國立臺灣大學工學院化學工程學研究所

碩士論文

Department of Chemical Engineering

College of Engineering

National Taiwan University

Master Thesis

雙金屬超分子高分子或 N-甲基吩噻嗪離子液體

應用於電致色變元件

Electrochromic Devices Based on Heterometallo-supramolecular

Polymer or N-methylphenothiazine Derived Ionic Liquid

蕭力尹

Li-Yin Hsiao

指導教授：何國川 博士

Advisor: Kuo-Chuan Ho, Ph.D.

中華民國 107 年 7 月

July 2018

國立臺灣大學碩士學位論文
口試委員會審定書

雙金屬超分子高分子或 N-甲基吩噻嗪離子液體
應用於電致色變元件

Electrochromic Devices Based on Heterometallo-Supramolecular Polymer or N-methylphenothiazine-Derived Ionic Liquid

本論文係蕭力尹君（R05524050）在國立臺灣大學化學工程學研究所完成之碩士學位論文，於民國 107 年 7 月 23 日承下列考試委員審查通過及口試及格，特此證明

口試委員：

_____（簽名）
（指導教授）

_____   _____

_____   _____

系主任、所長 _____（簽名）

致謝

首先要感謝我的指導教授何國川老師。相較於其他推甄生，我是成績比較普通的考試生，非常感謝老師還是願意讓我進入實驗室學習，同時在進入實驗室後老師的鼓勵與指導讓我對自己以及研究更有信心，也讓我學習到如何以正確的態度從事研究。也要感謝老師給我很多磨練的機會，不論是平常以英文報告實驗結果、出國參加會議口頭報告論文、或是撰寫論文後投稿到國際期刊、以及執行工研院研究計畫等，更重要的是要感謝老師讓我有機會赴日交換學習，開拓我的國際視野和啟發我的想法，讓我萌生前往美國取得博士學位的念頭。研究生涯中能待在何老師的實驗室真的獲益良多，這樣紮實的訓練讓我對於未來不論要從事學術研究或是就業工作，心理以及知識上都有完好的建設。

在此我要感謝實驗室的成員給我的幫助。我要感謝從進實驗室到現在一直給我很多指導和建議的昕則學長和廷祥學長，還有在碩一給我許多鼓勵的馮皓學長和旻翰學長，以及碩二給我很多想法的旻鑫學長，如果沒有你們的指導和幫助，我想我不會對實驗和研究產生興趣。在此也要感謝給我許多意見的學長姐，包括聖淵、致維、鑫福、妙璇、奕鈞、方賢、怡琳。也感謝同居平常修課、研究一同努力的秀玲和偉婷。也很感謝這段過程中，平時會一直討論實驗的彥安、柏勳、冠逸、程勗、書銘、語彤，與你們相處總是充滿歡樂。感謝旻軒、皓瑋、芳宇、宛霓、漢庭、宣百在平時實驗室討論會中分享研究成果，讓我學到更多在自身研究主題外的知識。最後我要感謝一路上相互扶持的彥鈞，從平常一起討論實驗、一起參加研討會到執行計畫，特別感謝你兩年來照顧。

感謝台大高分子所鄭如忠教授所提供的管柱層析設備予我從事純化工作。我也要感謝鄭教授實驗室的吳建欣博士和黃英治學長，很感謝你們願意教導我純化方法和討論實驗結果，在有機合成上也給我許多寶貴的指導和建議，讓我學習到許多有關合成的知識和技巧。

感謝 Higuchi-san 願意讓我進入他們的實驗室進行暑期交換，在日本 NIMS 實驗室做實驗對我來說是非常寶貴的經驗。也非常感謝 Ninomiya-san 在日本很親切地帶我做實驗，及時我回國後，還是很熱心地與我用 e-mail 討論實驗。在 NIMS 的這段期間，不只我學習到了許多合成相關知識和技巧，更重要的是開拓我的視野，讓我對研究更加充滿熱忱與想法。

感謝此次願意為學生進行論文審查以及口試的周澤川教授、戴子安教授、林正嵐教授及

何國川教授，因各位教授們的細心指導與建議，得以讓此篇研究更加完整。也希望此篇研究有機會提供其他研究者幫助，為知識的傳播盡一份心力。

感謝科技部予我的經費補助，讓我這兩年可以專注在研究上，不用擔心生活費的問題，也感謝科技部補助我參加美國研討會，讓我有機會出國口頭報告自己的研究，並且與其他學者交流，對於我是莫大的幫助。

最後最重要的是要感謝我的父母親。在我求學生涯中，不吝嗇地給予我幫助，這一路以來我都未曾因為學雜費和生活費擔憂過，父母親平常一直關心我的課業和生活作息是否正常，也很支持我所做的決定，你們的支持是我求學生涯中最重要的支柱。之後我會懷著感恩的心繼續努力，並用積極樂觀的態度迎接接下來的各種挑戰。謹以此論文獻給我摯愛的家人，以及所有曾經幫助過我的夥伴們。

<div align="right">

力尹

2018 年 7 月

</div>

中文摘要

在本論文中，本研究主要製備了兩種電致色變元件並加以探討其電化學性質，組成第一種電致色變元件的變色材料為釘鐵雙金屬超分子高分子和普魯士藍，第二種電致色變元件則由 N-甲基吩噻嗪離子液體和苯基紫精所製備而成。

在本研究第三章，首先製備出釘鐵雙金屬超分子高分子，並對其單膜電化學性質仔細探討。另外，由於普魯士藍是廣為人知非常穩定的電變色材料，且在光學表現上在 600 至 800 nm 處有不錯的吸收強度，而釘鐵雙金屬超分子高分子具有 400 到 600 nm 之強烈吸收峰，因此我們提出藉由此兩種材料之搭配，製備出能吸收全波段可見光的電致色變元件。為了防止漏液，此元件的電解質採用高分子電解質，當操作電位在 1.3 V 和 -2.2 V 之間，此元件在分別 503、580 和 690 nm 之波長下具有 52.7%、46.9% 和 28.0% 穿透度變化，在 503 nm、580 nm 波長下有小於 0.5 s 的快速著去色時間，還發現此元件具有特殊的三段式著色效率變化，而最大著色效率為 525.1 cm^2/C。另一方面，本研究還探討了記憶效應與長期穩定性相關性，藉由添加酸化過後的多壁奈米碳管，其表面所具有酸化官能基可以吸附過氯酸根離子，因此當釘鐵雙金屬超分子高分子加入些許多壁奈米碳管，在經過 200 秒之後，在相較記憶效應不好的 503 奈米波段，此薄膜仍可以維持 42% 原來之最高去色穿透度。

在本研究第四章，藉由五種步驟反應成功合成出全新之帶有 N-甲基吩噻嗪的離子液體，分別為硫化、脘基化、取代反應、離子化和陰離子製換。且每步驟之中間產物和最終產物之結構皆用核磁共振和質譜儀確認。首先，在三級式之電解槽中對 N-甲基吩噻嗪的離子液體做電化學分析，發現接上離子液體後，因為分子結構由原本平面分子(N-甲基吩噻嗪)改變為非平面分子，導致 N-甲基吩噻嗪離子液體之吸收波長從 520 奈米偏移到 575 nm 之位置，顏色從紅色變為紫色。為了進一步確認 N-甲基吩噻嗪離子液體在元件中電化學表現，我們使用穩定度很高的苯基紫精與之作為搭配來組成電致色變元件，此元件 0 V 與 1.2 V 的操作下，在 575 nm 波段下具有 69.2% 之光學穿透度化，小於 4 s 的著去色響應時間、高著色效率(531 cm^2/C)，在 10,000 圈操作後仍保持其最初 97.8% 之光學度穿透度變化。由此可知，本研究所合成出來的新型氧化著色材料：N-甲基吩噻嗪的離子液體同時保有 N-甲基吩噻嗪的高吸收度變化和離子液體的高穩定性。

關鍵詞：電致色變元件；全波段吸收；金屬超分子高分子；N-甲基吩噻嗪離子液體；多壁奈

米碳管

Abstract
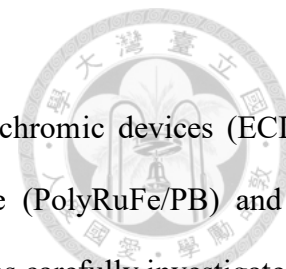
In this thesis, the electrochromic (EC) performance of two electrochromic devices (ECDs), Ru(II)/Fe(II)-based heterometallo-supramolecular polymer/Prussian blue (PolyRuFe/PB) and N-methylphenothiazine-based ionic liquid/phenyl viologen (NMP-IL/PV) was carefully investigated.

Firstly, Ru(II)/Fe(II)-based heterometallo-supramolecular polymer (PolyRuFe) has been successfully synthesized and the electrochromic properties are carefully investigated. Also, Prussian blue (PB) is selected as counter electrode owing to its good stability and large absorbance change of UV-visible spectra from 600 to 800 nm, which is cooperated with main absorbance change of PolyRuFe from 400 to 600 nm. The PolyRuFe/PB ECD has been successfully fabricated with panchromatic characteristic and the mechanism is proposed. Switching between -1.3 and 2.2 V, the proposed ECD utilizing the gel-typed electrolyte based on PMMA preventing the leakage problem exhibits the transmittance changes of 52.7%, 46.9%, and 28.0% at 503, 580, and 690 nm, respectively. Moreover, the fast response time of less than 0.5 s could be observed at 503 and 580 nm for both coloring and bleaching. The PolyRuFe/PB ECD also exhibits three-step coloration efficiency and the highest values are 525.1 cm^2/C at 503 nm. Furthermore, we proposed the relationship between the long-term stability and the memory effect of PolyRuFe/PB ECD. It was found that PolyRuFe incorporated with multi-walled carbon nanotubes (PolyRuFe-MWCNT) exhibits longer memory effect than bare PolyRuFe thin film. PolyRuFe-MWCNT remained 75%, 59% and 42% of their initial saturated bleaching state at 503 nm after 50, 100 and 200 s, respectively.

In the second part, we synthesized the novel NMP-based IL via five-step reaction, including thionation, methylation, substitution, ionization and anion exchange that no one demonstrated before. Each structure of intermediates was confirmed by 1H-NMR, 13C-NMR and mass spectra. When the functional groups graft on the benzene, the obvious absorbance change to 575 nm is found. It is explained that molecular structures changes from open ion-radical to hindered ion-radical. Namely, the planar structure of NMP convert into NMP-IL which belongs to hindered system. In order to investigate the EC performance of NMP-IL in ECD, the complementary ECD was fabricated

incorporating the cathodically coloring material, PV, which is well-known for its high optical contrast and good stability. The NMP-IL/PV ECD exhibits largest transimittance change of 69.2% and desirable coloration efficiency of 531 cm^2/C at 575 nm, which is contributed to the additive absorbance change of both coloring material. Moreover, the short switching times of less 4 s and good long-term stability (remained 92%, 96.2% and 97.8% of its original ΔT after 10,000 cycles at 430, 575 and 710 nm respectively) is obtained. These evidences reveal that the new potential anodically coloring material, NMP-IL, combining both the advantages of NMP and ionic liquid have successfully synthesized.

Table of contents

List of tables

List of figures

Nomenclatures

Abbreviation	Full name
ACN	Acetonitrile
BF_4^-	Tetrafluoroborate anion
CNT	Carbon nanotube
CE	Counter electrode
CV	Cyclic voltammogram
DCM	Dichloromethane
DIW	Deionized water
DMF	Dimethylformamide
DMPZ	5,10-dimethyl-5,10-dihydrophenazine
DMSO	Dimethyl sulfoxide
DWCNT	Double-walled carbon nanotube
EA	Ethyl acetate
EC	Electrochromic
ECD	Electrochromic device
ES	Everitt's salt
Fc	Ferrocene
$Fe(NO_3)_3$	Iron(III) nitrate
HV	Heptyl viologen
ITO	Indium tin oxide
IL	Ionic liquid
$LiClO_4$	Lithium perchlorate
M	Redox mediator
MEPE	Metallo-supramolecular polymer
MWCNT	Multi-walled carbon nanotube

NaClO$_4$	Sodium perchlorate
NiO	Nickel oxide
NMP	N-methylphenothiazine
OCV	Open-circuit voltage
PANI	Polyaniline
PB	Prussian blue
PC	Propylene carbonate
PEDOT	Poly(3,4-ethylenedioxythiophene)
PMMA	Poly-(methyl methacrylate)
PProDOT	Poly(3,4-propylenedioxythiophene)
PSS	Poly(styrene sulfonate)
PV	Phenyl viologen
RE	Reference electrode
R^2	Coefficient of determination
TBABF$_4$	Tetrabutylammonium tetrafluoroborate
TCO	Transparent conducting oxide
TMPD	N,N,N',N'-tetramethyl-p-phenylenediamine
UV-Vis	Ultraviolet-visible
V	Viologen
WE	Working electrode

Abbreviation	Latin / Meaning
etc	*et cetera* / and other things
et al.	*et alii* / and others, and co-workers

English symbol	Meaning (unit)
A	Surface area (cm^2)
D$_{app}$	Diffusion coefficient (apparent diffusivity) (cm^{2}s^{-1})

E	Potential (V)
E_{onset}	Onset potential (V)
E_{pa}	Anodic peak potential (V)
E_{pc}	Cathodic peak potential (V)
F	Faraday constant: 96485 (C/mol)
i	Current (A)
i_d	Diffusion limited current (mA)
i_p	Peak current (A)
j_{col}	Coloring current density (mA/cm^2)
j_{mea}	Measured current density (mA/cm^2)
j_{rec}	Recombination current density (mA/cm^2)
L	Diffusion length (μm)
n	Number of electrons transferred (-)
Q_d	Deposited charge density (C/cm^2)
R_s	Serial resistance (Ω)
R_s'	Resistance contributed by the electrolyte (Ω)
T_c	Transmittance at colored state (%)
T_b	Transmittance at bleached state (%)
t	Elapsed time (s)
t_c	Coloring time (s)
t_b	Bleaching time (s)
V	Volume (L)
V_c	Potential bias during coloring state (V)
V_b	Potential bias during bleaching state (V)
ΔA	Absorbance change (-)
ΔOD	Optical density change (-)
ΔT_n	Percentage of transmittance change remained after n cycles (%)

$\Delta T\%$	Transmittance change (%)
$[V^{+\bullet}]$	Total amount of $V^{+\bullet}$ (mol)
$[V^{+\bullet}]^R$	Amount of $V^{+\bullet}$ in bulk solution (mol)
$[V^{+\bullet}]^*$	Amount of $V^{+\bullet}$ on counter electrode (mol)

Greek symbol	**Meaning (unit)**
ε	Molar absorptivity ($dm^3\,mol^{-1}\,cm^{-1}$)
η	Coloration efficiency (cm^2/C)
η_e	Effective coloration efficiency (cm^2/C)
λ_{max}	Wavelength with maximum transmittance change (nm)
ν	Scan rate (mV/s)
σ	Ionic conductivity (mS/cm)

Chapter 1

Introduction
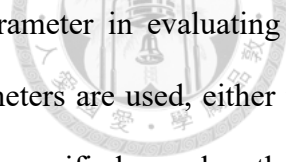
1.1 Overview of electrochromism

The term, chromism, refers to a phenomenon that materials undergo reversible changes of their optical characteristics induced by some form of stimulus [1], such as light [2-4], heat [5] or electricity [6-7]. In generally, chromism is based on a change in the electron states of molecules, which can be induced by several external stimuli which can alter the electron density of the substances. According to such unique properties of chromatic materials, the technology of electrochromism is developed by harnessing the reversible change of a chemical species between two redox states [8-9]. As the result, electrochromism can be defined as the capability of a material under an applied potential biases [10] to transform its optical properties within the whole electromagnetic spectrum, including visible region from 400 to 800 nm or the near-infrared (NIR) region [11-14]. Since 1969, the first literature reported about EC technology by S. K. Deb [15] , the various electrochromic devices (ECDs) utilize the optical changes of EC materials have been investigated, contributing to the well-being for humanity. To the begin, we firstly introduced several important parameters that determine the performance of the ECD and EC material as a start.

1.2 Electrochromic performance parameters

(a) Optical contrast

Electrochromic optical contrast is probably the most important parameter in evaluating an electrochromic material [16]. In order to quantify this parameter, two parameters are used, either the largest change of absorbance (ΔA) or transmittance ($\Delta T\%$) occurring at a specified wavelength. In general, we use transmittance change ($\Delta T\%$) due to the direct information about the percentage of light attenuated by this EC material on which the ECDs for light attenuation purpose focus. To obtain the transmittance change of the ECDs, we measure both firstly the transmittance under coloring state (T_c) and bleaching state (T_b) and the transmittance change is equal to Tb minus Tc. The larger transmittance change, the more amount of light is attenuated at the wavelength with maximum transmittance change (λ_{max}). For some instances, it is more practical to report a contrast over a specified range rather than a single wavelength. If so, variation in lightness (L*) or relative lumince change (Δ) [17] regarding the entire visible wavelength of both the colored and bleached states would be recorded in order to compare the amount of optical contrast among the visible region.

Usually, the optical characteristics of EC materials are judged by measuring their change of absorbance and transmittance because the change and shade of pigment are observed directly for human. On the contrary, fewer studies investigate the reflection in electrochromic field owing to less application of reflection, except for mirrors. The most of researchers aim at developing the multi-color or high optical contrast characteristic instead of reflective properties due to the wider application of smart window in electrochromic field. For this reason, the reflection would not be discussed in this thesis.

(b) Response time

The response time of the EC materials and devices is used to quantify the time required to switch between coloring and bleaching states. There are a lot of definitions to quantify this parameter. Therefore, according to the previous part, we use transmittance change as the parameter to define it. Follow some reliable literatures, we quantify the response time as the time required to reach 95% of

the largest transmittance change from either coloring or bleaching states. Thus, coloring time (t_c) and bleaching time (t_b) are obtained.

The response times of the EC materials and devices are usually restricted by diffusion rate of the ion diffusing in the electrolyte or thin film. Subsequently, the porous characteristic of the EC thin film and the ion conductivity of the electrolyte are crucial for the response time. Nevertheless, not all ECD applications required a short switching time. For instance, the ECDs applied in glazing products or smart windows designed for sunlight attenuation usually prefer longer response time to prevent unnecessary disturbing to the users during switching. On the other hand, the ECDs used in anti-glare mirror on the vehicles are expected to have short response time to respond to the needs of the users [18].

(c) Long-term stability

The evaluation of the long-term stability (write-erase stability) is to quantify the coloring-bleaching cycles that can be performed by the EC materials and devices. Similar to response time, there is no consistent method to quantify the long-term stability. Typically, the durability of electrochemical devices is based on the remained performance of this device, for instance, battery depending on the storage charge remained. Nevertheless, the stability of ECDs is not appropriate for only considering the charge since it could not directly reflect to the optical contrast. Thus, we evaluated the long-term stability by how much EC performance remained after cycling between coloring and bleaching states. Therefore, we use the remained transmittance change after n cycles (ΔT_n) as a standard for long-term stability in this thesis.

It is obvious that good long-term stability is an important criterion for commercialized ECDs. Generally, a gel-typed electrolyte utilizing polymer inside would be regarded as a better candidate to improve the durability of electrolyte owing to leakage. In addition, the stability is also affected by the completeness of sealing. For the EC materials, the problem is more intricate. The factors such as the ion diffusion inside the EC thin film, or the diffusion of the diffusible redox activity would also attribute to possible degradation of the ECD.

(d) Coloration efficiency

The term, coloration efficiency (η) also referred to as electrochromic efficiency, specified the ratio of optical density change (ΔOD) to the deposited charge density (Q_d) for EC materials or an ECD, as given by the Eq. (1-1) [19].

$$\eta = \frac{\Delta OD}{Q_d} = \frac{\log \frac{T_b}{T_c}}{Q_d} \tag{1-1}$$

The optical density change is defined as the optical contrast between bleaching (T_b) and coloring (T_c) states in logarithm, and the required charge for ECD represents the charge deposited into an ECD during coloring process. Required charge for an ECD, namely, the amount of charge necessary to arise the optical change is usually calculated through integrating the current with a defined time that assures the reaction reaching the steady state in fixed applied potential bias. The coloration efficiency indicates the relationship between optical contrast and the energy costed during the operation of an ECD. Therefore, the EC material and device showing higher coloration efficiency could be considered as a more efficient one.

1.3 Introduction of electrochromic materials

To date, various classes of EC materials have been developed as chromophores in ECDs. Generally, classification could be divided into anodically coloring and cathodically coloring materials based on the coloring behavior [20]. Typically, EC materials could possess both bleaching (transparent) and coloring states. The term, anodically coloring EC materials, indicates that these EC materials are darkened in the oxidative state. On the contrary, cathodically coloring materials are transparent in reductive state. Besides, there are materials that don't demonstrate significant color change but still be utilized in ECDs as ionic storage layer.

Nonetheless, classification based on the coloring behavior of the EC materials doesn't clarify the chemical and physical properties of these materials. Therefore, an alternative method is often utilized by researchers, which is, dividing those EC materials into groups that have similar structures or intrinsic properties [20]. In this section, we will focus on several classes of EC materials that we utilize in this thesis.

(a) Metallo-supramolecular polymers

One of the newest EC materials, named as metallo-supramolecular electrochromic materials has been developed by Kurth et al [21]. Generally, organic polymers are synthesized through the polymerization of monomers, which is accompanied by the formation of covalent bonds. On the contrary, metallo-supramolecular polymers, which are synthesized through the complexation of equivalent metal ions and ditopic organic ligands, are a new type of polymers, in which the polymer backbone consists of coordination bonds [22]. Polymers built up through weak interactions can assemble, disassemble and reconstruct in a dynamic fashion under ambient conditions [23], indicating the chain length of metallo-supramolecular polymer is not fixed in solution owing to the equilibrium reaction of complexation [22]. Han et al. successfully synthesized a series of metallo-supramolecular polymers via combination Fe^{2+}, Ru^{2+} and Co^{2+} metal ions and corresponding ligands, achieving a variety of color changing behaviors [24-25]. The synthetic route was expressed in Fig. 1-1 while the color presented by the obtained Fe^{2+}, Ru^{2+} and Co^{2+} based metallo-supramolecular polymers were shown

in Fig. 1-2. The mechanism of metallo-supramolecular polymer to change its color can be explained by the energy diagram shown in Figure 1-3. At coloring state, the energy falls in the range of visible light, which requires for electron to leap across energy gap between HOMO (the highest occupied molecular orbital) and LUMO (the lowest unoccupied molecular orbital). The different metal ions and ligands cause the various energy gaps, attributed to metal-to-ligand charge transfer (MLCT) [26]. Take the Fe^{2+}-based metallo-supramolecular for example, shown in Fig. 1-3. Its deeply blue color that illustrated in Fig. 1-4 attributed to its strong light absorption at 580 nm, which enable the electron at HOMO level to leap to LUMO level. While Fe^{2+} is oxidized to Fe^{3+} state, the colorless state is due to the elimination for electron undergoing MLCT, which caused by the increasing gap between HOMO and LUMO [22].
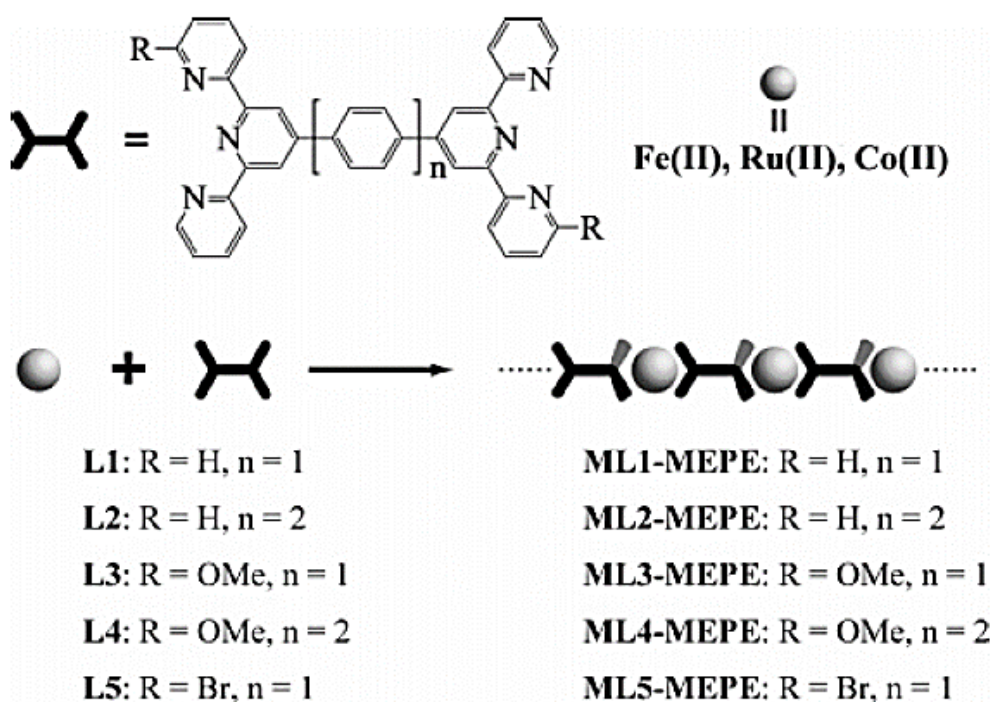
Fig. 1-1 Coordination of metal ions and various ligands L1 ~ L5 [25].

Fig. 1-2 Colors of Fe^{2+}, Ru^{2+}, Co^{2+} based metallo-supramolecular polymers and with various ligands L1 to L5, respectively [25].
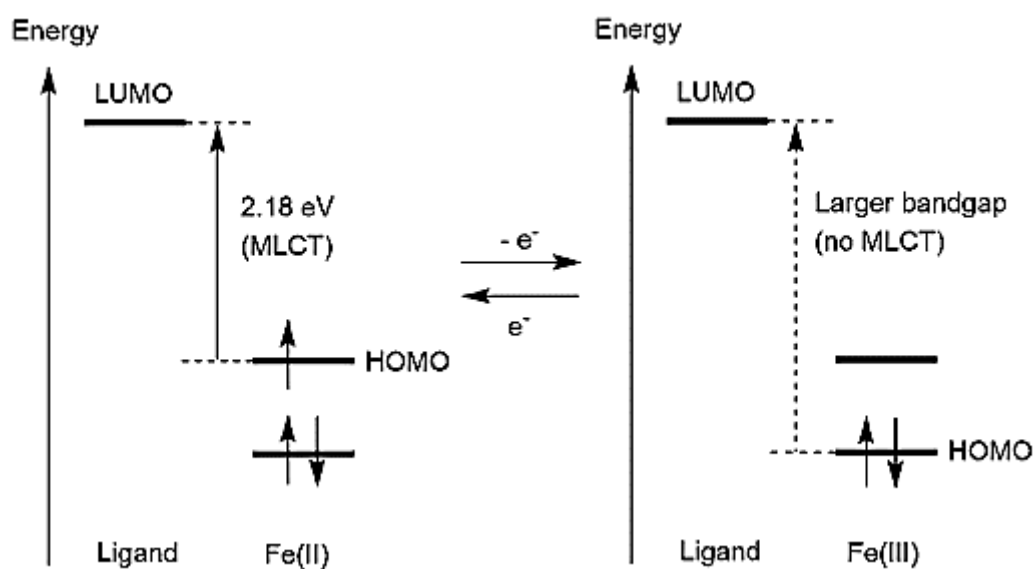
Fig. 1-3 Energy diagrams of Fe^{2+} based metallo-supramolecular polymer under redox states [22].
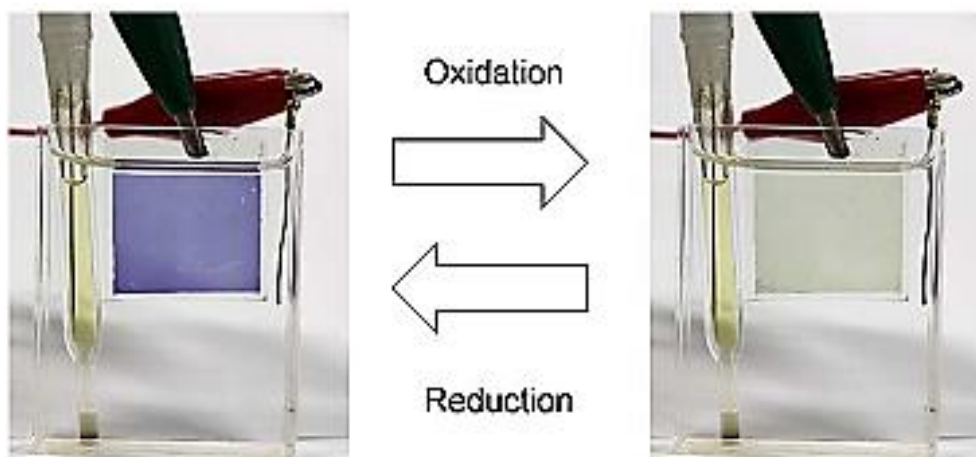
Fig. 1- 4 Images of Fe^{2+} based metallo-supramolecular under different redox states [22].

As mentioned before, the selection of the ion in the electrolyte affect the EC performance of thin-film EC material. For MEPE system, the anions play the crucial role owing to adsorption by MEPE thin film during oxidation. CVs of the Ru(II)-based metallo-supramolcular polymer (PolyRu) films with different counter anions are shown in Fig. 1-5 [27]. PolyRu-TFSI, PolyRu-PF$_6$, PolyRu-ClO$_4$ and PolyRu-CF$_3$SO$_3$ exhibit reversible cycle; however, the poor electrochemical properties and stability of PolyRu-BF$_4$, PolyRu-Cl and PolyRu-CO$_3$ can be observed. Among all of them, PolyRu-ClO$_4$ shows the highest current density and the appropriate redox potential, indicating perchlorate ions are the best anion for MEPE.
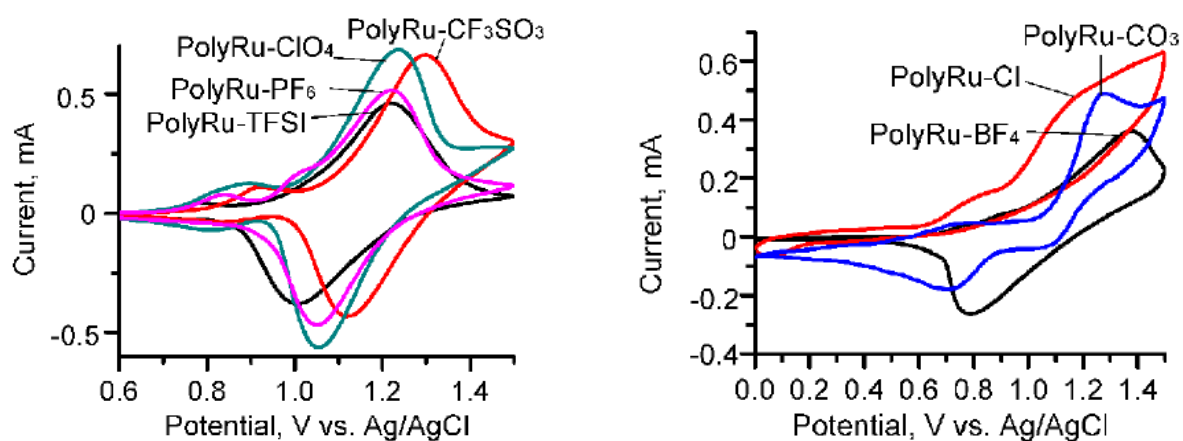
Fig. 1-5 Cyclic voltammograms of PolyRu-TFSI, PolyRu-PF$_6$, PolyRu-ClO$_4$, PolyRu-CF$_3$SO$_3$, PolyRu-BF$_4$, PolyRu-Cl and PolyRu-CO$_3$ [27].

(b) Prussian blue and its analogues

Prussian blue, (PB, iron (III) hexacyanoferrate (II)) is a well-known and widely used anodically coloring EC material. After first, Prussian blue was merely used as a pigment in industry. The early reports for Prussian blue revealed that it possesses EC property, which shows a large optical change from its ES (Everitt's salt, Li$_2$Fe^{2+}[Fe^{2+}(CN)$_6$]) to PB (LiFe^{3+}[Fe^{2+}(CN)$_6$]) states in the presence of Li ion, namely, from transparent to blue. The outstanding optical contrast, long-term stability, and desirable response time allow Prussian blue to be utilized in various EC studies [28-32]. In general, Prussian blue is fabricated as a thin film through electrodeposition [33], while some new methods were

also progressed to prepare Prussian blue nanoparticles [34-36].

The Prussian blue analogues, refers to the analogues that different with the metal inside the crystal, comparing to Prussian blue. The different Prussian blue analogues lead to various EC property, for instance, switching from transparent to yellow (Nickel hexacyanoferrate) [35], or maintaining colorless in both redox states (Zinc hexacyanoferrate) [36]. The multiple EC property of Prussian blue analogues, is one of the attractive characteristic, making them as promising EC materials for researchers. In Fig. 1-6, the colors of several Prussian blue analogues are presented, implying the potential of new EC materials that could be developed in the future [37].
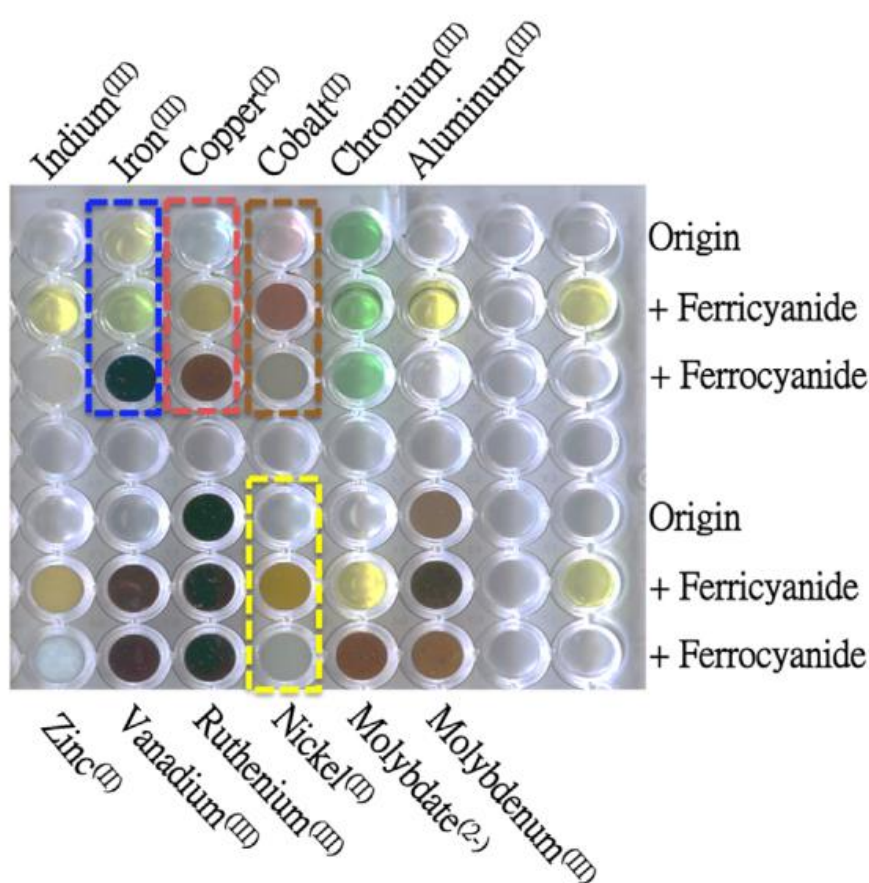
Fig. 1-6 The images of Prussian blue analogues that show the various colors at different redox states [37].

(c) Solution-type EC materials

In previous parts, the EC materials are mostly utilized as an EC thin film, namely, the EC materials are immobilized or coated on the electrode, and the transfer of electrons and ions through the thin film are followed by the doping or dedoping into it. There is another kind of EC materials that freely diffuse in the electrolyte and give or release electron onto the electrode, referring as solution-type EC materials [16]. Separating from the EC thin films, the solution-type EC materials are not confined on the electrodes but diffusing in the electrolytes. Therefore, the EC property of solution-type EC materials are different from those of thin films as the conductivity, or the diffusion coefficient of the thin film. The electrochromic performance of the solution-type EC materials mainly depends on the property of the molecule and the electrolyte in the ECD. Furthermore, compared to EC thin films, the absorbance spectrum of solution-type EC materials is more transparent at bleaching state in usual. There are several EC materials that belong to this class, such as the viologens, quinones, phenazines, and tertiary amines.

One of popular solution-type EC materials, 5, 10-dimethyl-5, 10-dihydrophenazine (DMPZ) [16], exhibits three stable redox state, that is, DMPZ, DMPZ$^+$, and DMPZ^{2+}. The structure of DMPZ and the absorbance spectra of DMPZ$^+$ and DMPZ^{2+} are presented in Fig. 1-6. As shown, a significant absorbance change between 400 to 500 nm, leading to a color change from transparent to lime-green [16, 38], can be observed while the reaction triggers the oxidation of DMPZ into DMPZ$^+$ [39].
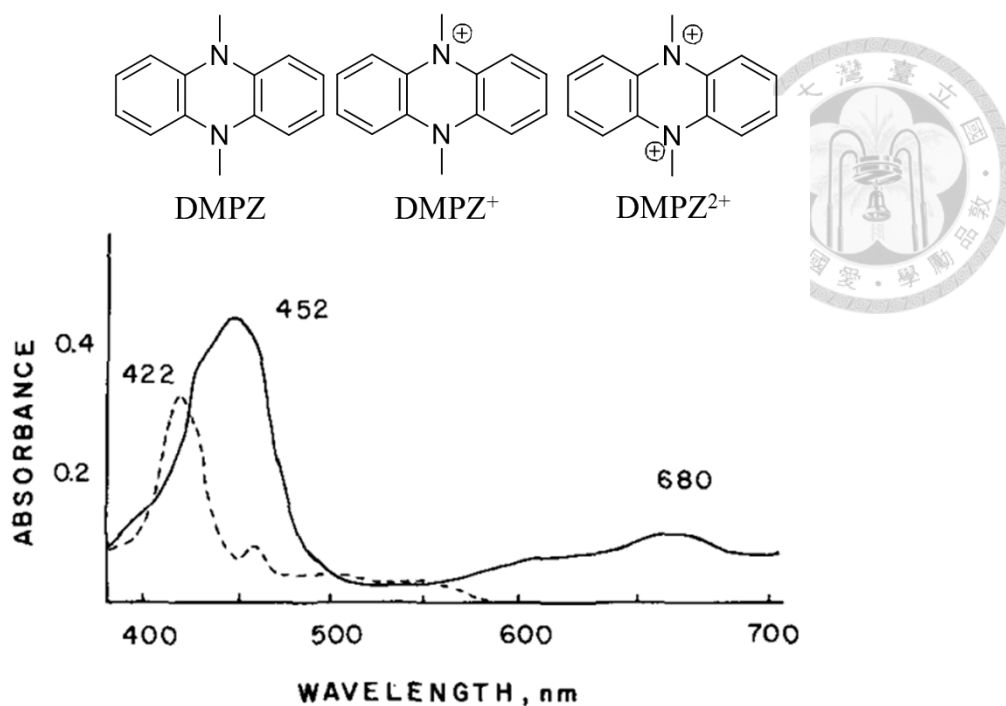
Fig. 1-7 The structures of DMPZ, DMPZ$^+$, and DMPZ^{2+} and the absorbance spectra of DMPZ$^+$ (solid line) and DMPZ^{2+} (dot line) [38].

Another solution-typed EC material has been investigated widely is phenothiazine, which has the similar structure with DMPZ. Phenothiazines are a class of important heterocycles and widely used as common building blocks for the synthesis of medical drugs, antitubercular agent, cholinesterase inhibitor, and so on [40-41]. In addition, phenothiazine derivatives have been found frequently in other important molecules such as optoelectronic materials, antioxidants, polymerization inhibitors, industrial dyes and other agrochemical compounds [42-45]. Recently, molecules and polymers containing phenothiazine moieties have attracted much research interest due to their unique electro-optical properties and their potential in diverse applications such as light-emitting diodes [46-47], chemiluminescence [48] and transistors [47]. Furthermore, the N-substituted phenothiazine derivatives (PDs) were synthesized and their corresponding ECDs were assembled. Most of PDs exhibit the transparent and red color in the reduced state and oxidized state, respectively. The structures, properties and electrochromism of PDs are presented in Fig. 1-7 and Fig. 1-8. It is found that PDs, with electron-rich characteristic due to presence of sulfur and nitrogen heteroatoms, could be easily oxidized to form stable polaron while resulting in a noticeable color change in visible

11

region, enabling PDs to be utilized in many ECDs [49-50]. Another important class of solution-type EC materials are the viologens on which many researchers and companies focus on, and we will give our discussion in next section.
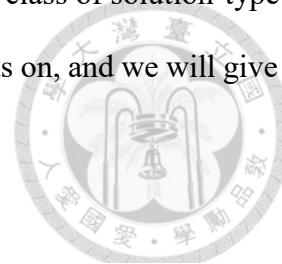
Compound	R	Formula	T (°C)	Mp (°C)/form	Electrochromic color	Yield (%)
1	H	$C_{12}H_9NS$	–	183	Green	–
2a		$C_{16}H_{17}NS$	40	Viscous liquid	Red	55
2b		$C_{18}H_{21}NS$	40	Viscous liquid	Red	60
2c		$C_{20}H_{25}NS$	40	Viscous liquid	Red	62
2d		$C_{24}H_{33}NS$	80	Viscous liquid	Red	64
2e		$C_{15}H_{14}NS$	40	Viscous liquid	Red	48
2f		$C_{19}H_{16}NS$	40	103	Red	82
2g		$C_{21}H_{18}NS$	80	98	Red	74
2h		$C_{18}H_{11}N_3O_4S$	110	83	Red	66

Fig. 1-8 The part of PDs, concluding temperature, melt point, electrochromic color and yield [49].
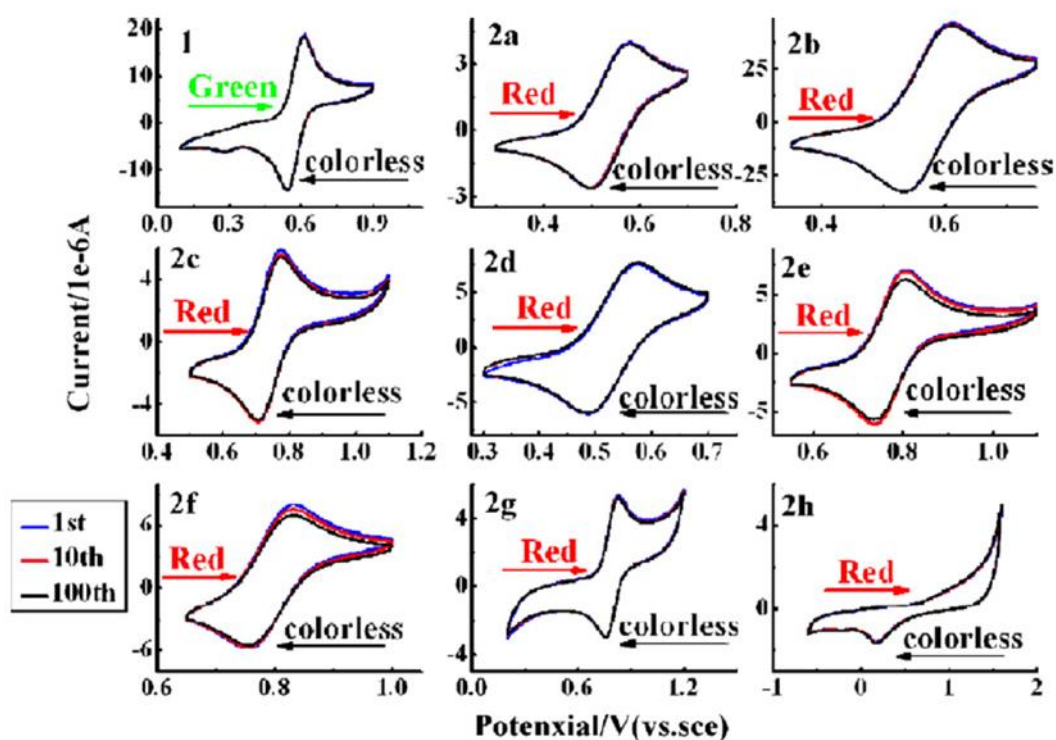
Fig. 1-9 CV of PDs containing 0.1 M TBAP in DCM at room temperature. The first, 10th and 100th cycles are shown and the scan rate is 100 mV/s. [49]

(d) Viologens

Among all electrochromic materials, the viologens (V), also referring as N, N-substituted bipyridinium salts [51], draw much attention for their dramatic and highly reversible optical change. Generally, Viologens exhibit three redox states, including dication state (V^{2+}), radical cation state ($V^{+\bullet}$), and neutral state (V^0). While switching between dication state (bleached) and radical cation state (colored), it leads to a significant change of optical contrast; however, the lower optical change is founded when switching to the radical cation state. With their electrochemical redox activity, each three redox states exhibit electrochromism. The di-cation is the usual starting material for their studies because it is the most stable of the three. As for the radical-cation state, it is also one of organic radicals. In solution the color of the radical will prolong almost indefinitely in the absence of oxidizing agents, such as ferrocene, although the reaction with oxygen is rapid [52]. Di-reduced compounds are occasionally called bi-radicals owing to their reactivity [53]. Di-reduced viologens may reduce hydrogen ion to hydrogen gas because they are very powerful reducing agents [54]. Nevertheless, di-reduced species are colored in red-brown to scarlet-red [54], depending on the substituents, that the intensity of the color is lower than radical-cation one since no optical charge transfer or internal transition corresponding to visible wavelengths is accessible. Thus, we usually switch between dication state and radical cation state for considering its coloration efficiency and long-term stability.

The structures of the three redox states of viologens are presented in Fig. 1-10. Typically, there are two anions (X^-) accompanying with the N, N-substituted bipyridinium, bearing both positive and negative charges in molecules, making the viologen a zwitterion. The nomenclature typically used is to name it by the substituent groups on the bipyridinium. For instance, if the substituent groups are phenyl groups (R = C_6H_5), the viologen would be named as phenyl viologen (PV) [55].
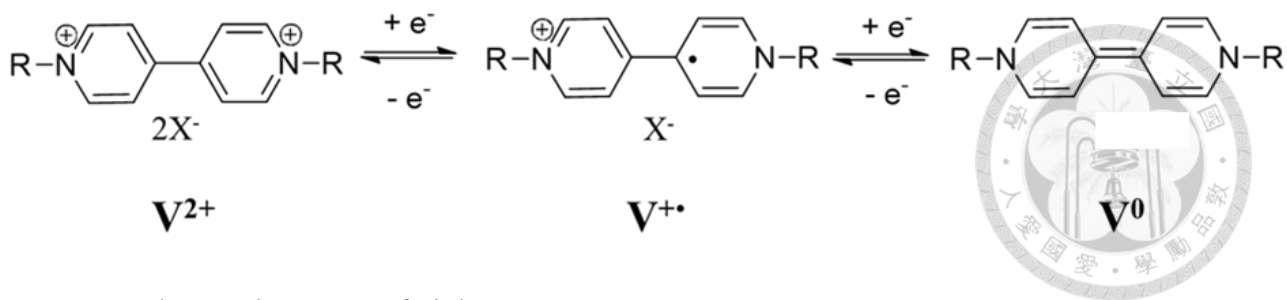
Fig. 1- 10 Three redox states of viologens.

The first time the name, viologen, was given to the N, N-substituted bipyridinium found in 1933 by L. Michaelis et al. [56], and the violate color was observed from methyl viologen dication [56]. Many researchers focus on studying viologen derivatives not only for their large optical contrast, but also for their highly reactive radical reaction, allowing various structural modifications for different purposes. As cathodically coloring EC materials, viologen derivatives probably are the most popular materials as solution-type EC materials. Thus, there are many reviews or handbooks about viologens have been published [16, 57-58].

1.4 Electrochromic devices

At the beginning, an important concept about fabricating ECDs is the idea of complementary ECD. Namely, an ECD is often composed of one anodically coloring material and another cathodically coloring material that both can react simultaneously. An alternative combination is to choose one major coloring material and another material balances the charge in the ECD, referring as ion storage layer. Herein, the strategy of the complementary ECDs could combine the optical contrast of both two coloring materials, leading to higher coloration efficiency is quite important [59]. In addition, the ohmic drop in the ECD could be decreased by introducing another electrochemically active material, leading the ECD to be operated at a significantly lower potential window and the stability could also be enhanced.

Generally, an ECD would consist of several parts, including the glasses, transparent conductor coated on the glass, EC materials, and the electrolyte. The most widely used of transparent conductor is indium tin oxide (ITO) since it is considered to have outstanding conductivity and transparency. On the other hand, there are many novel transparent conductor are under developed, such as conducting polymer and graphene [60-61].

(a) Thin-film type ECDs
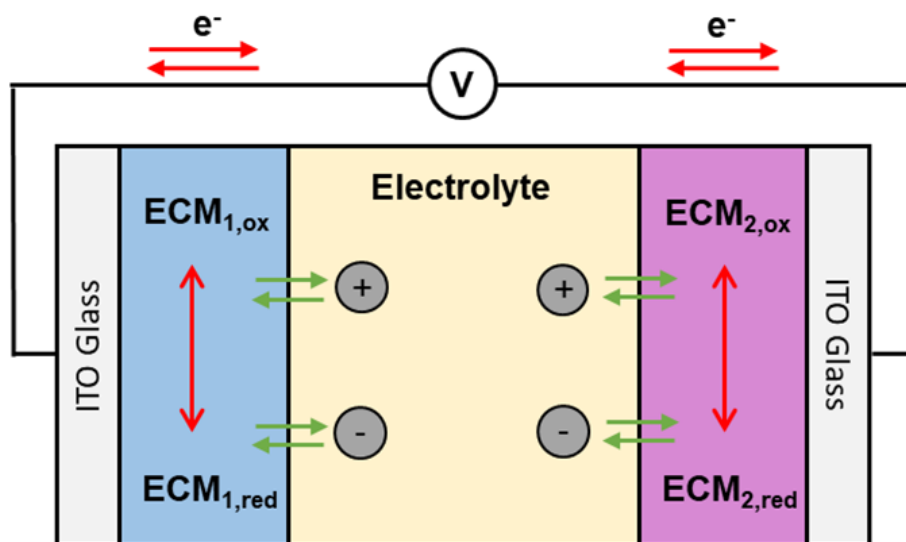
Fig. 1-11 Working principle of a thin-film type ECD.

The research fields of ECDs according to the properties of EC materials can separate into three parts, the thin-film-type [62], the solution-type [63], and hybrid type ECDs [64]. The structure and working principle of a thin-film type ECD were illustrated in Fig. 1-11 [16]. For this type of ECDs, two EC materials are immobilized or coated compactly on the electrode as solid thin films. The functions of this kind of EC materials depend on the electron transfer and ion diffusion inside the thin films. Thus, the performances of thin-film type EC materials and devices are significantly affected by both the charge transfer resistance and the diffusion coefficient of ions inside the EC thin films. Thus, the ion in the electrolyte plays a key role in the EC performance of the thin-film type ECDs [65-67]. The electrochromic characteristics of thin-film type are quite long of the memory time, which ranging from several minutes to even hours, and faster coloring/bleaching time comparing to other categories of ECDs.

As mentioned before, there would be two EC materials or ionic storage layer as a complementary pair. Since most of the EC materials could be fabricated as thin films, such as metal oxides, conjugated polymers, and Prussian blue analogues, considering the candidates for fabricating this kind of ECD. For instance, NiO/WO_3 [68], PANI/PEDOT [69], and Prussian blue/ WO_3 [59] are thin-film-type ECDs that composed of anodically and cathodically coloring thin films. On the other hand, there are several studies focus on using one EC thin film contributing most of the optical change, and the other one only working as balancing the charge, namely, the ion storage layer. For example, Prussian blue/Zinc hexacyanoferrate [36], and PANI/indium hexacyanoferrate [70].

(b) Solution-type ECDs
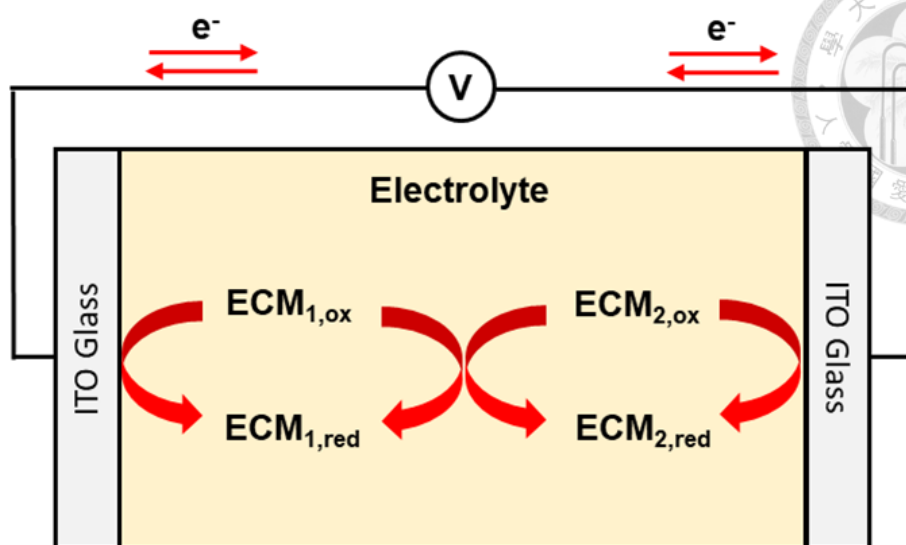
Fig. 1-12 Working principle of a solution-type ECD.

Differently, the solution-type ECDs consist of EC materials that are redox active species dissolving in the electrolyte. As shown in Fig. 1-12 [71], two redox couples are frequently used in a solution-type ECD. Generally, viologens are often used as the cathodically coloring material in this class of ECDs. Anodically coloring materials such as phenothiazine-based groups, phenylene diamine and ferrocene are utilized in such ECDs in general.

Without any driving voltage, both EC materials are thermodynamically stable at the bleaching state. While a potential bias is applied, these two materials would respectively diffuse to the surface of different electrode to undergo oxidation and reduction, forming color change from transparent. The colored materials would diffuse back to bulk solution owing to the concentration gradient and charge transfer between them happen, namely, recombination reaction. The recombination reaction occurs simultaneously because the EC materials prefer to the thermodynamically stable state, bleaching state. Therefore, the recombination reaction would progress continuously until all colored materials disappear. This self-erasing characteristic could be applied in the anti-glare rearview mirror. Nevertheless, to maintain the solution-type ECD at coloring state, constant current is required to continuously supply the colored species and resist the recombination reaction. It leads to the energy dissipation.

Consequently, the faster surface reaction is often controlled by the diffusion rate of EC materials between bulk solution and the surfaces of electrodes. For most cases, compared with thin-film type, longer switching time is required in solution type ECDs. There are many combinations of redox couple utilizing in solution-type ECDs, such as TMPD/HV [72], ferrocene/methyl viologen [73], hydroquinone/ethyl viologen [74], and DMPZ/methyl viologen [75].

(c) Hybrid-type ECDs
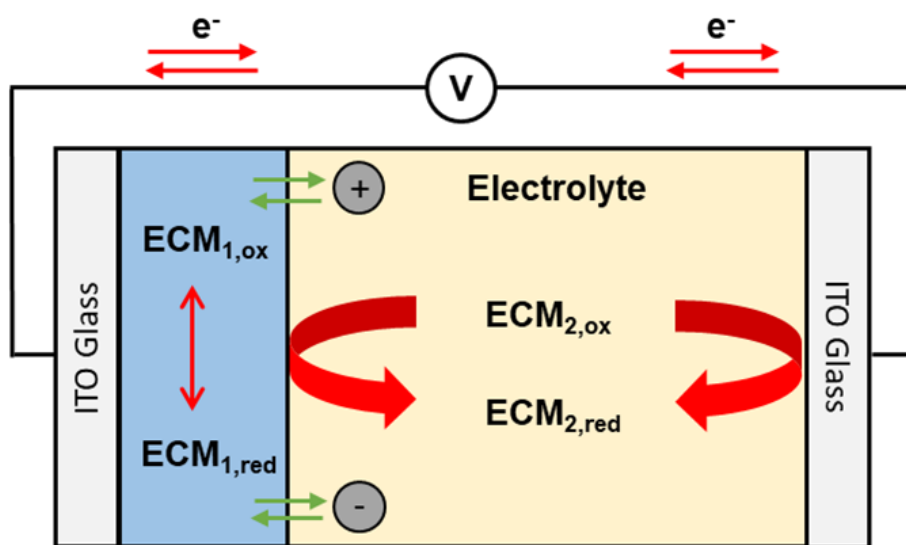
Fig. 1-13 Working principle of a hybrid type ECD.

The term, hybrid-type ECDs, referring as an ECD composing both thin film and electrochromic specie, namely, redox couple that dissolved in the electrolyte, which illustrated in Figure 1-13. As there is one redox couple dissolving in electrolyte, recombination reaction between electrochromic solid thin-film and dissolved redox couple consistently occurs. This eliminates the memory effect observed in thin-film type ECDs. On the other hand, the response time of such device is often determined by the relatively slower diffusion reaction of redox couples. The color transition time scale therefore is also in the range of seconds. There are still some studies using this system to develop the possibility of the combination of EC materials, such as the literature proposing Prussian blue/HV [64], and NiO/dimethyl terephthalate [76].

1.5 Scope of this thesis

In this thesis, expect for the introduction (Chapter 1), experimental (Chapter 2), and conclusions and suggestions (Chapter 5), in the rest of the thesis, we will put out effort to introduce our development on Ru(II)/Fe(II)-based heterometallo-supramolecular polymer (PolyRuFe) and the novel N-methylphenothizine derived ionic liquid (NMP-IL). There are two different chapters, discussing about the electrochromic device composed of PolyRuFe and Prussian blue in Chapter 3. In Chapter 4, we focus on synthesizing the novel NMP-IL and utilizing in the ECD with phenyl viologen. The framework of this thesis is illustrated in Fig. 1-14. In the following paragraphs, we will introduce the motivation and the expected research goal of chapter 3 and chapter 4.

In chapter 3, we aim at fabricating a panchromatic ECD based on metallo-supramolecular polymer (MEPE). As mentioned before, MEPEs show many attractive EC properties; however, there are few studies fabricating the ECD composed MEPEs owing to their technological difficulties. Herein, the Prussian blue (PB) is selected as anodically coloring material because it is a popular EC material for its dramatic long-term stability. Further, the obvious absorbance change of PB at 600~800 nm is utilized to fabricate the proposed ECD composed of PolyRuFe, which provides the high optical contrast at 400~600 nm. Also, the memory effect of PolyRuFe is investigated carefully, which is considered a crucial advantage of thin-film type EC material. In this chapter, we incorporated multi-walled carbon nanotubes (MWCNTs) with PolyRuFe, abbreviated as PolyRuFe-MWCNT, to enhance the memory time at bleaching state by utilizing the adsorption ClO_4^- of MWCNTs, which is regarded as the most suitable anion for MEPE thin film.

In chapter 4, we would like to synthesize the novel NMP-based IL that no one has synthesized before. ILs are well-known for enhancing the durability of electrochemical device since the high boiling points of ILs and the higher ionic conductivity of the electrolytes with the presence of ILs. It is suitable for introduce the ILs in the ECD. On the other hand, the NMP as the phenothiazine-based group which is investigated its electrochromism recently owing to its high optical contrast and good stability. In this chapter, we synthesize the NMP-IL via five-step reaction, including thionation, methylation, substitution, ionization and anion exchange. Further, each structure of intermediates was

confirmed by 1H-NMR, 13C-NMR and mass spectra. In order to investigate the EC performance of NMP-IL in ECD, the complementary ECD was fabricated incorporating the cathodically coloring material, PV, which is well-known for its high optical contrast and good stability. The NMP-IL/PV ECD exhibits the high absorbance change, fast response time, large coloration efficiency and impressive long-term stability, revealing the NMP-IL is the potential anodically coloring material.

```
┌─────────────────────────────────────────────────────────┐
│ Electrochromic devises based on heterometallo-supramolecular │
│    polymer or N-methylphenothiazine derived ionic liquid  │
└─────────────────────────────────────────────────────────┘
                              │
(Chapter 1 & 2)               ↓
        ┌───────────────────────────────────────┐
        │  Introduction & Experimental Procedure │
        └───────────────────────────────────────┘
                              │
         ┌────────────────────┴────────────────────┐
         ↓                                          ↓
(Chapter 3)                               (Chapter 4)
┌─────────────────────────┐     ┌─────────────────────────┐
│ A panchromatic electro- │     │ N-methylphenothiazine    │
│ chromic device composed │     │ derived ionic            │
│ of Ru(II)/Fe(II)-       │     │ liquid as redox couple   │
│ based heterometallo-     │     │ with phenyl              │
│ supramolecular polymer   │     │ viologen for ECD         │
│ and Prussian blue        │     │                          │
└─────────────────────────┘     └─────────────────────────┘
         └────────────────────┬────────────────────┘
                              │
(Chapter 5)                   ↓
        ┌───────────────────────────────┐
        │   Conclusions & suggestions    │
        └───────────────────────────────┘
```

Fig. 1-14 Framework of this thesis.

Chapter 2

Experimental Procedure

In Chapter 2, the experimental details in this thesis will be discussed carefully. Separately, the general experimental procedure will be introduced firstly in section 2.1, and the details about chapter 3 and chapter 4 will be discussed in section 2.2 and 2.3, respectively.

2.1 General experimental details

2.1.1 Materials

Sodium ferrocyanide (Na$_4$Fe(CN)$_6$, >99%), Iron(II) acetate (Fe(OAc)$_2$, >99.99%), 4',4''''-(1,4-Phenylene)bis(2,2':6',2''-terpyridine) (L$_0$), 10-methylphenothiazine (98%), lithium perchlorate (>98%), 1-Butylimidazole (98%), 1, 4-dibromobutane (99%), propylene carbonate (PC, 99.7%), ethylene glycol (EG), methanol (MeOH), acetone (>99%), tetrahydrofuran (THF), dichlorobenzene, dichloromethane (DCM), toluene, ethyl acetate (EA), hexane(Hex), N,N-dimethylformamide (DMF) were all purchased from Sigma-Aldrich; cis-tetrakis(dimethylsulfoxide)-dichlororuthenium(II) (RuCl$_2$(DMSO)$_4$, 98%) was purchased from Strem Chemicals, Inc.; anhydrous sodium perchlorate (NaClO$_4$) was purchased from Wako; 4-Hydroxydiphenylamine (>95%), methyl methacrylate poymer (PMMA), iodine were purchased from Tokyo Chemical Industry (TCI); iron(III) nitrate (Fe(NO$_3$)$_3$) was purchased from Nacalai Tesque, Inc.; sulfur powder (99.5%) was purchased from Alfa Asear. All chemicals were used as received without further purification.

Throughout this thesis, ITO-coated glass (ITO glass, Solaronix SA, R$_{sh}$ = 7 Ω/sq.) was utilized as a substrate for ECD owing to its desirable conductivity and transparency. To start with, the purchased ITO glasses would be cut into 3.0 x 4.0 cm^2 small pieces. After that, they were ultrasonically cleaned in a sonciator by isopropanol, acetone and DIW for 15 min respectively and then dried in a N$_2$ flow. The active area of the ITO glasses for three-electrode system were controlled at 2.0 x 2.0 cm^2.

2.1.2 Apparatus

A potentiostat/galvanostat was used for electrochemical experiments on an ALS/CHI model 612B electrochemical workstation (CH Instruments, Inc.). A conventional three-electrode system was used with the ITO glass as the working electrode, platinum wire as the counter electrode, and a homemade Ag/Ag$^+$ electrode in ACN with 0.1 M TBAP and 0.01 M AgNO$_3$ as the reference electrode. Spectroelectrochemical measurement was carried out by a spectrophotometer (Shimadzu UV-3600). CIE (Commission Internationale de l'Eclairage) coordinates of the devices were acquired by using the same spectrophotometer (Shimadzu UV-3600). All electrochemical measurements of ECDs were obtained under two electrode system configuration.

2.2 Experimental detail related to Chapter 3

2.2.1 Synthesis of PolyRuFe and preparation of PolyRuFe thin film

PolyRuFe was synthesized according to the previous literature [77]. First, 108.125 mg (0.2 mmole) L$_0$ and 48.45 mg (0.1 mmole) RuCl$_2$(DMSO)$_4$ were mixed and stirred at 150 °C in the 25 ml nitrogen-saturated absolute ethylene glycol (EG) for 24 hr. After that, 17.4 mg (0.1 mmole) Fe(OAc)$_2$ dissolved in EG was added to the reaction mixture and stirred at 100 °C in the nitrogen-saturated condition for 24 hr. After the reaction, the solution was cooled down to the room temperature and then THF was added in the solution until it turns colorless. The precipitated polymers were collected by filtration and washed two times by THF, and then dried under vacuum overnight to obtain the PolyRuFe in around 90% yields. The PolyRuFe film was prepared by spin-coating 100 μl of the polymer solution (4 mg/ml in methanol) at 40 rpm for 5 min and finally dried at 50 °C for 30 min.

2.2.2 Synthesis of PB nanoparticles preparation of PB thin film

For water-dispersible PB nanoparticles, 3.23 g Fe(NO$_3$)$_3$·9H$_2$O were mixed with 2.90 g Na$_4$Fe(CN)$_6$·10H$_2$O in 45 ml deionized water (DIW) [78]. The obtained precipitate was centrifuged at 4000 rpm for 6 times to remove the residual reactants, and then 0.542 g Na$_4$Fe(CN)$_6$·10H$_2$O was added into the mixed solution as surface modifier and stirred for 3 days. After that, water-dispersible

PB nanoparticles were obtained by removing DIW by rotary evaporator. The PB thin film was obtained also by spin-coating 80 µl of the uniformly dispersible aqueous solution (100 mg/ml) at 4000 rpm for 30 s, and then heated at 90 °C for 30 min.
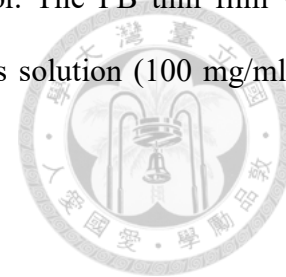
2.2.3 Preparation of PolyRuFe-MWCNT thin film

First, 0.5 mg MWCNT was dispersed in the 1 ml methanol uniformly, and then 4 mg PolyRuFe was added in the mixing solvent. The PolyRuFe-MWCNT film was prepared by spin-coating 100 µl of the polymer solution with MWCNT at 40 rpm for 5 min and finally dried at 50 °C for 30 min.

2.2.4 Cell assembly

All PolyRuFe and PB thin films were pretreated by cyclic voltammetry (CV) in a three-electrode system before assembling the ECD. The charge density of thin films was optimized for fabricating a complementary ECD with the maximum transmittance change. The gel-typed electrolyte was prepared by stirring the NaClO$_4$, PMMA, PC and acetone with the ratio of 3:7:20:70 for 8 hr. The PolyRuFe/PB ECD was obtained by gel-typed electrolyte sandwiching between two films. The cell gap of 60 µm was controlled by one layer of DuPont Surlyn. For subsequent research, the PolyRuFe coated ITO electrode was used as working electrode in a two-electrode system.

2.3 Experimental detail related to Chapter 4

2.3.1 Synthesis of NMP-IL

As a major studied target in this chapter 4, we synthesized the novel EC material, NMP-IL, by serial reactions. Fig. 2-1 shows the structures and synthesis route of each intermediates and final product. Each step of reactions were referred in literatures while the details were optimized by ourselves [79-85]. TLC analysis was used in each reaction except ion exchange reaction to confirm whether the reactants ran out and how many products generated. The detail of each synthesis steps will be be discussed carefully at following section.
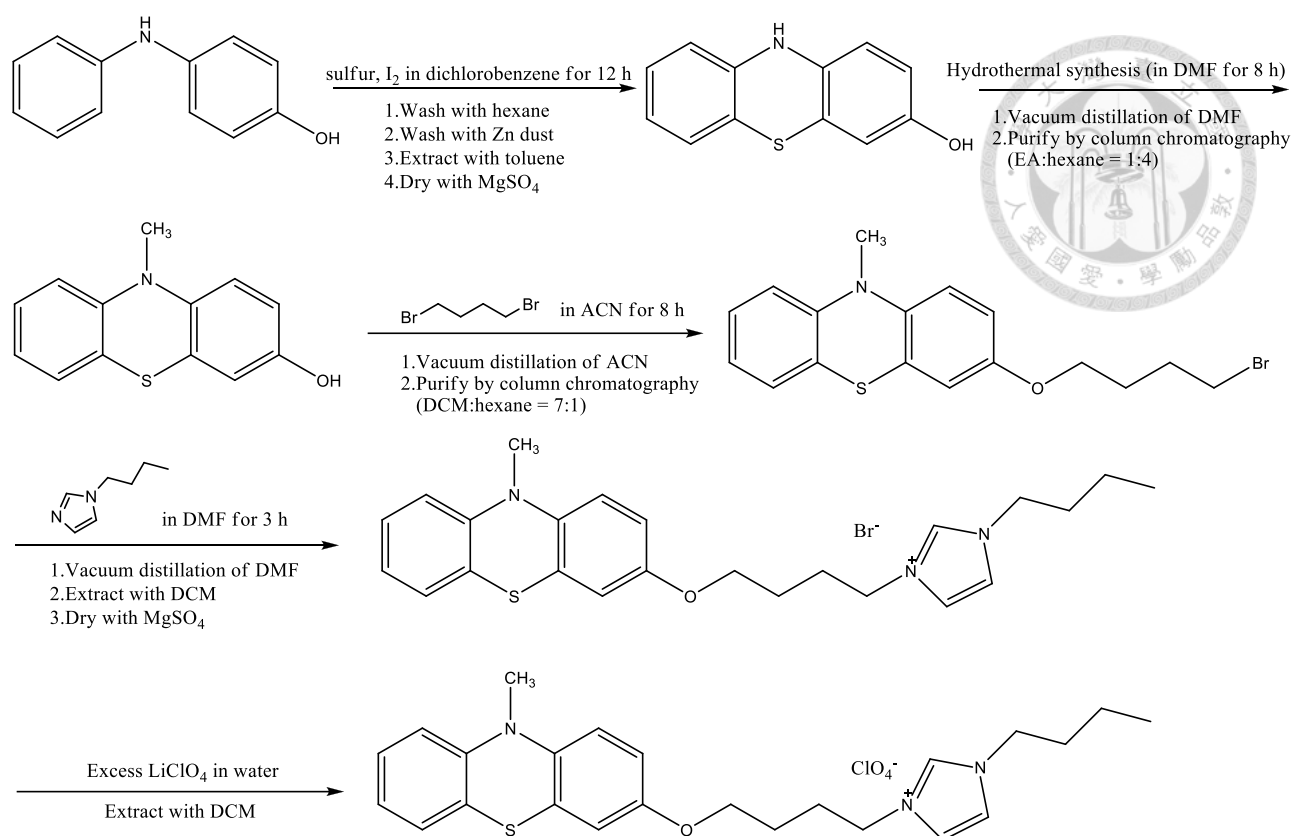
Fig. 2-1 The serial synthesis steps of NMP-IL.

2.3.1.1 Synthesis of 10H-phenothiazine-3-ol (HMP-OH)

The HMP-OH was prepared by thionation of the substituted 4-hydroxydiphenylamine according to the following method [80]. A mixture of the substituted 4-hydroxydiphenylamine (0.01 mole), sulfur (0.02 mole), and traces amount of iodine was refluxed in 10 ml of 1,2-dichlorobenzene at 145 °C for 12 h. Precipitation of the crude product was obtained, and effected by the addition of hexane to the resulting green-colored viscous mixture. After that, viscous mixture was filtered to remove hexane. The dark precipitate on the filter paper was washed with more hexane, and then washed with zinc dust to remove the extra sulfur. Extraction with toluene left a large residue, which was found to be charred matter. The yellow solid of HMP-OH was obtained on evaporation of the toluene extract. The yield of HMP-OH is 90%.
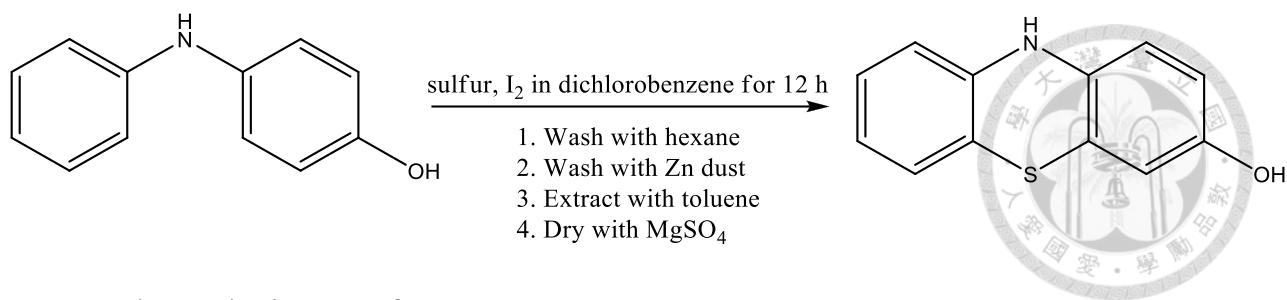
Fig. 2-2 The synthesis steps of HMP-OH.

2.3.1.2 Synthesis of 10-methylphenothiazine-3-ol (NMP-OH)

The NMP-OH was prepared by methylation of the substituted HNP-OH. However, there are secondary amine and hydroxyl group on the HMP-OH, methylation reaction was definitely going upon both functional groups no matter which base and solvent was used. Compared to other literatures [81-82], we didn't use the base as initiator to avoid the methylation reaction occurring on the hydroxyl group. HMP-OH (0.15 mmole), CH_3I (0.9 mmole), which excess six time of HMP-OH for reacting completely, and 20 ml of DMF in bomb reactor at 90 °C for 8 h. Furthermore, compared to DMSO, DMF is an ideal solvent for this reaction, resulting the less needless product. After reaction finished, DMF was removed by vacuum distillation and left crude residue. The residue was purified by column chromatography on silica gel by eluting with ethyl acetate (EA) and hexane to provide NMP-OH. Because the structure of target product, NMP-OH, is similar than the structures of other needless product, it is difficult to separate pure NMP-OH from others on silica gel by eluting with EA and hexane only. The pure beige solid, NMP-OH, can be obtained using column chromatography on silica gel again by eluting with DCM and hexane (DCM:hexane=10:1). By hydrothermal reaction, the yield of NMP-OH increase to 68% from ca 30% while adding base in the reaction.
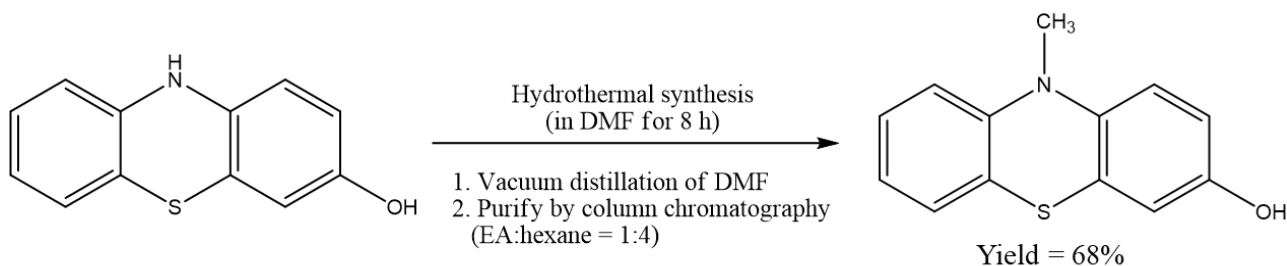
Fig. 2-3 The synthesis steps of NMP-OH.

2.3.1.3 Synthesis of 3-(4-bromobutoxy)-10-methylphenothiazine (NMP-Br)

The NMP-Br was prepared by substitution reaction according to the following method [83-84]. A solution of 5 mmol 1, 4-dibromobutane in ACN was added dropwise to a stirred mixture of 1 mmol NMP-OH and 3 mmol K_2CO_3 in ACN at 85 °C for 8 h. After reaction finished, which checked by TLC analysis, ACN was evaporatered and the mixture was obtained. The mixture was purified by column chromatography on silica gel by eluting with DCM and hexane to provide white solid, NMP-Br.
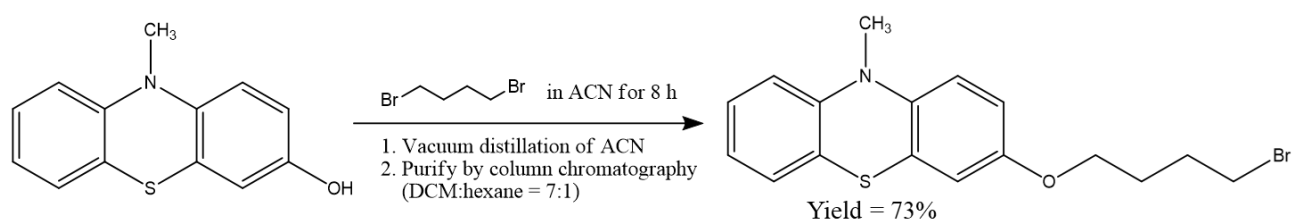
Fig. 2-4 The synthesis steps of NMP-Br.

2.3.1.4 Synthesis of 1-butyl-3-(4-(10-methylphenothiazin-3-yloxy)butyl)-imidazol-3-ium bromide (NMP-IL-Br)

The NMP-Br was prepared by ionization reaction [84]. The equivalent of NMP-Br and 1-butylimidazole were reacted in the DMF at 150 °C for 3 h. After that, DMF were removed by vacuum distillation and the black viscous residue was obtained, NMP-IL-Br. For this reaction, the temperature plays a crucial role. We tried to use toluene or ACN as solvent during reaction; nevertheless, the lower temperature could not induce the reaction owing to the larger functional group of NMP. For this reason, DMF is the better choice as reaction solvent having chemical stability and higher boiling point.
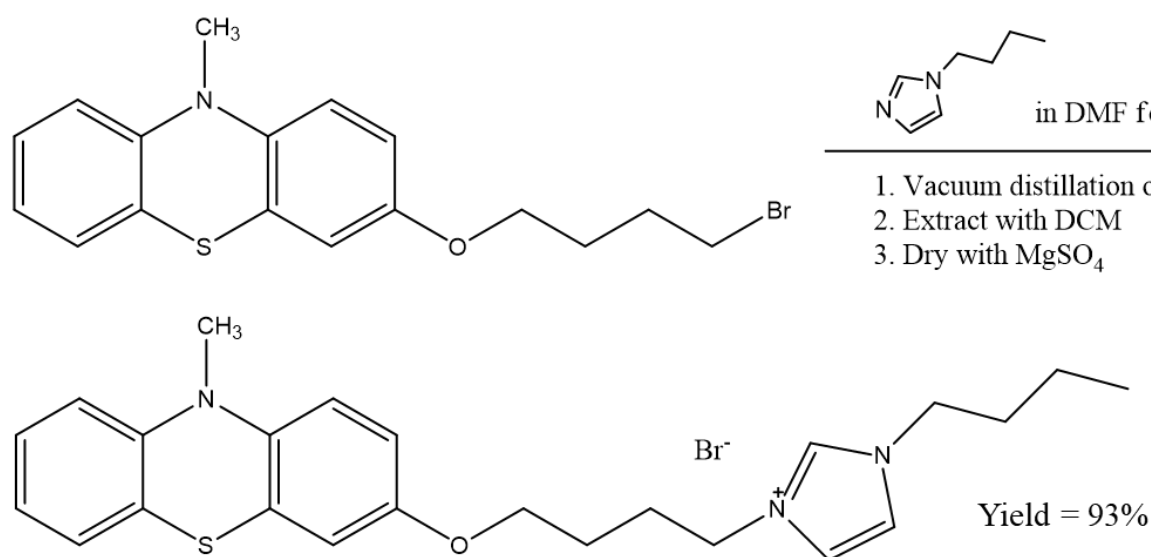
Fig. 2-5 The synthesis steps of NMP-IL-Br.

2.3.1.5 Synthesis of 1-butyl-3-(4-(10-methylphenothiazin-3-yloxy)butyl)-imidazol-3-ium perchlorate (NMP-IL)

The last step in the synthesis involved an anion exchange form bromide to chlorate because the better solubility of chlorate anion in organic solvent [85]. A solution of NMP-IL-Br in water was added excess LiClO₄, and the mixture was stirred at room temperature for 3 h. The dark precipitate could be observed during reaction. After that, extracted with DCM and DIW, and removed DCM getting the pure NMP-IL.
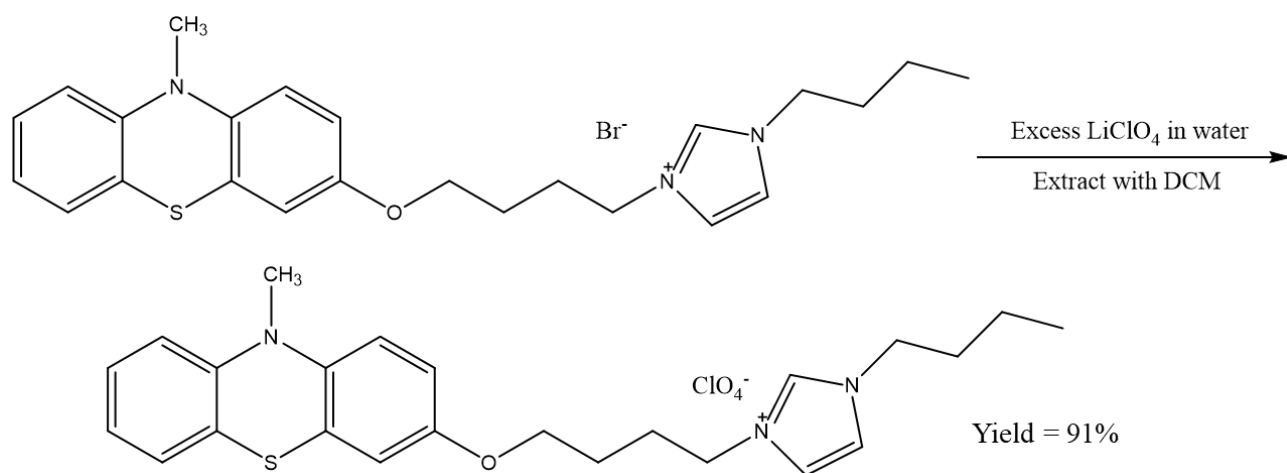
Fig. 2-6 The synthesis steps of NMP-IL.

2.3.2 Preparation of PV (PV(BF₄)₂)

1.54 mmol PVCl₂ was dissolved in 1 mL DIW and 18.85 mmol NaBF₄ was dissolved in 4 mL DIW. The aqueous solution was then mixed in ice bath, and the mixture was centrifuged at 13,000 rpm for 30 min. After that, the precipitate was further washed by DIW for 3 times. Finally, the beige PV(BF₄)₂ powder was collected by drying in vacuum for 24 hours.

2.3.3 Cell assembly

All-in-one EC materials and supporting electrolyte containing 0.03 M NMP-IL, 0.03 M PV and 0.1 M TBABF₄ in PC was sandwiched between ITO substrates. The 60 μm cell gap was controlled by one layer of DuPont Surlyn.

Chapter 3

A Panchromatic Electrochromic Device Composed of Ru(II)/Fe(II)-Based Heterometallo-supramolecular Polymer and Prussian Blue

3.1 Introduction

Among all electrochromic materials, metallo-supramolecular polymers draw much attention due to their promising electrochromism as inorganic-organic hybrid materials. The polymers show various colors and impressive optical properties owing to metal-to-ligand charge transfer (MLCT) absorption and intervalence charge transfer (IVCT), which are triggered by the electrochemical redox reaction of the metal ions [86]. Recently, terpyridine ligands are most commonly used because of their rich coordination chemistry, thermal stability, and high binding affinity towards transition metal ions [87], including Fe(II), Ru(II), Co(II), and other transition metals, which have proved to play a key role in the MEPEs based on d-d* transition or MLCT absorbance [88-90]. Through different ligands and corresponding metal ions combination, new polymers, which exhibit unique electrochromism, can be created [91]. Furthermore, the multi-color characteristic could be observed for the polymers, which utilize different kinds of ligands or consist of two metal ion species [92-93].

Meanwhile, many researchers aim at developing black-to-transmissive ECD recently for a growing demand of novel displays, which are energy-efficient simultaneously like e-paper or e-book. However, it is a challenging task to achieve high optical change over the entire visible wavelength, and only a few materials have been successfully demonstrated. For examples, Beaujuge et al. reported on the use of the donor–acceptor approach to make a black-to-transmissive polymer thin film [17]. Hsu et al. proposed the Co(II)-based metallo-supramolecular polymer (PolyCo) which showed the black-to-transmissive electrochromism [94]. In addition, some ECDs have been fabricated with easy to show panchromatic optical change by using multiple EC materials [95-98]. MEPEs draw much attention for high optical contrast, fast response time, and outstanding stability [89]; however, scarcely any of researchers fabricated the ECD which exhibits the panchromatic characteristic based on MEPEs.

Herein, we demonstrate the panchromatic ECD composed of Ru(II)/Fe(II)-based heterometallo-

supramolecular polymer (PolyRuFe) and Prussian blue (PB, Iron(III) hexacyanoferrate(II)), for PB provides the strong absorbance from 600nm to 800nm, and PolyRuFe provides the large optical change from 400 nm to 600 nm. Moreover, anodically coloring PB is selected as counter electrode in this study owing to it is a well-known inorganic material for fairly good stability and large optical change [99-100]. In general, it is operated between two states, one is Prussian blue state (oxidized form) the other is colorless Everitt's salt (ES) (reduced form) and it can be cycled reversibly for more than thousands times in whether aqueous or non-aqueous solvents [78]. Meanwhile, to tackle the leakage problem in a solution-typed electrolyte, the ECD utilize gel-typed electrolyte based on poly-(methyl methacrylate) (PMMA), it leads to safety and better stability of the ECD. It is expected that an ECD exhibits panchromatic absorbance change, fast response time and well cycling stability.

3.2 Results and discussion

3.2.1 Characterization of PolyRuFe in a three electrode system

3.2.1.1 CV of PolyRuFe in a three-electrode system

A cyclic voltammorgram (CV) of PolyRuFe performed in a three-electrode system is shown in Fig. 3-1. Upon the variation of the potential bias, the current density dropped or increased significantly at certain potential, indicating the happen of two redox reactions. The first redox couple at 0.77 and 0.70 V (*vs*. Ag/Ag$^+$) could be attributed to the redox reaction between metal ions Fe(II) and Fe(III). The second redox couple at 0.93 and 0.84 V (*vs*. Ag/Ag$^+$) could be described to the redox reaction between Ru(II) and Ru(III). Furthermore, according to previous literature of PolyCo [94], we proposed the mechanism as Eqs. (3-1) and (3-2) attributed to the redox of Fe(II) and Ru(II), respectively.

$$[(PolyRu(II)Fe(II)]_n \cdot (4n)ClO_4^- + nClO_4^- \leftrightarrow [(PolyRu(II)Fe(III)]_n \cdot (5n)ClO_4^- + ne^- \qquad (3\text{-}1)$$
$$\qquad \text{(purple)} \qquad\qquad\qquad\qquad \text{(orange)}$$

$$[(PolyRu(II)Fe(III)]_n \cdot (5n)ClO_4^- + nClO_4^- \leftrightarrow [(PolyRu(III)Fe(III)]_n \cdot (6n)ClO_4^- + ne^- \qquad (3\text{-}2)$$
$$\qquad \text{(orange)} \qquad\qquad\qquad\qquad \text{(light green)}$$
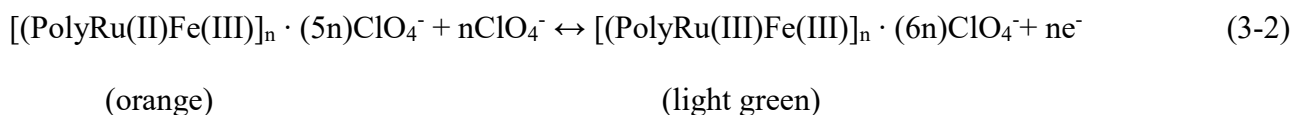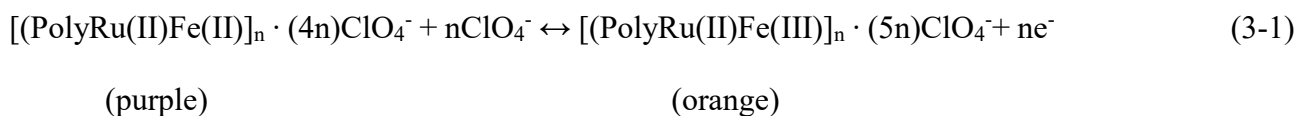
At the time when the potential bias was larger the peak potential at 0.77 V, the PolyFe(II)Ru(II) would be oxidized to PolyFe(III)Ru(II), leading a color variation from purple to orange. The color change from orange to light green when switching to 0.93 V attributed to the oxidation of PolyFe(III)Ru(II), forming PolyFe(III)Ru(III).
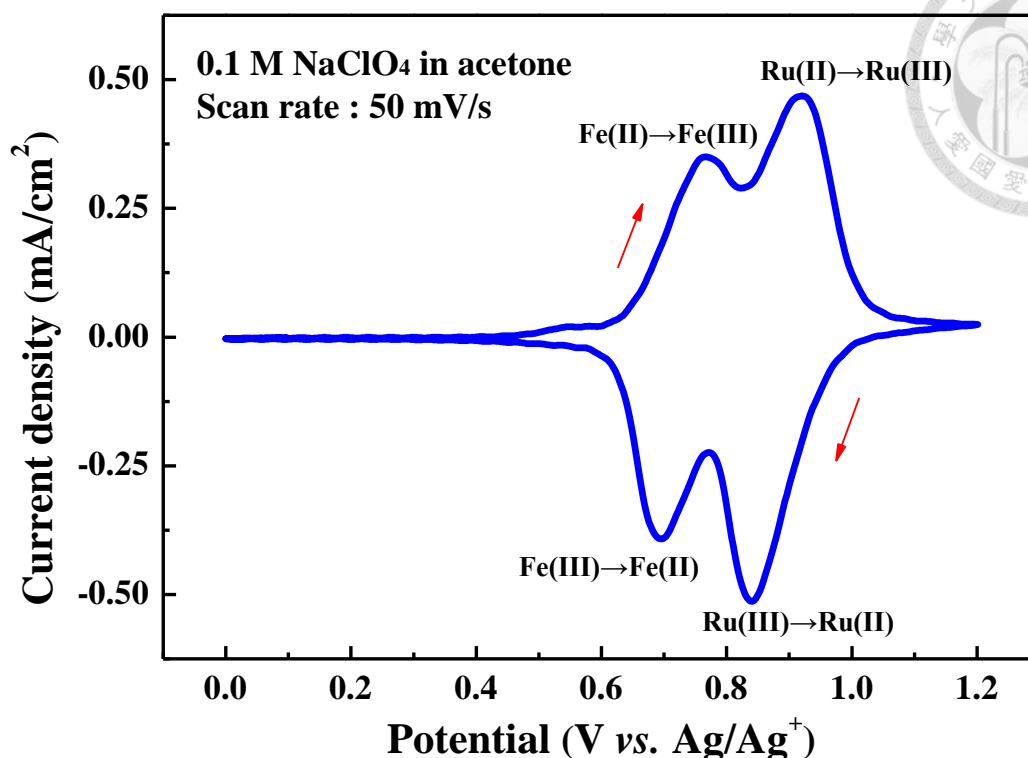
Fig. 3-1 CV of PolyRuFe and 0.1 M NaClO$_4$ in acetone at a scan rate of 50 mV/s in a three-electrode system.

3.2.1.2 UV-Vis absorbance spectra of PolyRuFe in a three electrode system

The absorbance spectra with various applied potential bias are shown in Fig. 3-2. Two significantly optical changes occurred with the peaks at 503 nm and 580 nm when the applied potential bias arrived at 1.2 V (*vs*. Ag/Ag$^+$). PolyRuFe is synthesized with the equimolar ratio of Fe(II) and Ru(II); however, the absorbance of Ru(II) complex portion at 503 nm is much stronger than that of the Fe(II) complex portion at 580 nm. It is attributed to the larger absorption coefficient (ε) value of Ru(II)-based MEPE (PolyRu) than that of Fe(II)-based MEPE (PolyFe). According to the previous literatures, the reason is that stronger π-conjugated of ligand (L$_0$) to the Ru(II) metal ions than to F(II) metal ions and a stronger dynamic chelate effect of Ru(II) metal ion to ligand (L$_0$) compared to that of Fe(II) [101].
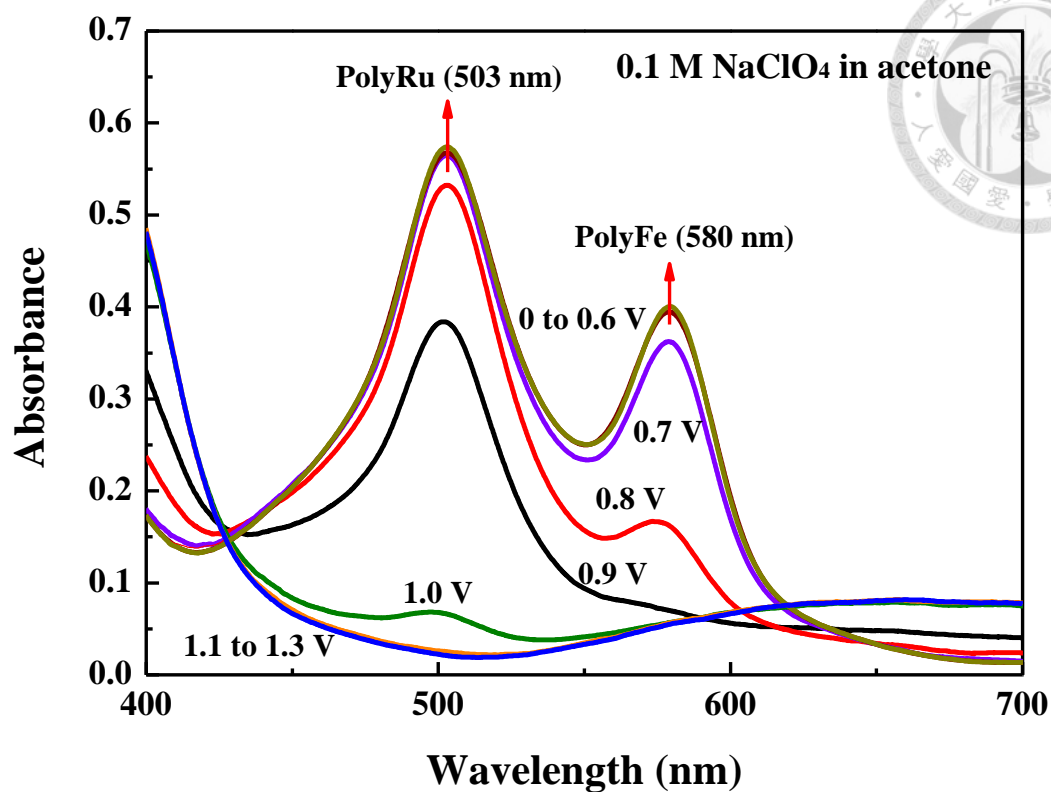
Fig. 3-2 UV-Vis absorbance spectra of PolyRuFe with maximum absorbance in acetone.

3.2.1.3 Image of PolyRuFe at 0, 0.9 and 1.2 V (*vs.* Ag/Ag$^+$)

The images of PolyRuFe at 1.2 V (bleaching state), 0.9 V and 0 V (coloring state) in three electrode system are shown in Fig. 3-3, it shows the multi-color characteristic, the light green, orange and dark purple color could be observed at 1.2, 0.9 and 0 V, respectively.

Fig. 3-3 Images of PolyRuFe at 1.2 V (bleaching state), 0.9 V and 0 V (coloring state) in three electrode system (*vs.* Ag/Ag$^+$).

3.2.1.4 Dynamic transmittance responses at 503 and 580 nm for PolyRuFe

Fig. 3-4 shows the dynamic transmittance responses at 503 and 580 nm for PolyRuFe with a potential bias stepped between 1.3 V (bleaching) and 0 V (coloring) with 10 s interval. The measured values of T_b, T_c, ΔT, t_b and t_c are summarized in Table 3-1. As demonstrated, PolyRuFe thin film exhibits a large ΔT of 68.8% and 58.7% at 503 and 580 nm respectively. The coloring and bleaching responses shorter than 1 s could be observed at each wavelength. To verify the above results, which is measured from optical contrast, the formula of diffusivity in kinetics shown in Eqn. 3-3 was utilized, where t_d is the diffusion time (s), l is the diffusion distance (cm), and D is the diffusivity of ions.

$$t_d = \frac{l^2}{D} \tag{3-3}$$

As mentioned before, the ClO_4^- ions would adsorb and desorb from the PolyRuFe film during oxidation and reduction of PolyRuFe, respectively. To estimate the diffusion time of ClO_4^- in PolyRuFe thin film, diffusion distance was set as the thickness of PolyRuFe thin film, which around 200~300 nm; the diffusivity of ClO_4^- ions in the film, D, was set as 10^{-9} cm^2/s, which was the ca. values of ions diffusion in the thin film. The t_d was calculated as 0.4~0.9 s, which is close to the values of tb and tc. Consequently, the dynamic of ClO_4^- diffusion can give evidence of the response time of optical contrast.
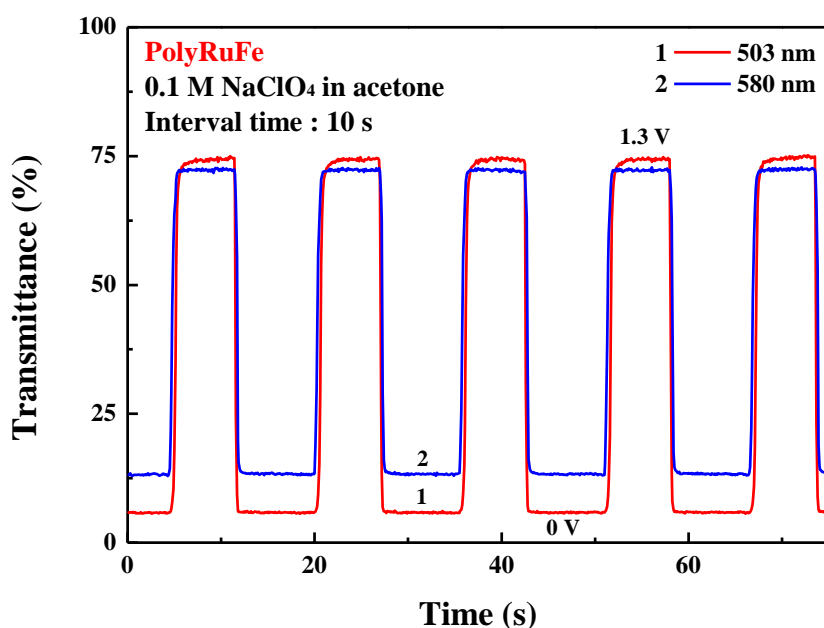
Fig. 3-4 Dynamic transmittance responses at 403 and 580 nm for PolyRuFe performed with a

potential step between 0 and 1.3 V.

Table 3-1 Dynamic transmittance response of the PolyRuFe.

λ_{max} (nm)	T_b (%)	T_c (%)	ΔT (%)	t_b (s)	t_c (s)
503	74.7	5.9	68.8	0.3	0.9
580	72.1	13.4	58.7	0.8	0.5

4.2.1.5 Long-term stability of PolyRuFe in a three electrode system

The long-term stability of the PolyRuFe based on their write-erase ability were investigated by stepping the PolyRuFe between 0 V (coloring state) and 1.3 V (bleaching state) with an interval time of 10 s for both coloring and bleaching processes. Dynamic transmittance response cycled for 1000 cycles between coloring and bleaching state at 503 and 580 nm are shown in Fig. 3-5 and Fig. 3-6, respectively. To qualify the long-term stability, the remained ΔT after n cycles (ΔT_n) of PolyRuFe are collected in Table 3-2.

As shown in Fig. 3-5 and Fig. 3-6, good stability that remained around 95% after 1000 cycles could be observed for PolyRuFe at both 503 and 580 nm, indicating the quite high redox reversibility of PolyRuFe compared to the normal conducting polymers and metal oxides. It is explained that the EC mechanism is different with the other organic or inorganic EC material. The main driving force to cause the strong color changes is according to the intensity of MLCT, which increases or decreases by the redox reaction of the centre metal ions.

Table 3-2 Dynamic transmittance response of the PolyRuFe.

λ_{max} (nm)	ΔT (%)	ΔT_{500} (%) / Retention (%)	ΔT_{1000} (%) / Retention (%)
503	68.8	68.1 / 99.0	64.7 / 94.0
580	59.6	59.5 / 99.8	58.4 / 98.0
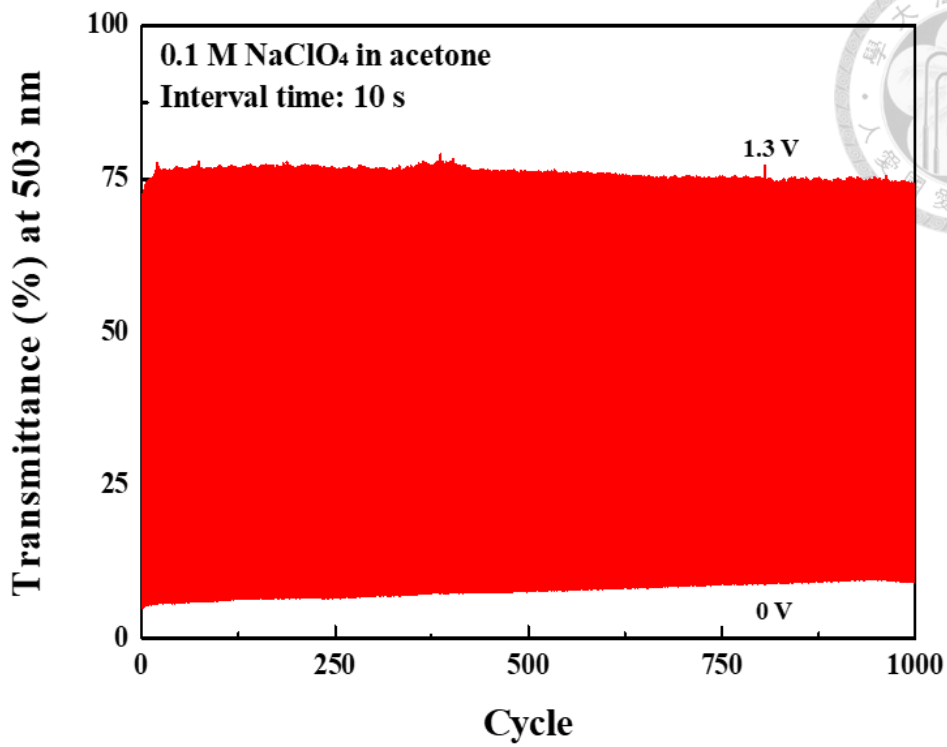
Fig. 3-5 Long-term stability of PolyRuFe at 503 nm.
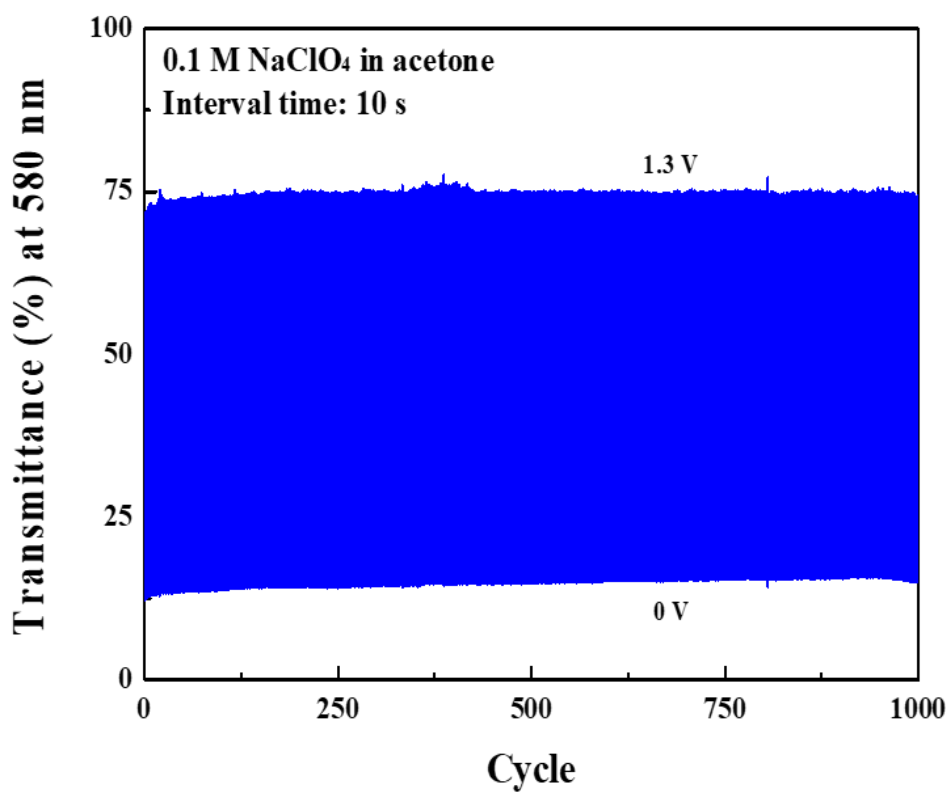
Fig. 3-6 Long-term stability of PolyRuFe at 580 nm.

36

3.2.2 Characterization of PB in a three electrode system (*vs*. Ag/Ag$^+$)

3.2.2.1 CV of PB

A CV of PB performed in a three-electrode system is shown in Fig. 3-7. The redox couple could be attributed to the following reaction, presented in Eq. (3-3):

$$Na_4Fe(II)_4[Fe(II)CN_6] \quad \leftrightarrow \quad Fe(III)_4[Fe(II)CN_6] + 4e^- + 4Na^+ \qquad (3-4)$$

$$\text{(ES, colorless)} \qquad\qquad \text{(PB, blue)}$$
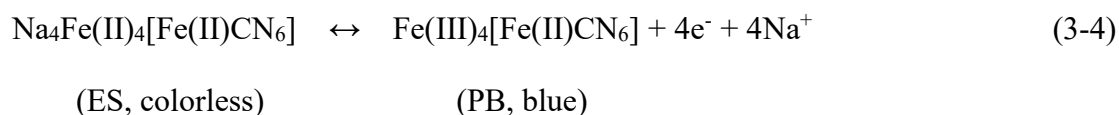
It shows the cycled reversible stability in acetone and the upper applied oxidative potential is controlled at 0.3 V to avoid the appearance of the second redox peak, forming the Berlin Green.
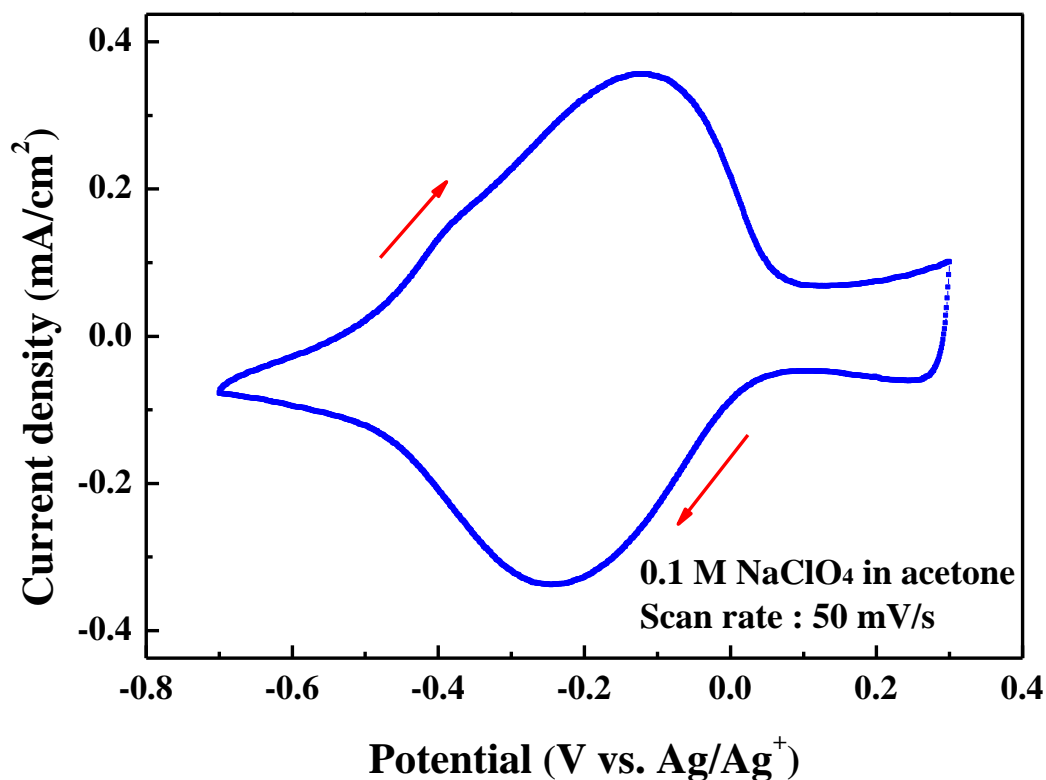
Fig. 3-7 CV of PB in acetone at a scan rate of 50 mV/s in a three-electrode system.

3.2.2.2 UV-Vis absorbance spectra of PB

The absorbance spectra of PB with various applied potential bias are shown in Fig. 3-8. When negative potential more than -0.4 V is applied, high transparency was observed. When the applied potential bias reached to 0.3 V, a strong absorbance spanned from 600 nm to 1000 nm is noticed and the maximum absorbance peak locates at 690 nm. It is expected that an ECD composed of PolyRuFe and PB would exhibit panchromatic characteristic.
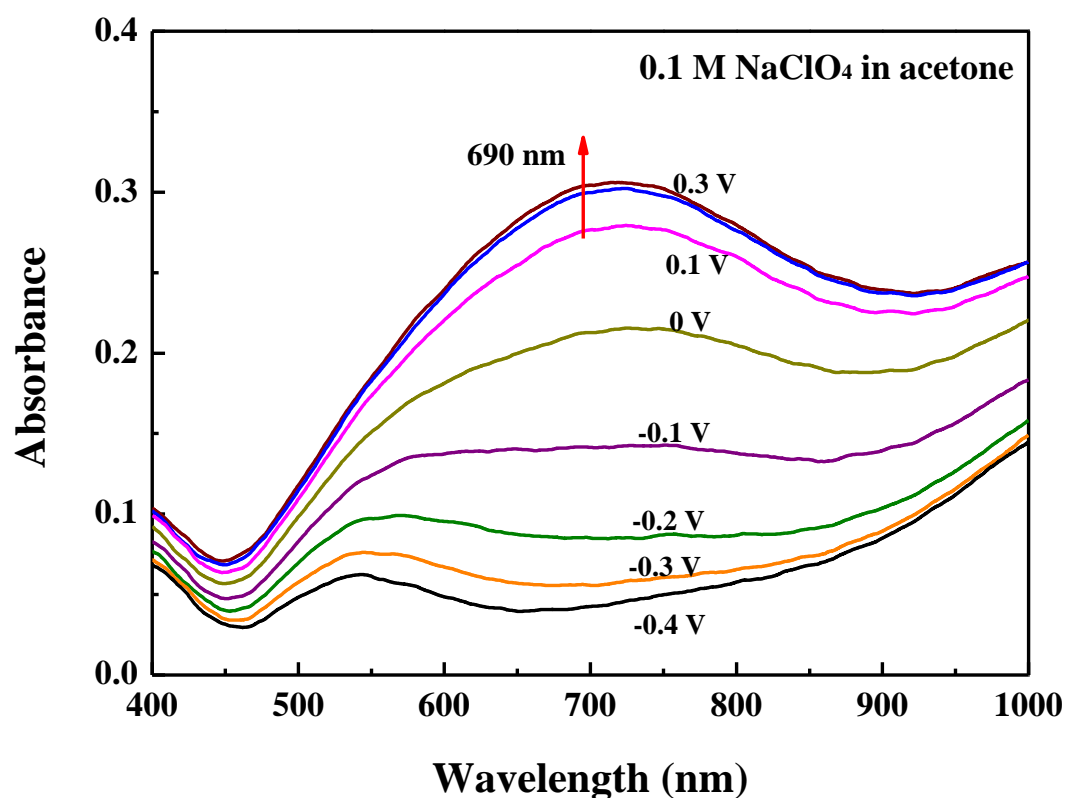
Fig. 3-8 UV-Vis absorbance spectra of PB at various potential biases from -0.4 to 0.3 V.

3.2.3 Characterization of PolyRuFe/PB ECD

3.2.3.1 CV of PolyRuFe/PB ECD

Further, we fabricated a PolyRuFe/PB ECD. A CV of the ECD is presented in Fig. 3-9 and three redox peaks could be observed. These two redox couples (a1, c1 and a2, c2) could be described to the redox reaction of PolyRuFe and PB. As shown, the peak separation of these two redox peaks are similar as PolyRuFe thin film, implying the PB is an ideal counter electrode for the MEPE system. We proposed the mechanism Eq. (3-4) of the PolyRuFe/PB ECD by combination of Eqs. (3-1), (3-2) and (3-3), as follow:

$$[(PolyRu(II)Fe(II)(ClO_4^-)_4]_n + (n/2)Fe(III)_4[Fe(lI)(CN)_6]_3 + 2nNa^+ + 2nClO_4^-$$

(near black)

$$\leftrightarrow$$

$$[(PolyRu(III)Fe(III)(ClO_4^-)_4]_n + (n/2)Na_4Fe(II)_4[Fe(II)(CN)_6]_3 \qquad (3-5)$$
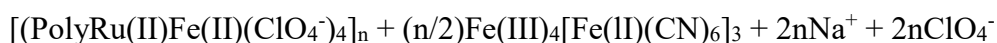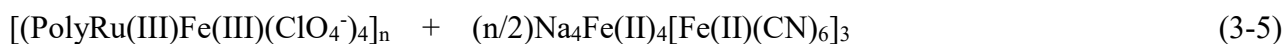
(light green)

Nevertheless, it is still observed the third redox couple (a3, c3) in the CV measurement. This could be attributed to the side reaction of PB due to the mismatch charge density of the PolyRuFe and PB. Owing to the quite small charge density of PolyRuFe, it cannot provide sufficient charge to lead PB redox completely even though PB film is very thin. Thus, the wider potential is applied to lead PB redox completely in order to form the uniform color change of the proposed ECD at coloring state.
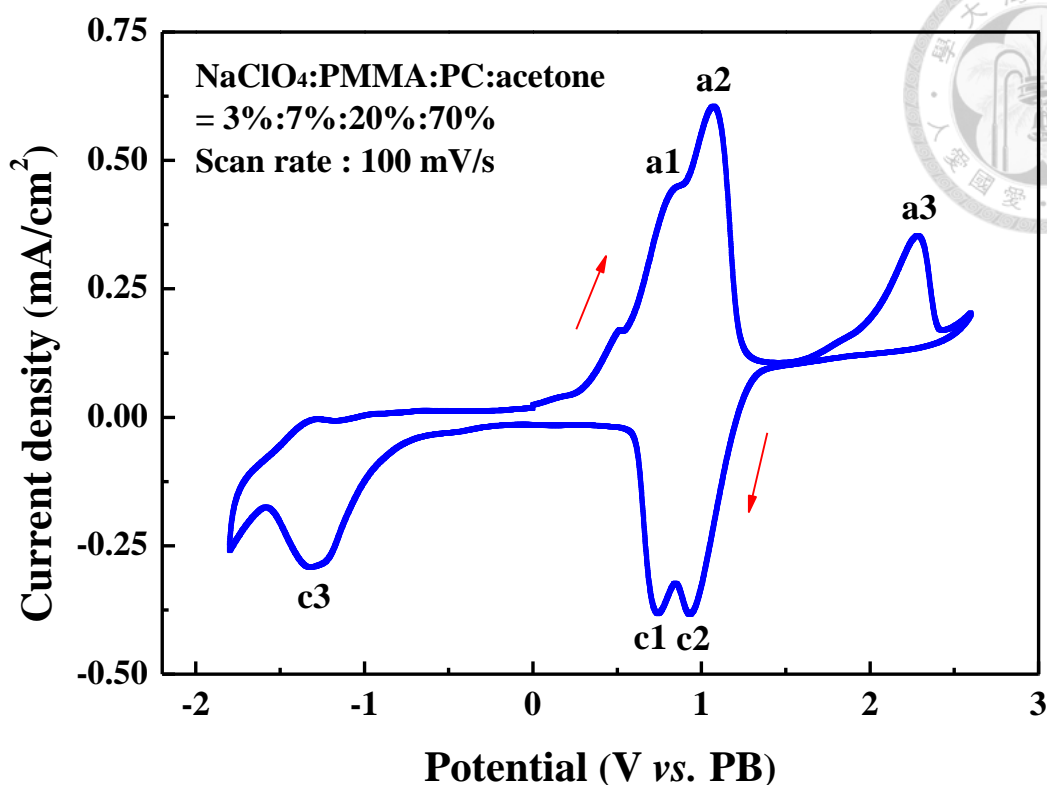
Fig. 3-9 CV of the PolyRuFe/PB ECD with gel-type electrolyte.

3.2.3.2 UV-Vis absorbance spectra of PolyRuFe/PB ECD

In order to investigate electrochromic properties of the PolyRuFe/PB ECD with the gel-typed electrolyte, UV-vis absorbance spectra of the proposed ECD were measured between 2.2 to -1.3 V, shown in Fig. 3-10. The proposed ECD shows panchromatic feature and well absorbance change in the visible region. When the applied negative potential bias reached over 0 V, two obvious peaks at 503 nm and 580 nm could be noticed. The large increment at 503 nm and 580 nm are mainly attributed to the redox reaction of Ru(II) and Fe(II) ions, respectively. Similarly, the high optical change could also be perceived from 600 nm to more than 800 nm, and it is mainly described by the redox of PB. Originally, the absorbance of Ru(II) complex portion at 503 nm is much stronger than that of the Fe(II) complex portion at 580 nm, according to the larger absorption coefficient (ε) value of Ru(II)-based MEPE. It could be noticed that the increment of absorbance change at 580nm due to the overlapping the absorbance of PB. When the applied potential bias is over 1.4 V, the ECD reach to bleaching state; however, the light green is also observed. In order to redox PB completely, the more positive and

negative potential biases of 2.2 and -1.3 V were applied. As shown in Fig. 3-10, when applied the -1.3 V, the larger absorbance increases at 690 nm compared to 503 and 580nm.
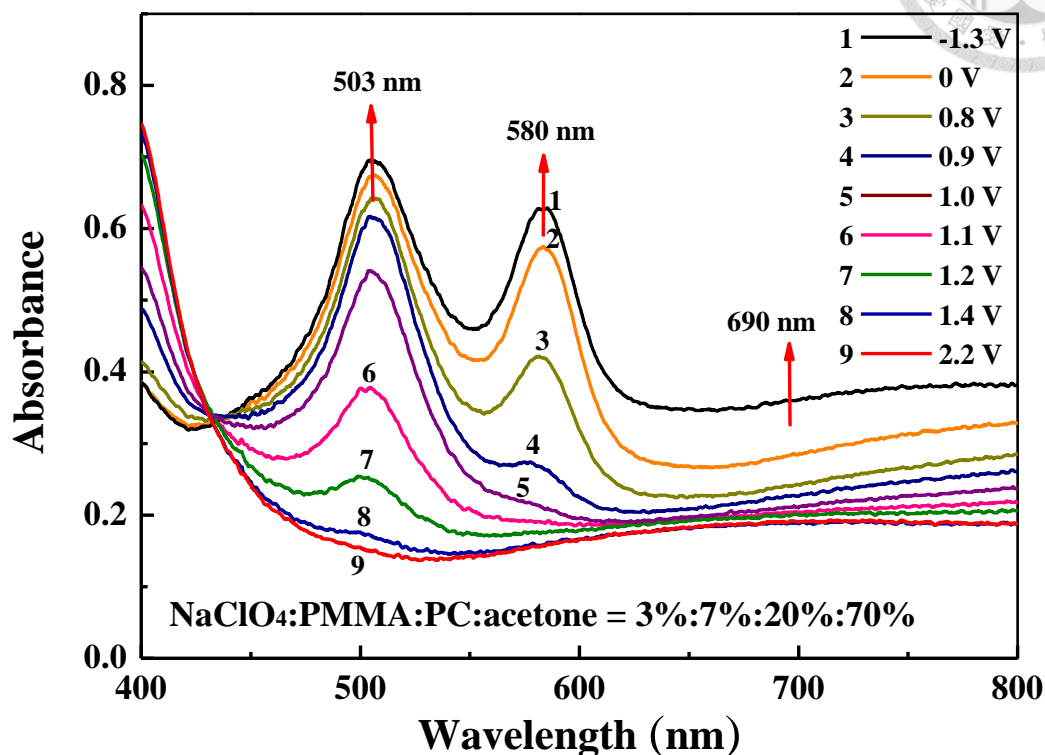
Fig. 3-10 UV-vis absorbance spectra of the PolyRuFe/PB ECD at different potential bias from -1.3 V to 2.2 V.

3.2.3.3 Dynamic transmittance change at 503, 580 and 690 nm of PolyRuFe/PB ECD

The dynamic transmittance curves of the PolyRuFe/PB ECD, which were collected at characteristic absorbance peaks of 503, 580 nm and the absorbance peak of PB at 690 nm, are presented respectively in Fig. 3-11. The bleaching potential and the coloring potential are 2.2 V and -1.3 V, respectively. The data are also summarized in Table 3-3. The highest transmittance change (ΔT) of 52.7% at 503 nm could be observed, according to strong π-conjugated of ligand (L_0) to the Ru(II) metal ions. Moreover, the transmittance change (ΔT) of 46.9% and 28.0% could be observed at 580 nm and 503 nm, respectively. It shows less transmittance change (ΔT) at 690nm owing to the thinner PB film that in order to match the charge-density with a PolyRuFe film. The proposed ECD

at 690 nm exhibits a short response time of less than 4 s. Furthermore, it is remarkable that the quite short response time of less than 0.5 s at 503 nm and 580 nm could be observed for both coloring and bleaching process. The PolyRuFe/PB ECD shows the advantage of ECD based on MEPEs completely.
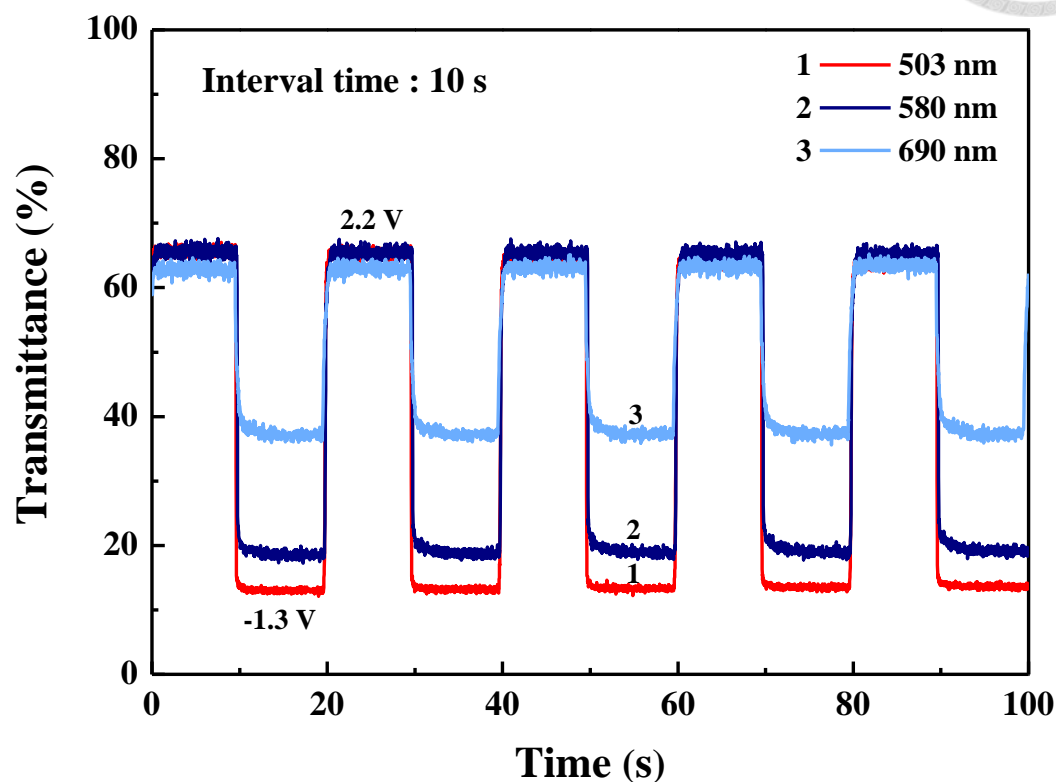
Fig. 3-11 Dynamic transmittance response of the PolyRuFe/PB ECD at 503, 580 and 690 nm.

Table 3-3 Dynamic transmittance response of the PolyRuFe/PB ECD.

λ (nm)	T_b (%)	T_c (%)	ΔT (%)	t_b (s)	t_c (s)
503	66.3	13.6	52.7	0.3	0.2
580	66.2	19.3	46.9	0.5	0.3
690	64.5	36.5	28.0	0.9	3.6

3.2.3.4 Coloration efficiency of PolyRuFe/PB ECD

To investigate the optical density change (ΔOD) and the required driving voltage for the PolyRuFe/PB ECD, the relationship between ΔOD at three different wavelengths and the charge density (Q_d) under various potential bias are presented in Fig. 3-12. The measured charge densities were calculated by integration of the measured current densities against the fixing time (5 s). The coloration efficiency (η) is obtained by Eq. (3-5):

$$\eta = \Delta OD/Q_d \qquad\qquad (3\text{-}6)$$

The coloration efficiencies of the PolyRuFe/PB ECD were calculated to be ca. 525.1, 61.4 and 57.7 cm^2/C at 503 nm; 114.3, 413.6 and 114.7 cm^2/C at 580 nm; 53.6 and 140.9 cm^2/C at 690 nm, corresponding to the portion of Ru(II), Fe(II), and Prussian blue, respectively. The value of coloration efficiency at 503 nm decreased dramatically while that at 503 nm increased at larger potential bias (0.9~2.2 V), which can be attributed to the prior reduce reaction of Ru(II) compared to Fe(II). In Fig. 3-9, the oxidation peak a1 of Fe(II) is on the left compared to the peak a2 of Ru(II), indicating the formal oxidation potential of Ru(II) is higher than Fe(II). In other words, Ru(II) is much easier reduced than Fe(II) so that Ru(II) was reduced first when applying higher range of potential bias (0.9~2.2 V); while major part of Fe(II) was reduced when applying lower range of potential bias (0.6~0.9 V). Finally, the large absorbance change at 690 nm when applied potential bias from 0.6 to -1.3 V and coloration efficiency of PB was collected as 140.9 cm^2/C, which is the largest values, compared to 503 and 580 nm, upon these potential biases. These results lead the three-step values of the coloration efficiency.   Furthermore, the quite large coloration efficiency 525.1 and 413.6 cm^2/C were obtained, respectively, at 503 nm and 580 nm, demonstrating that only a little charge density needed to drive EC reactions.
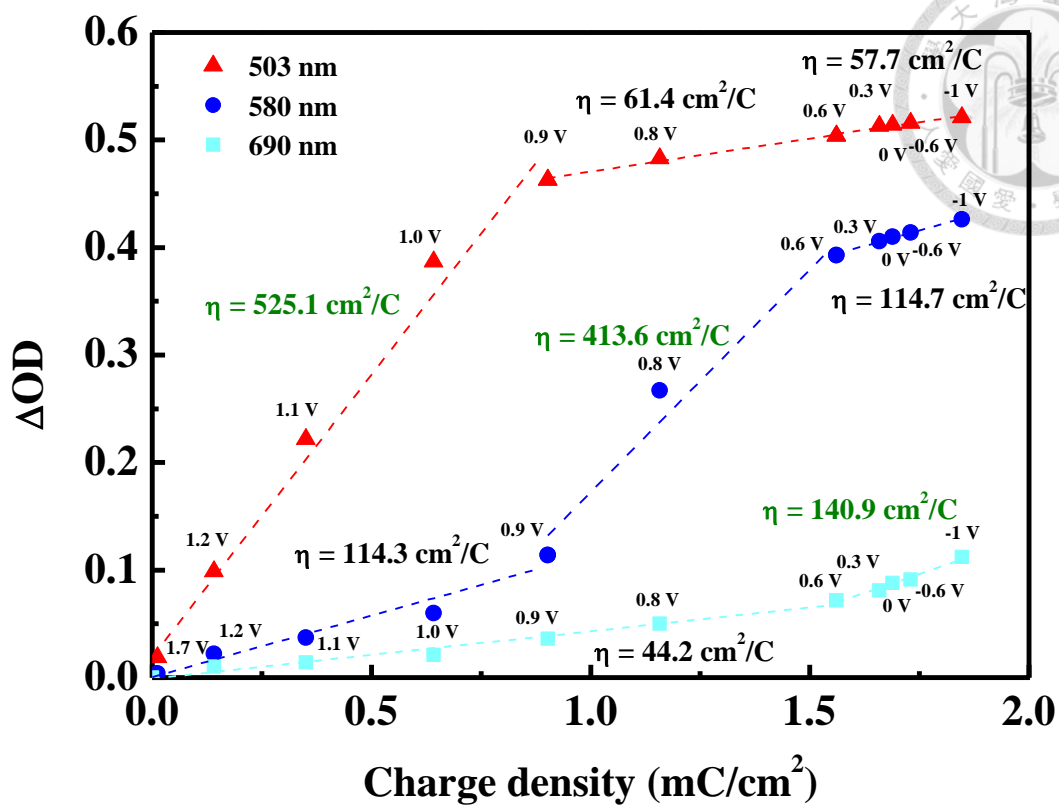
Fig. 3-12 The relationship between the optical change (ΔOD) and the applied charge density with 5 s sampling time of the PolyRuFe/PB ECD at 503, 580 and 690nm.

3.2.3.5 CIE 1973 system of colorimetry for PolyRuFe/PB ECD

To scientifically evaluate the color change of ECD occurring on electrochemical switching, the ECD is subjected to colorimetric analysis by using CIE 1931 system of colorimetry, which is shown in Fig. 3-13. When the device is at bleaching state, the chromaticity coordinates (x=0.3391, y=0.3701). The chromaticity (x=0.3303, y=0.2428) could be observed at the coloring state. The position at coloring state in the chromaticity move toward purple area owing to the much stronger absorbance of PolyRuFe than the absorbance of PB. Further, the images of PolyRuFe ECD at bleaching (2.2 V) and coloring (-1.3 V) states are shown in Fig. 3-14.
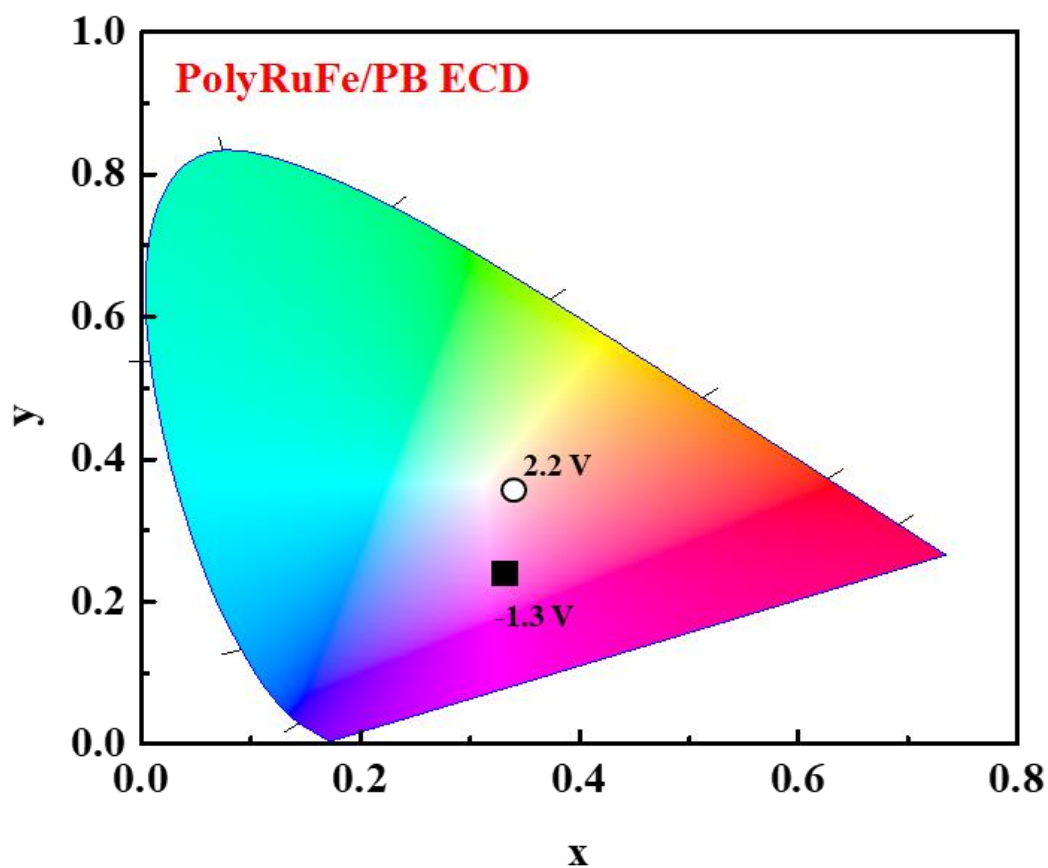
Fig. 3-13 Colorimetry (x-y diagram) of the PolyRuFe/PB ECD at the bleaching state (2.2 V) and coloring state (-1.3 V).
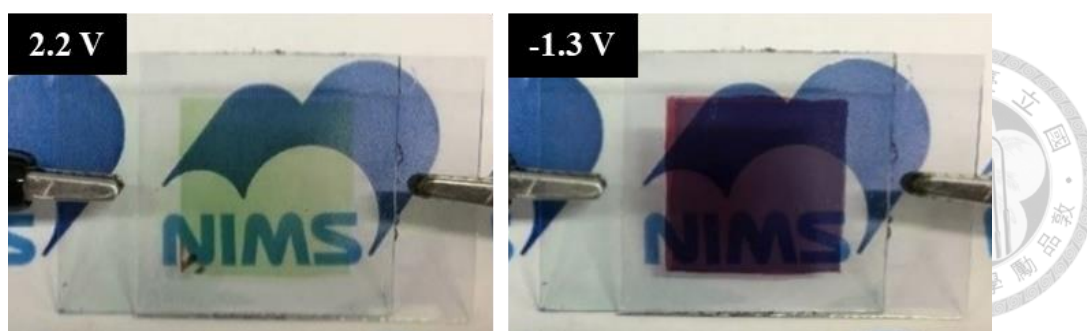
Fig. 3-14 Images of PolyRuFe/PB ECD at bleaching (2.2 V) and coloring (-1.3 V) states.

3.2.3.6 Long-term stability of PolyRuFe/PB ECD

A long-term cycling test for the PolyRuFe/PB ECD was performed and the results collected at 503, 580 and 690 nm are presented in Fig. 3-15. The quantitative EC switching performance of the ECD at the first and 200th cycle is recorded in Table 3-4. No significant decay in ΔT could be observed at both 580 and 690 nm, which are mainly contributed by PolyFe and PB, respectively. By comparing the performances before and after 200 cycles (4000 s in total), its ΔT remains 89.7% and 89.6% of its original value (at 580 and 690 nm, respectively). However, the value of the ΔT at 503 nm decreased from the initial 53.6% to about 17.2% at the end of 200 cycles. PolyRu exhibits stable redox reactions in the three electrode system, but may become unstable in the ECD owing to its higher redox potential window. The main reason we proposed is the worst memory effect of PolyRu compared to PolyFe. It leads the ineffective pretreatment of oxidation for the ECD, which is generally considered to be an important part before fabricating the ECD. As Fig. 3-15, it shows the dynamic transmittance responses when switching between 0 (coloring state) and 1.3 V (bleaching state). After switching to bleaching state, the PolyRuFe film was left in the open-circuit condition to investigate its memory effect. The results of the retention are collected in the Table 3-5. In the open-circuit condition, PolyRu turns to coloring state rapidly in 50 s. On the other hand, PolyFe exhibits better memory effect that could maintain 40 % of its saturated bleaching state for 150 s. Due to poor memory effect of PolyRu, it is found that PolyRu cannot be bleached gradually in the optical long-term stability measurement.
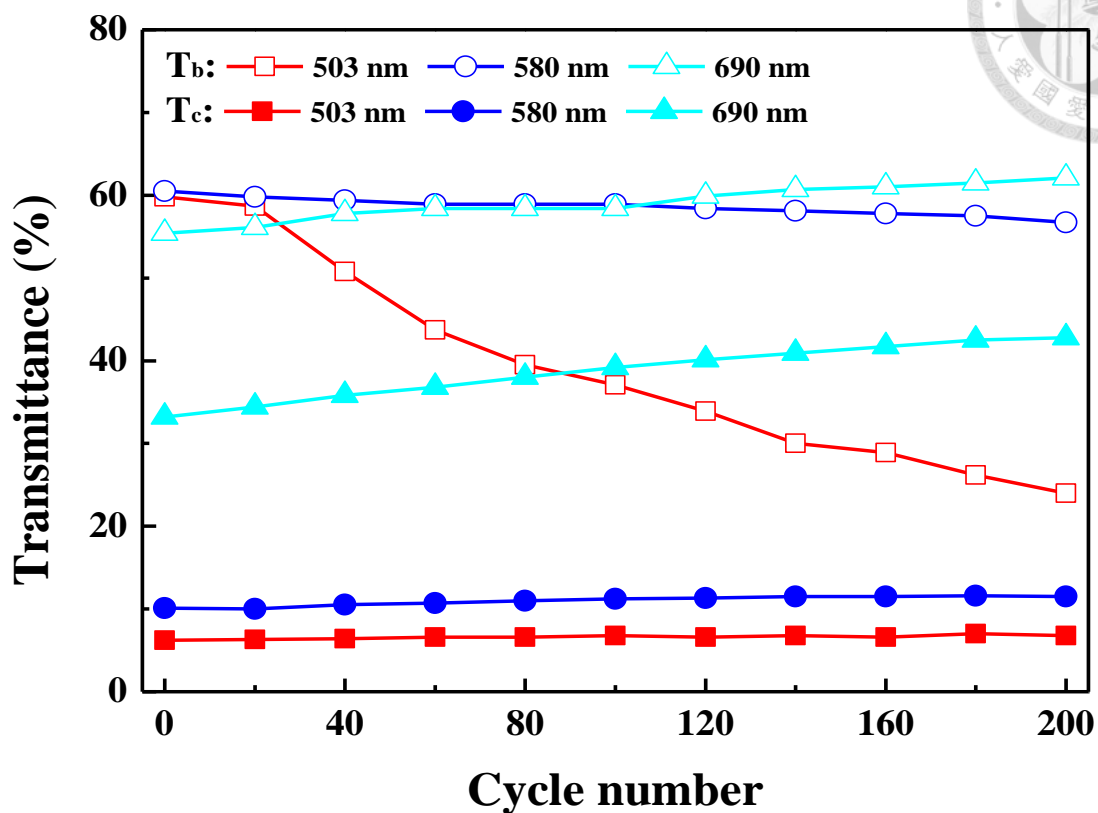
Fig. 3-15 Long-term transmittance change of the PolyRuFe/PB ECD. The ECD was switched between -1.3 V and 2.2 V for 200 cycles.

Table 3-4 EC performances of the PolyRuFe ECD at the 1st and 200th cycles.

Cycle	λ (nm)	Tb (%)	Tc (%)	ΔT (%)
1	503	59.8	6.2	53.6
200	503	24.0	6.8	17.2
1	580	60.5	10.1	50.4
200	580	56.7	11.5	45.2
1	690	55.4	33.2	22.2
200	690	62.1	48.2	19.9

3.2.3.7 Memory effect of PolyRuFe in a three electrode system

In order to improve the poor memory effect of PolyRu(III), the multi-walled carbon nanotubes (MWCNTs) is introduced in the PolyRuFe/PB ECD. According to the literature, oxidized MWCNTs promoted ClO_4^- adsorption due to the introduction of more oxygen-containing functional groups, which served as additional adsorption sites. As shown in Fig. 3-14 and Table 3-4, PolyRuFe-MWCNT exhibits longer memory effect than bare PolyRuFe. PolyRuFe-MWCNT remained 75%, 59% and 42% of their initial saturated bleaching state at 503 nm after 50, 100 and 200 s, respectively. On the other hand, the retention of PolyRuFe-MWCNT at 580 nm increases to 94%. Comparing to bare PolyRuFe, the memory effect of PolyRuFe-MWCNT greatly increases. It is expected to improve the long-term stability of PolyRuFe by enhancing the memory effect owing to adsorption amounts of ClO_4^-.
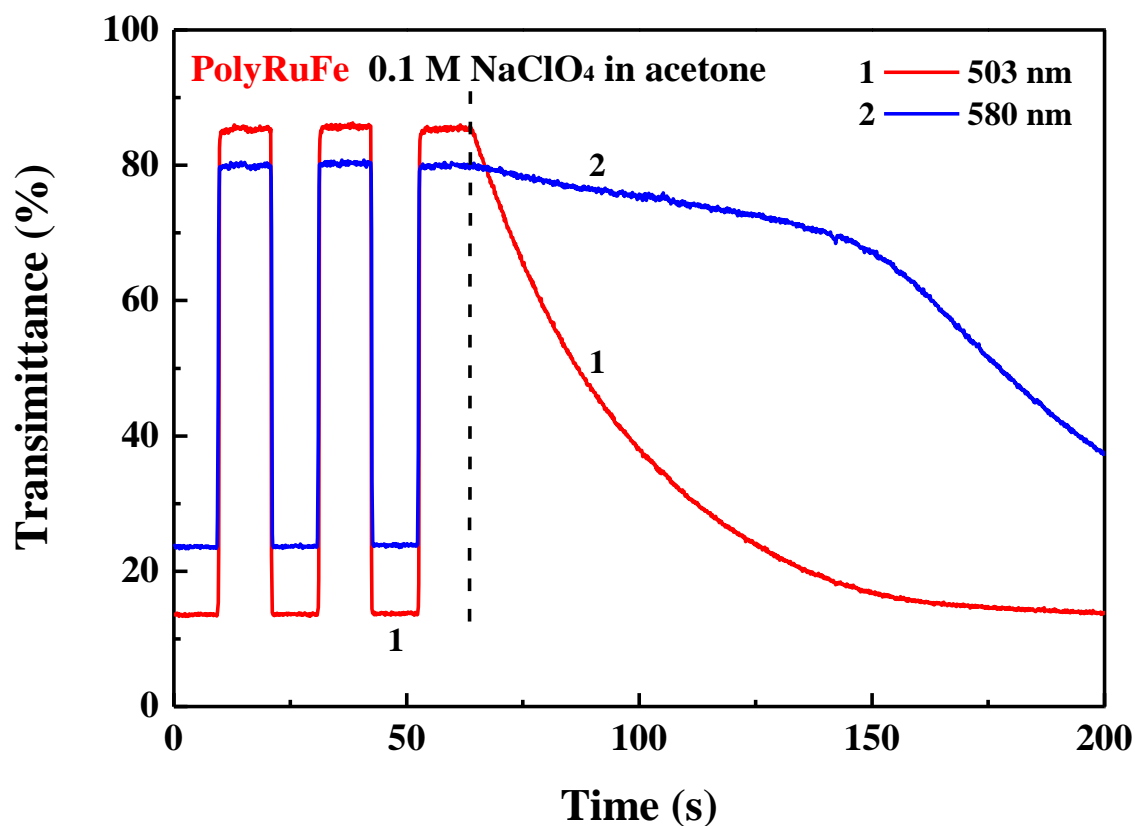
Fig. 3-16 The retention of the saturated bleaching state for PolyRuFe thin film at 503 and 580 nm.
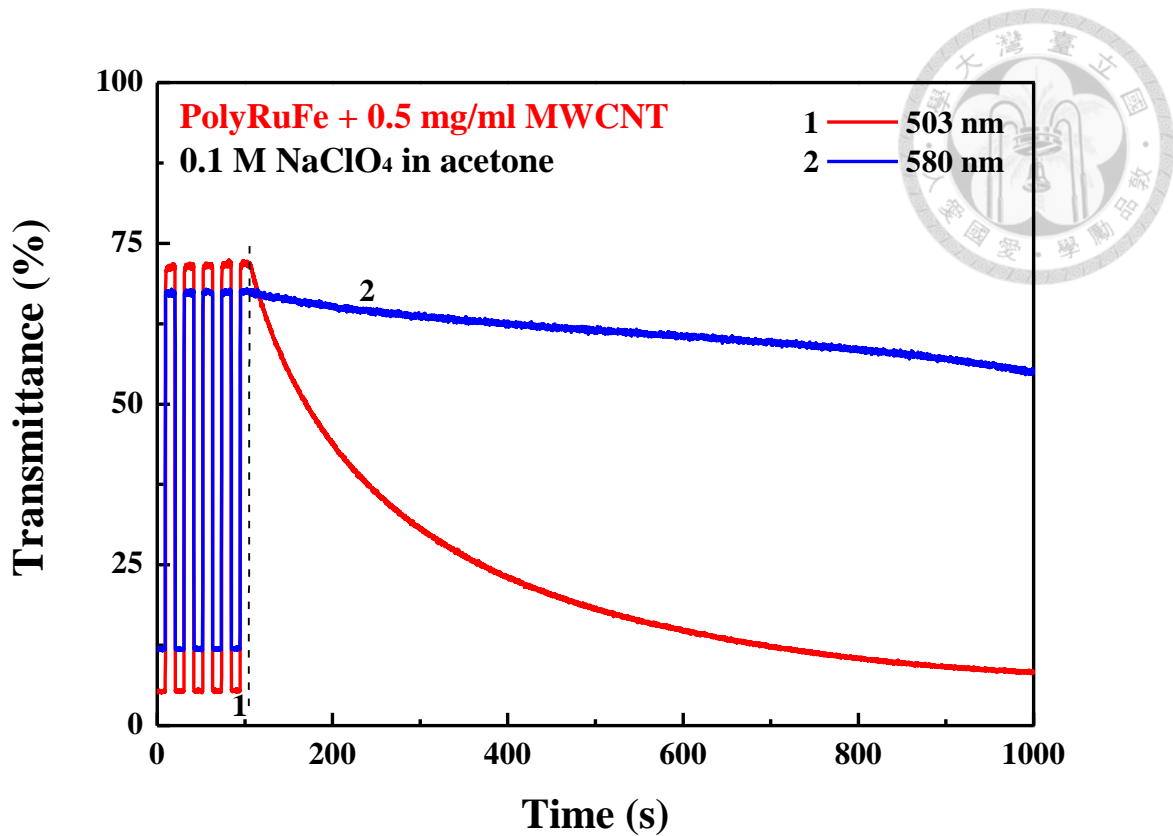
Fig. 3-17 The retention of the saturated bleaching state for PolyRuFe-MWCNT thin film at 503 and 580 nm.

Table 3-5 The memory effect of PolyRuFe and PolyRuFe-MWCNT.

Thin films	λ (nm)	T_b / R[a] (%) (initial)	T_b / R (%) (50 s)	T_b / R (%) (100 s)	T_b / R (%) (200 s)
PolyRuFe	503	85 / 100	29 / 34	15 / 18	-
	580	80 / 100	74 / 92	58 / 73	-
PolyRuFe-MWCNT	503	72 / 100	54 / 75	43 / 59	30 / 42
	580	67 / 100	66 / 98	65 / 96	64 / 94

[a] Retention of its initial T_b.

A comparing table based on the ECD composed of MEPE is shown in Table 3-6. As presented, there are few researchers aim at fabricating ECD based on MEPE. In particular, there are rare ECDs composed of PolyRu owing to the poor stability. However, the proposed PolyRuFe/PB ECD still exhibits lots of desirable EC properties, including larger ΔT and shorter response time, compared to other ECD based on MEPE. The relationship between long-term stability and memory effect were investigated and PolyRuFe-MWCNT was investigated to enhance memory time in this chapter. It is expected to improve the stability of PolyRu in the future.

3.2.3.8 EQCM analysis of PolyRuFe-MWCNT and PolyRuFe

To understand the ionic transport phenomenon, the electrochemical quartz crystal microbalance (EQCM) analysis was applied for the PolyRuFe-MWCNT and PolyRuFe films. EQCM is used to study the mass changes in a gold-disk electrode by measuring the frequency change of the crystal. In order to calculate the accumulated mass, ΔM, a correlation equation is shown in Eq. 3-6.

$$\Delta M = -\left[\frac{A \times N \times r_q}{-f_0{}^2}\right] \times \Delta f \qquad (3\text{-}7)$$

ΔM is the change of mass (g), f_0 represents the resonant frequency of the initial mode of quartz crystal (8.88 MHz), A is the surface area of the gold-disk electrode (0.196 cm^2), N is the shear modulus of quartz (167 KHz cm), R_q is the density of the quartz crystal (2.684 g/cm^2), and Δf is the measured change of resonant frequency.

Fig. 3-18 (a) and (b) show in situ mass change of PolyRuFe and PolyRuFe-MWCNT films during the potential cycling between 0 to 1.3 V in 0.1 M NaClO$_4$ at a scan rate of 20 mV/s, respectively. Both of two films show the reversible and stable mass change during CV scan. When the cycling potential switched from ca 0.7 to 1.2 V, the increasing mass can be observed owing to the adsorption of ClO$_4^-$; the potential switched from ca 1.1 to 0.6 V, the decreasing mass was obtained due to the reduction of PoluRuFe leading the desorption of ClO$_4^-$. It is indicated that the adsorption and desorption of ClO$_4^-$ occurs accompanying the redox reaction of PolyRuFe cause the mass change of two films.
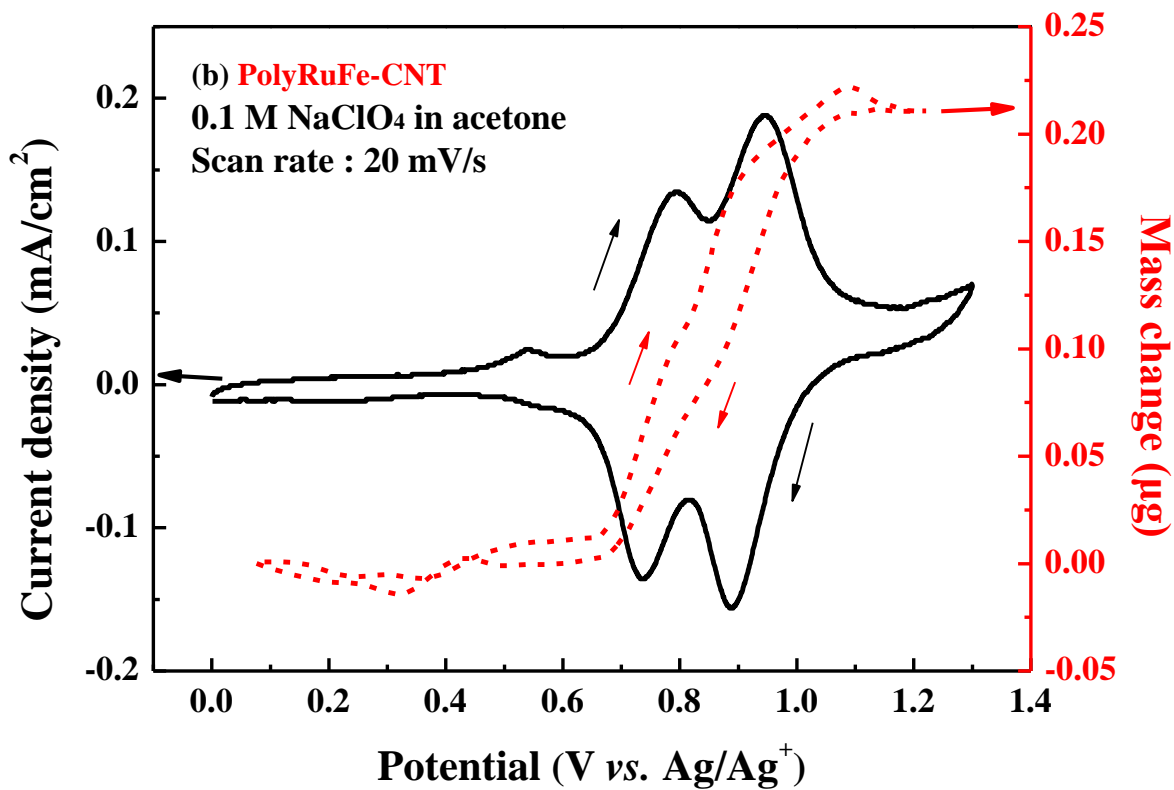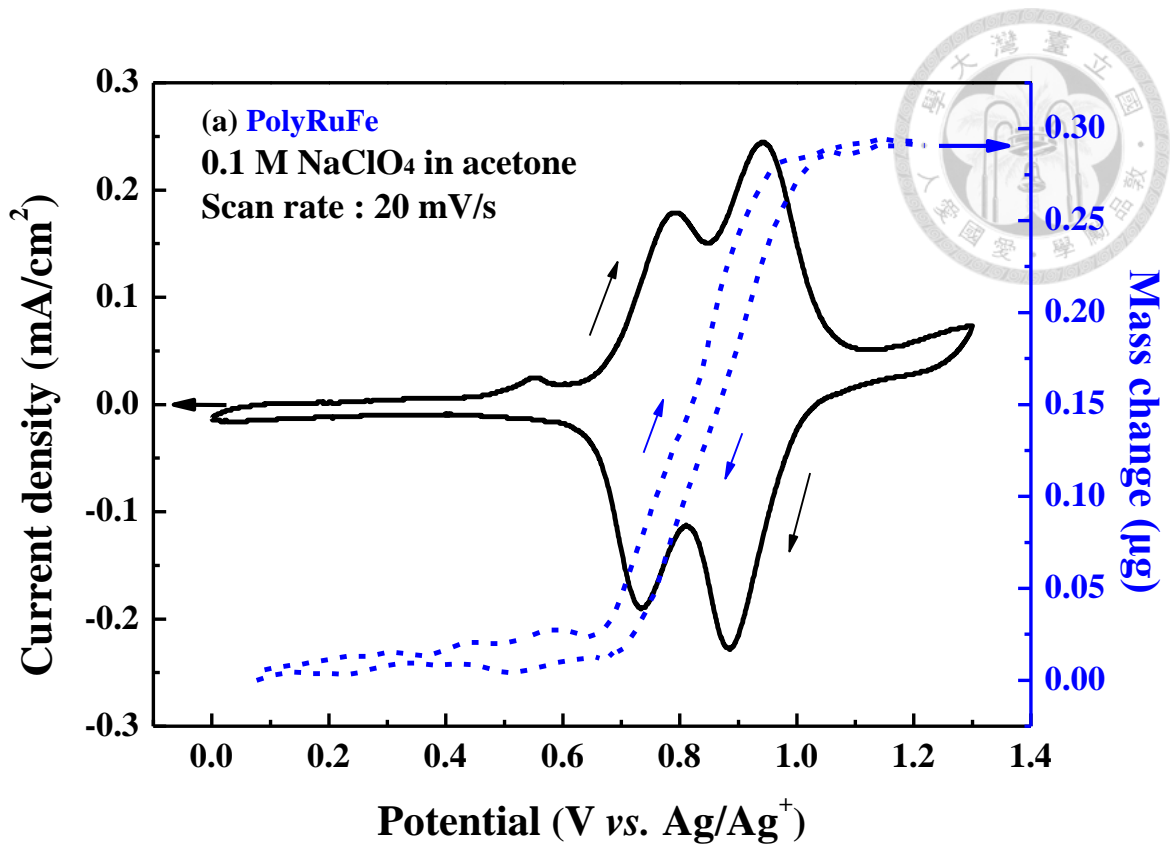
Fig. 3-18 Current density and accumulated mass change of (a) PolyRuFe and (b) PolyRuFe-MWCNT films on the gold-disk electrode of CV scan in the solution containing 0.1 M NaClO$_4$ at a scan rate of 20 mV/s.

3.2.3.9 QCM analysis of PolyRuFe-MWCNT and PolyRuFe films at OCV.

In order to investigate the relationship between memory effect and the adsorption of ClO_4^-, the quartz crystal microbalance (QCM) was measured at the open-circuit voltage (OCV) condition, shown in Fig. 3-19. As shown, the lower mass change of PolyFe-CNT can be observed at the OCV in 1000 s, compared to PolyRuFe, implying the effective adsorption of ClO_4^- by MWCNT. PolyRuFe-MWCNT exhibited the better memory effect, attributed to the slower desorption of ClO_4^-.
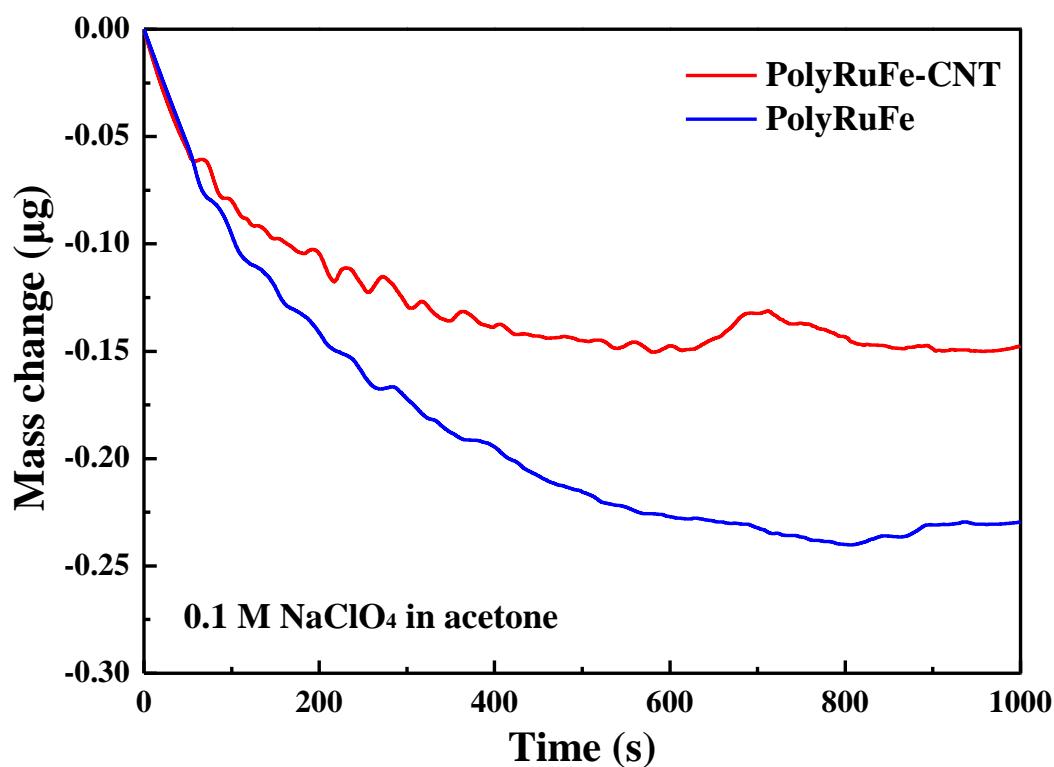
Fig. 3-19 Mass change of PolyRuFe-MWCNT and PolyRuFe films on the gold-disk electrode at OCV.

Table 3-6 Mass change of PolyRuFe-MWCNT and PolyRuFe films on the gold-disk electrode at OCV
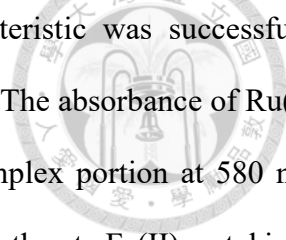
Samples	ΔM (μg) (200 s)	ΔM (μg) (400 s)	ΔM (μg) (600 s)	ΔM (μg) (800 s)	ΔM (μg) (1000 s)
PolyRuFe-MWCNT	-0.10	-0.14	-0.15	-0.14	-0.15
PolyRuFe	-0.14	-0.19	-0.23	-0.24	-0.23

Table 3-7 List of literatures on the EC performance of ECDs composed of MEPE

ECD	V_b/V_c (V)	t_b/t_c (s)	ΔT (%)	R^k (%) (n^{th} cycle)	Ref.
PolyFe/electrolyte[a]/VO$_x$[f]	1.6/0	-	36	-	[102]
PolyCu/electrolyte[b]/PANI[g]	1.5/0.8	0.2/0.4	21	99 (1500)	[103]
PolyRu/electrolyte[c]/PANI:PSS[h]	-1.5/1.5	1.3/4.0	40	-	[l]
PolyFe/electrolyte[d]/NiHCF[i]	0.8/0	1.0/0.5	45	95 (1500)	[m]
PolyCo/electrolyte[e]/Fc[j]	0/2.5	2.3/1.6	52.7	92 (500)	[n]
PolyRuFe/PB at 503 nm	2.2/-1.3	0.3/0.2	52.7	32.1 (200)	Chapter 3
PolyRuFe/PB at 580 nm	2.2/-1.3	0.5/0.3	46.9	89.7 (200)	Chapter 3

[a] 1.0 M LiClO$_4$ /PC thickened with a thermoplastic polymer. [b] 0.1 M tetrabutylammonium perchlorate in ACN with 1.0 mM HClO$_4$. [c] 0.1 M LiClO$_4$ in ACN with 1.0 mM HClO$_4$. [d] NaClO$_4$: PMMA : PC : ACN = 3 : 15 : 25 : 57 wt%. [e] 0.1 M LiClO$_4$ in acetone. [f] Vanadium oxide. [g] Polyaniline. [h] Polyaniline:polystyrene sulfonate. [i] Nickel hexacyanoferrate. [j] Ferrocene. [k] Retention of its initial ΔT after cycling. [l] Wan Hsuan's work. [m] Hsin-Che's work. [n] Sheng-Yuan's work.

3.3 Conclusions

In this section, PolyRuFe which exhibited the multi-color characteristic was successfully synthesized and the electrochromic properties were carefully investigated. The absorbance of Ru(II) complex portion at 503 nm is much stronger than that of the Fe(II) complex portion at 580 nm, attributed to the stronger π-conjugated of ligand (L_0) to the Ru(II) metal ions than to Fe(II) metal ions. The obtained PolyRuFe/PB ECD incorporating of the gel-type electrolyte based on PMMA not only eliminates the leakage drawback of the liquid-typed electrolyte, but also exhibits the panchromatic feature with well optical change of 52.7, 46.9, and 28.0% at 503, 580 and 690 nm, respectively. Moreover, the outstanding response time less than 0.5 s could be observed at 503 nm and 580 nm for both coloring and bleaching, it shows the advantage of the MEPE-based films completely. In addition, the three-step values of the coloration efficiency could be observed owing to the different redox potential between Fe and Ru. Ru(II) is much easier to reduce than Fe(II) so that Ru(II) was reduced first when applying higher range of potential bias (0.9 ~ 1.7 V); while major part of Fe(II) was reduced when applying lower range of potential bias (0.6 ~ 0.9 V); the large absorbance change at 690 nm when applied potential bias from 0.6 to -1.3 V. To scientifically evaluate the color change of ECD occurring on electrochemical switching, the ECD was also subjected to colorimetric analysis by the CIE 1931 system of colorimetry. Only 10.3% and 10.4% decays, corresponding at 580 and 690 nm respectively, were observed in the PolyRuFe/PB ECD after 200 continuous cycles at bleaching (2.2 V) and coloring (-1.3 V) voltages with an interval time of 10s. Much more decay could be observed at 503 nm, which is attributed to the poor memory effect of PolyRu. Compared to this result, the PolyRuFe-MWCNT exhibits longer memory effect than bare PolyRuFe. PolyRuFe-MWCNT remained 75%, 59% and 42% of their initial saturated bleaching state at 503 nm after 50, 100 and 200 s, respectively. It is expected to improve the long term stability of PolyRu in ECD by enhancing its memory effect.

Chapter 4

N-methylphenothiazine Derived Ionic Liquid as Redox Couple with Phenyl Viologen for ECD

4.1 Introduction

Since initial discovery in 1914, ionic liquids (ILs) have been widely researched in multiple chemistry disciplines [104]. Due to their unique properties, ILs have been investigated as potential electrolytes for application in electrochemical devices including lithium ion batteries [105-107], fuel cells [108-109], and solar cells [110-112]. As liquid salts, ILs are usually composed of an organic cation and an organic or inorganic anion, and they are dominated by strong electrostatic forces between their molecular ions [113]. The key properties that ILs offer is good chemical and electrochemical stability, low volatility, non-flammability, and high ionic conductivity. These make them potentially ideal as solvents and electrolytes. One of the attractive characteristics of ILs in organic synthesis is that the structures with the cationic or anionic components can be modified according to various requirement, so that they can be utilized in different applications. Recently, increasing attention has been focused on the use of ionic liquids as a means of immobilizing redox couples [114-116]. For examples, Forgie et al. synthesized the electroactive ionic liquid based on ferrocene and its electrochemical properties were investigated for the lithium-ions battery [117]. Zhang et al. reported on iodine-free redox couple, imidazolium functionalized TEMPO, for dye sensitized solar cell [118]. Gelinas et al. demonstrated an electrochromic device that uses ethyl viologen and ferrocene-based redox ionic liquids ([FcNTf]⁻) as the electroactive species [119].

Phenothiazine-based groups are a class of important heterocycles and widely used as common building blocks for the synthesis of pharmaceuticals [120]. Recently, several researchers aim to investigate phenothiazine-based group for applications in various electronic and electrochemical devices since they are good electron-donor and hole transport materials due to the presence of electron-rich sulfur and nitrogen heteroatoms [49]. For electrochromism, N-methylphenothiazine (NMP) exhibits noticeable color change in visible region and good cycling stability [50]. Up to now, only few

research that proposed anodically coloring ionic liquid could be found. In this chapter, we first synthesized the imidazolium ionic liquid composed of NMP. NMP-based ionic liquid (NMP-IL) combines the both advantages of NMP and ionic liquid that shows high optical change and good stability. Moreover, the NMP-IL exhibits the unique purple color (575 nm) owing to the assembling carbon chain on the NMP.

Among all of EC material, viologens draw much attention for their desirable optical contract and stability [121-123]. In order to investigate the electrochromism of NMP-IL in electrochromic device. We fabricated the solution-typed ECD composed of NMP-IL and Phenyl viologen (PV). In general, PV shows three states, including PV^{2+} (dicaiton state, colorless), $PV^{+\bullet}$ (radical cation state, green) and PV^{0} (neutral state, light brown). However, only the reaction between PV^{2+} and $PV^{+\bullet}$ is favored because PV^{0} would accelerate the aging process through crystallization and side reaction, also called comproportionation [124]. Another aging process in viologen system is aggregation. The $PV^{+\bullet}$ generated upon reduction tends to aggregate on the surface of electrode due to lack of solubility [125-126]. According to literature [52, 57], retardation of the diffusion rate of the viologens could decrease the aggregation of $PV^{+\bullet}$. Also, the incorporation of the redox couple into the ECD to improve the stability through the formation of $PV^{+\bullet}$ agglomerates. Following these two strategies, decreasing of the diffusion rate and incorporating the redox couples by adding NMP-IL had been regarded as a feasible way.

4.2 Results and discussion

In this section, the structure of NHP-OH, NMP-OH, NMP-Br and NMP-IL were confirmed by ^{1}H NMR, ^{13}C NMR and mass spectrometry first. DMSO-d_6 was utilized as d-solvent in ^{1}H NMR and ^{13}C NMR for characterization of all products. The obvious peak of products all located on 2.49 and 39.5 ppm in ^{1}H NMR and ^{13}C NMR, respectively was the signal of DMSO-d_6. Further, the peak located on ca 3.3 ppm was water.

4.2.1 Characterization of NHP-OH by ^{1}H NMR, ^{13}C NMR and mass spectrometry

The structure of NHP-OH was confirmed by ^{1}H NMR, ^{13}C NMR and mass spectrometry presented in Fig. 4-1, Fig. 4-2, Fig. 4-3, respectively. In Fig. 4-1, the peaks located on 8.9 and 8.2 ppm are the signals of hydroxyl group and secondary amine on the NHP-OH, respectively and 7 peaks located on 6.4~7 ppm belong to other hydrogens on the benzene rings of NHP-OH. In Fig. 4-2, 11 obvious peaks can be observed on ^{13}C NMR spectrum. Among 12 carbon of NHP-OH, only carbon j and k show the similar signal, overlapping at 114 ppm, owing to the asymmetric structure of NHP-OH. For mass spectrometry, shown in Fig. 4-3, the main molecular weight of 215.04 can be observed, which is exactly match of predict molecular weight of NHP-OH. It indicates that we have successfully synthesized NHP-OH via thionation.
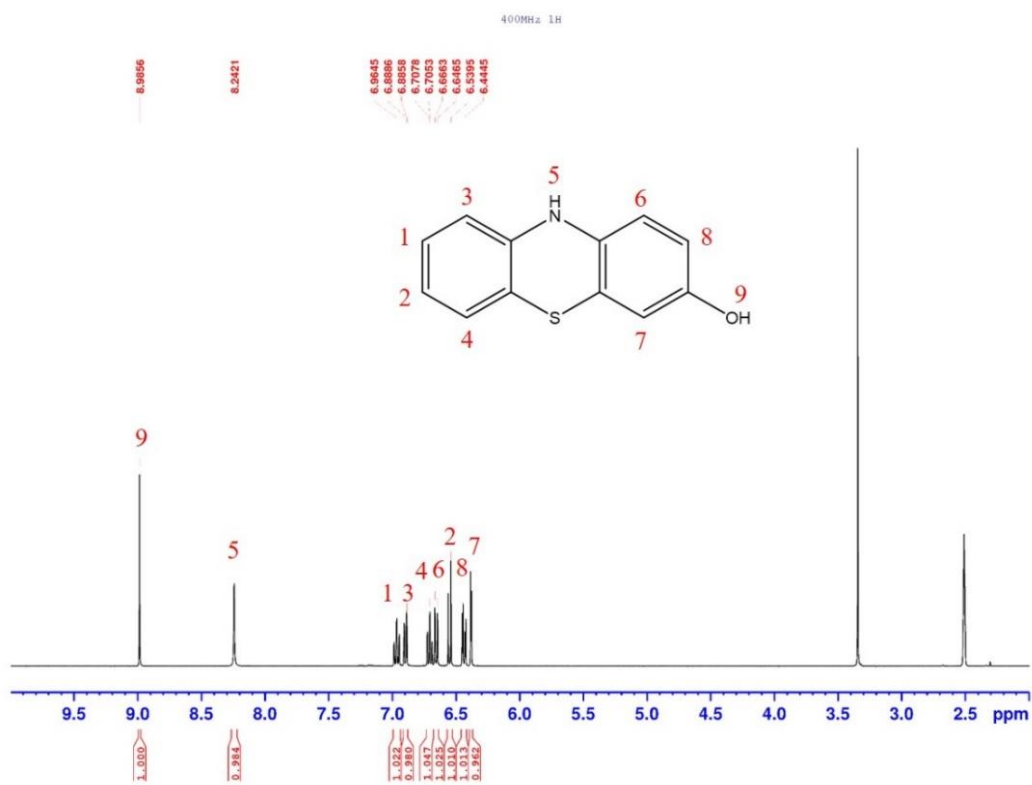
Fig. 4-1 ¹H NMR spectrum of NHP-OH.
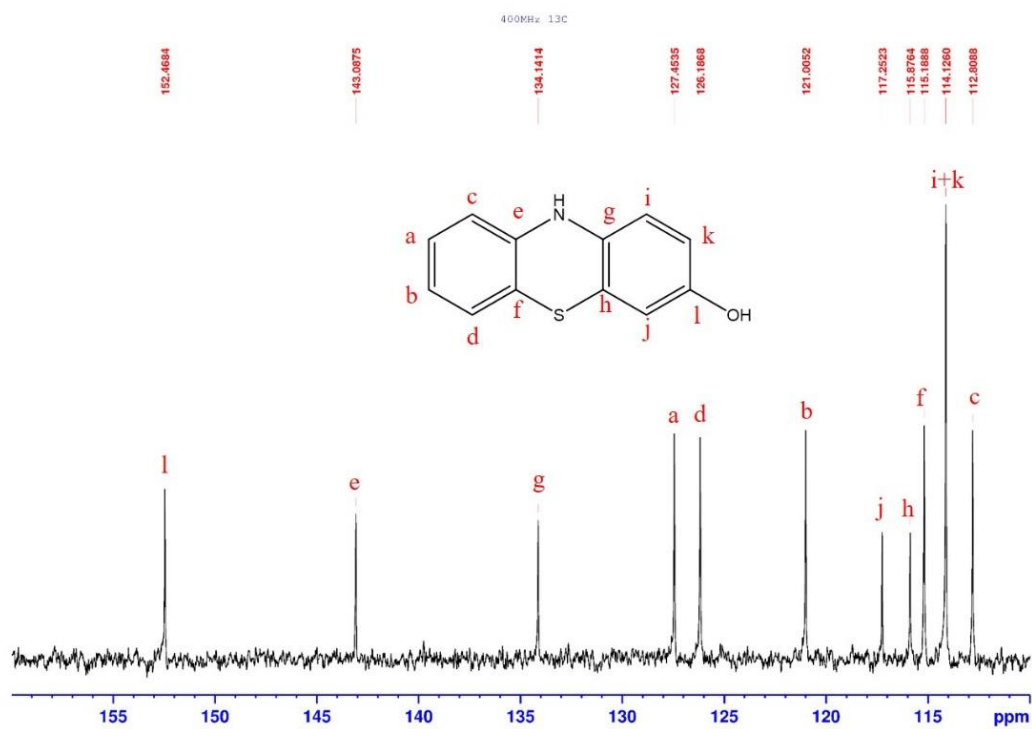
Fig. 4-2 ¹³C NMR spectrum of NHP-OH.

Fig. 4-3 Mass spectrum of NHP-OH.

4.2.2 Characterization of NMP-OH by ^{1}H NMR, ^{13}C NMR and mass spectrometry

The structure of NMP-OH was confirmed by ^{1}H NMR, ^{13}C NMR and mass spectrometry presented in Fig. 4-4, Fig. 4-5, Fig. 4-6, respectively. In Fig. 4-4, the peak at 9.0 which belongs to secondary amine of NHP-OH disappeared, and the new peak at 3.2 ppm generated, attributed to the methyl group of tertiary amine. In addition, the peaks of the hydroxyl group and seven hydrogens on NMP-OH were intact and clear, indicating that we had successfully synthesized the NMP-OH by the methylation reaction. For ^{13}C NMR, the thirteen peaks can be observed at totally different position corresponding to asymmetric NMP-OH. In Fig. 4-6, the accurate molecular weight was measured by mass spectrometry, imply the high purity of NMP-OH.
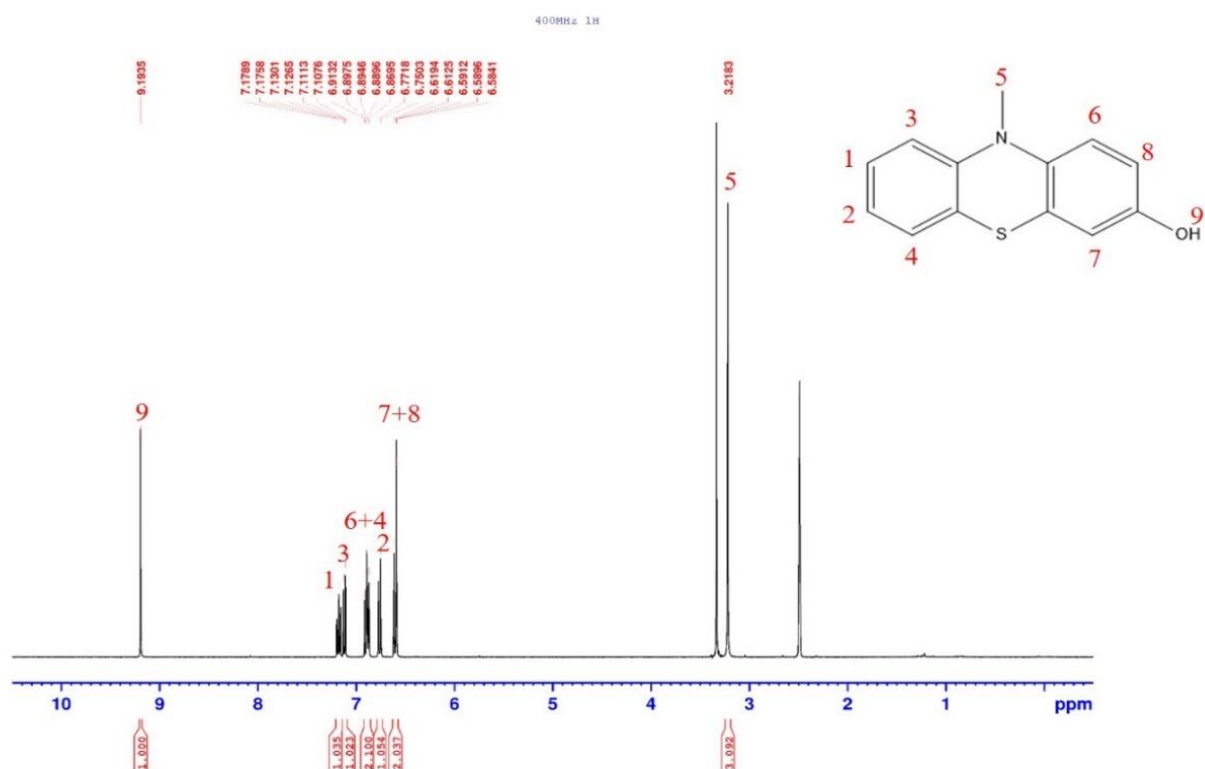
Fig. 4-4 ^{1}H NMR spectrum of NMP-OH.
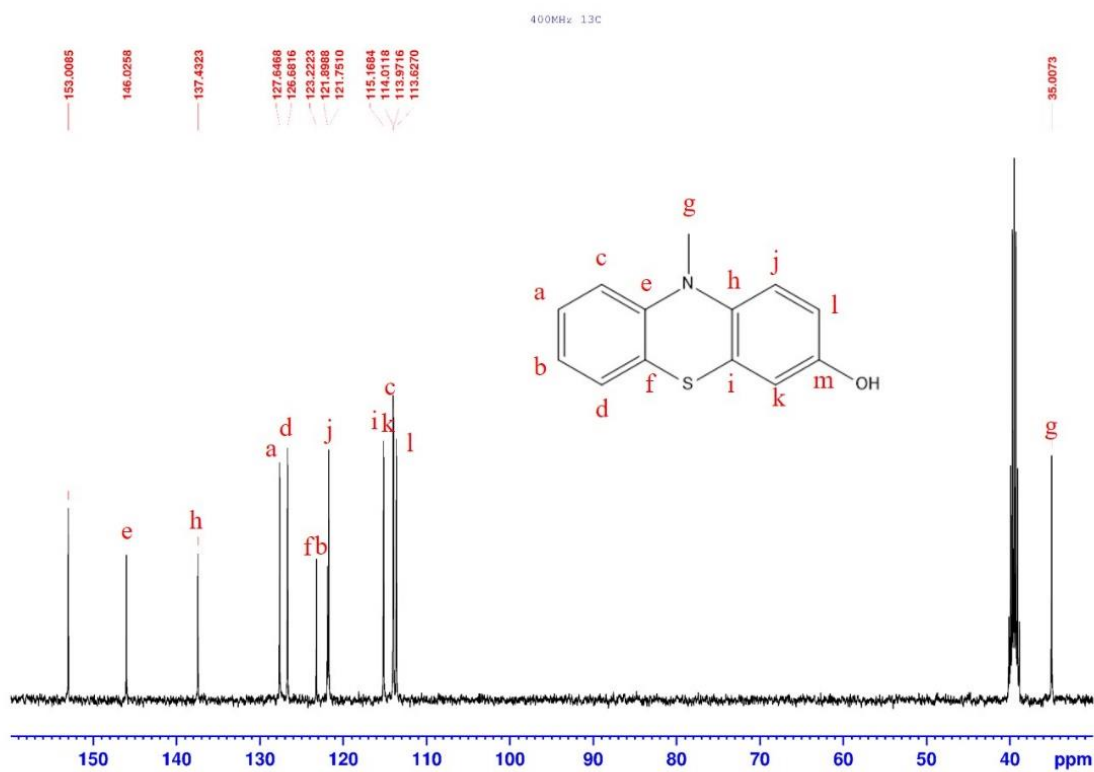
Fig. 4-5 ^{13}C NMR spectrum of NMP.
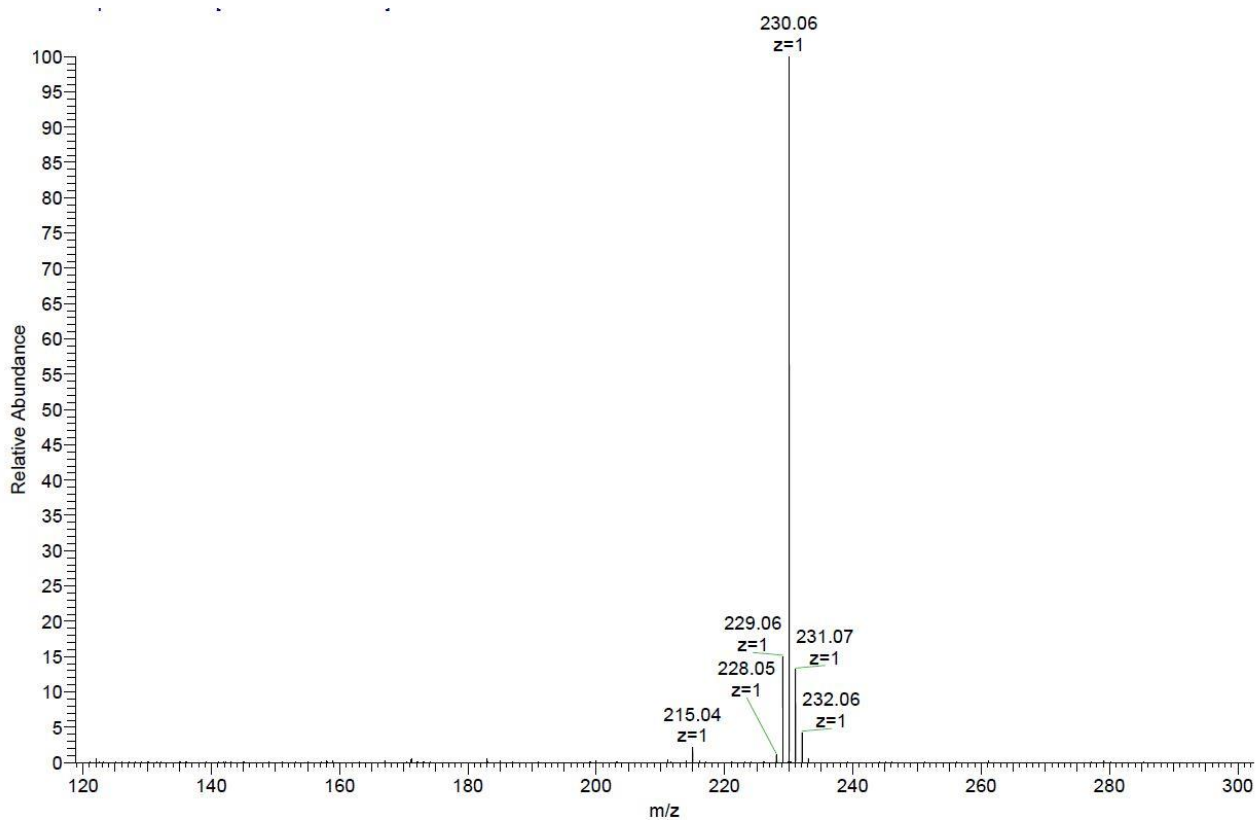
Fig. 4-6 Mass spectrum of NMP-OH.

4.2.3 Characterization of NMP-Br by ^{1}H NMR, ^{13}C NMR and mass spectrometry

The structure of NMP-Br was confirmed by ^{1}H NMR, ^{13}C NMR and mass spectrometry, shown in Fig. 4-7, Fig. 4-8, Fig. 4-9, respectively. The NMP-Br is produced by reacting NMP-OH and 1, 4-dibromobutane. For this reason, the hydroxyl group at ca 9 ppm is the target to judge if the substitution reaction occurs. In ^{1}H NMR, the peak located at ca 9 ppm, which belongs to hydroxyl group, disappeared and the peaks of number 9, 12, 11, 10 generated belonging to hydrogens on 4-bromobutoxy, implying the NMP-Br was synthesized successfully. Compared to ^{13}C NMR spectrum of NMP-OH, extra four peaks (n, o, p and q) of secondary carbon could be observed, attributed to the 4-bromobutoxy, presented in Fig. 4-8. Further, the seventeen peaks could be observed at totally different position corresponding to asymmetric NMP-Br. In Fig. 4-9, two peaks almost same tall could be observed owing to the two stable isotopes of bromine, ^{79}Br and ^{81}Br, resulting the two close values of molecular weight.
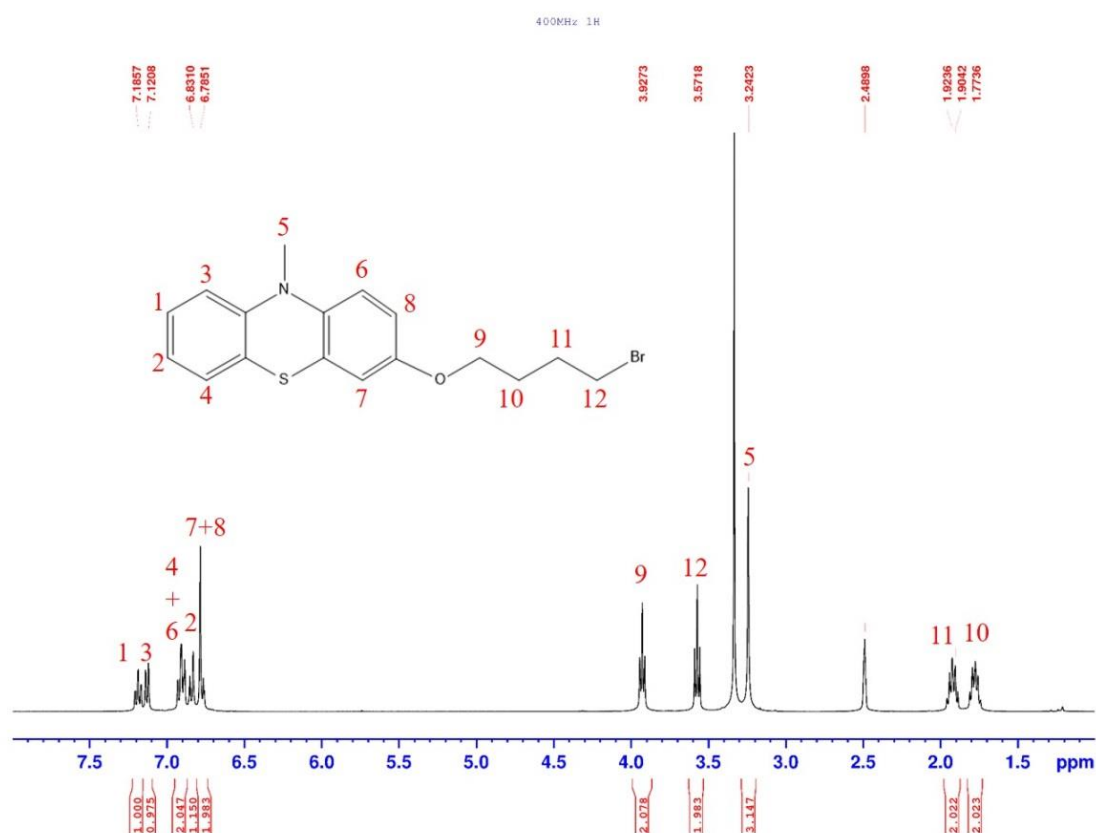
Fig. 4-7 ^{1}H NMR spectrum of NMP-Br.

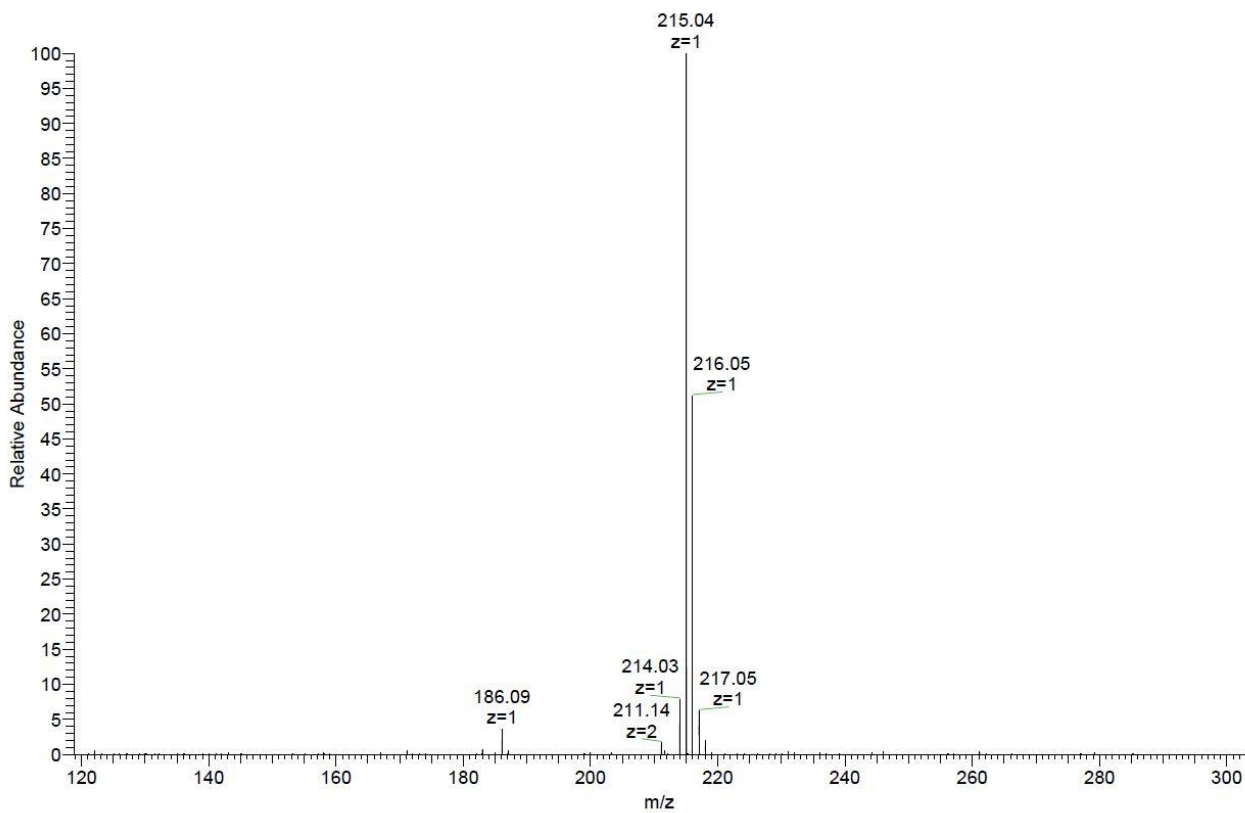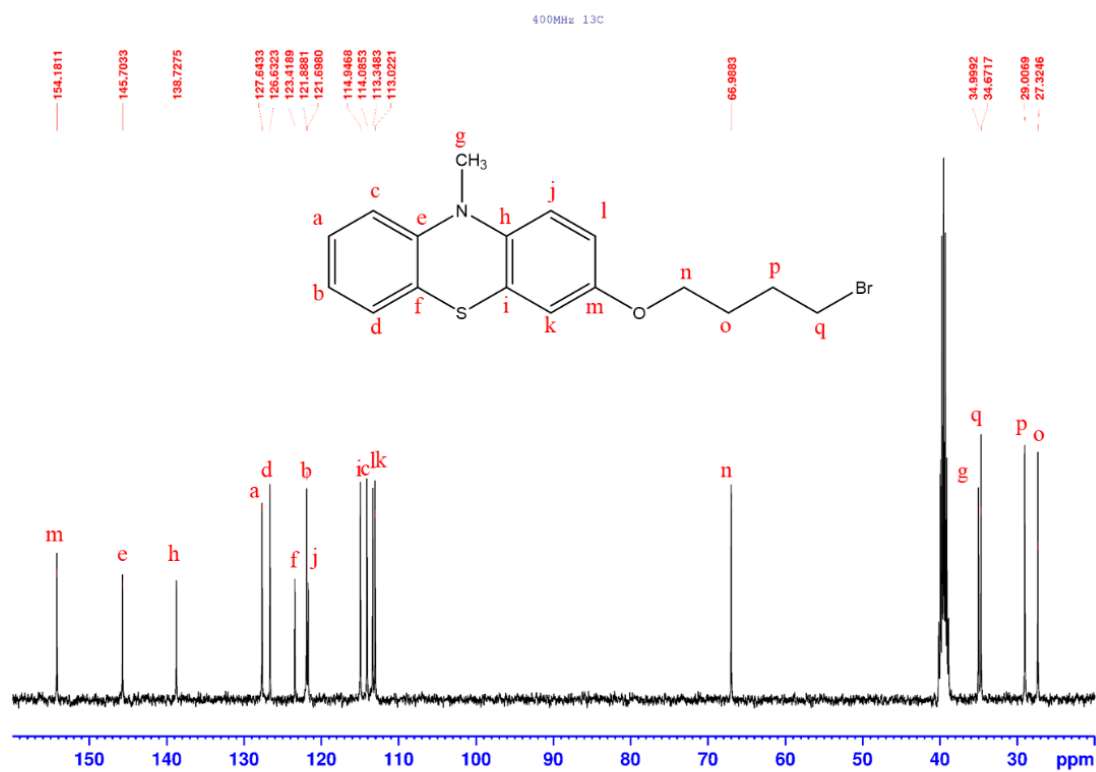**Fig. 4-8** ^{13}C NMR spectrum of NMP-Br.
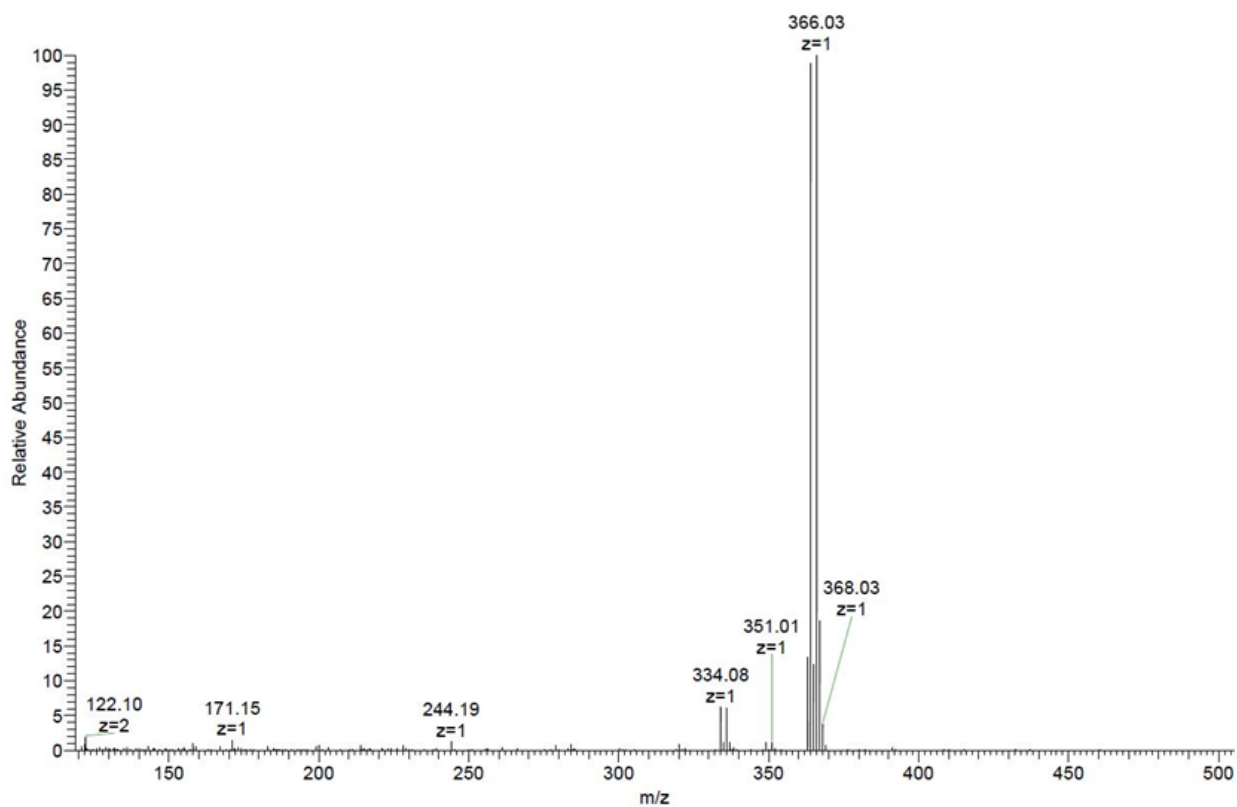
Fig. 4-9 Mass spectra of NMP-Br

4.2.4 Characterization of NMP-IL by ^{1}H NMR, ^{13}C NMR and mass spectrometry

The structure of NMP-IL was confirmed by ^{1}H NMR, ^{13}C NMR and mass spectrometry, shown in Fig. 4-10, Fig. 4-11, Fig. 4-12, respectively. In addition, the ^{1}H NMR, ^{13}C NMR and mass spectrum described the same results of NMP-IL-Br and NMP-IL owing to their similar structure, except anions. Therefore, we directly presented the results of our target product, NMP-IL. In Fig. 4-10, the hydrogens of number 12 and 11 were the crucial aims to confirm whether NMP-Br and 1-butylimidazole reacted completely. Compared to ^{1}H NMR spectrum of NMP-Br, shown in Fig. 4-7, it was found the shift of number 12 hydrogen (from 3.6 to 4.2 ppm) and number 11 hydrogen (from 1.9 to 1.2 ppm) of NMP-IL, indicating the ionization reaction occurred. For ^{13}C NMR spectrum, the signal of carbons of 1-butylimidazole could be observed significantly. Furthermore, only twenty-two peaks were able to obtained owing to the symmetry structure of imidazole, which exhibited the same position between carbon s and t located at 122.4 ppm; carbon u and q located at 48.6. In Fig. 4-12, the precise molecular weight excluding anion was measured via mass spectrometry. In consequently, the high purity and qualify of NMP-IL enable to be evaluated from these results.
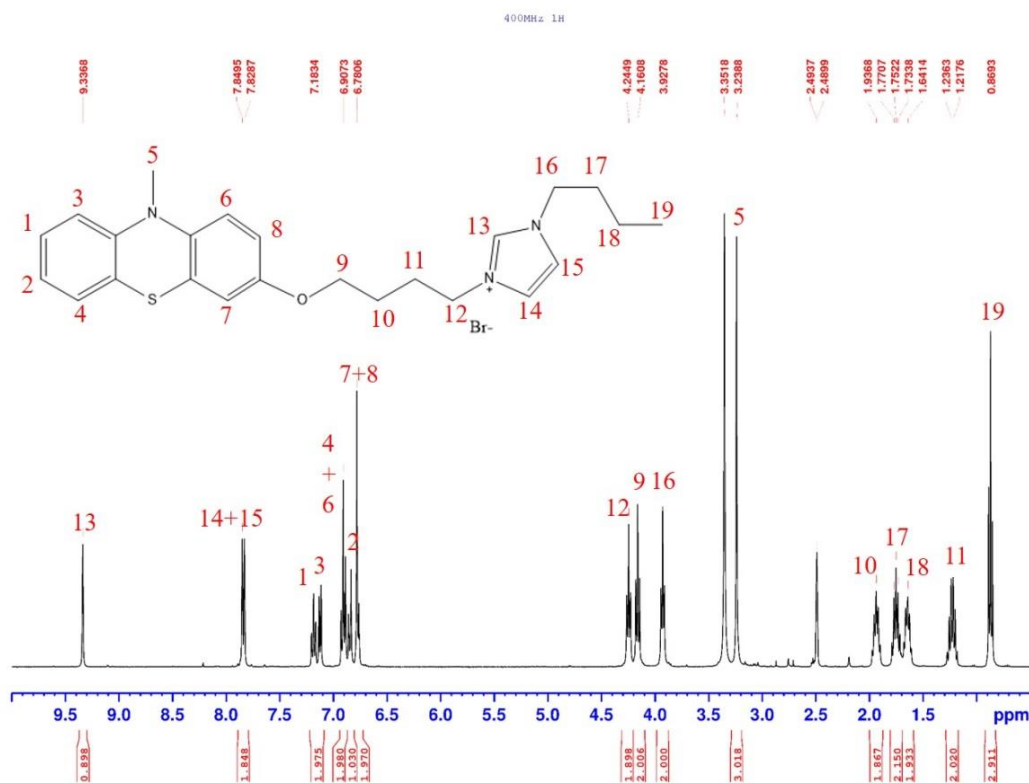
Fig. 4-10 ^{1}H NMR spectrum of NMP-IL.
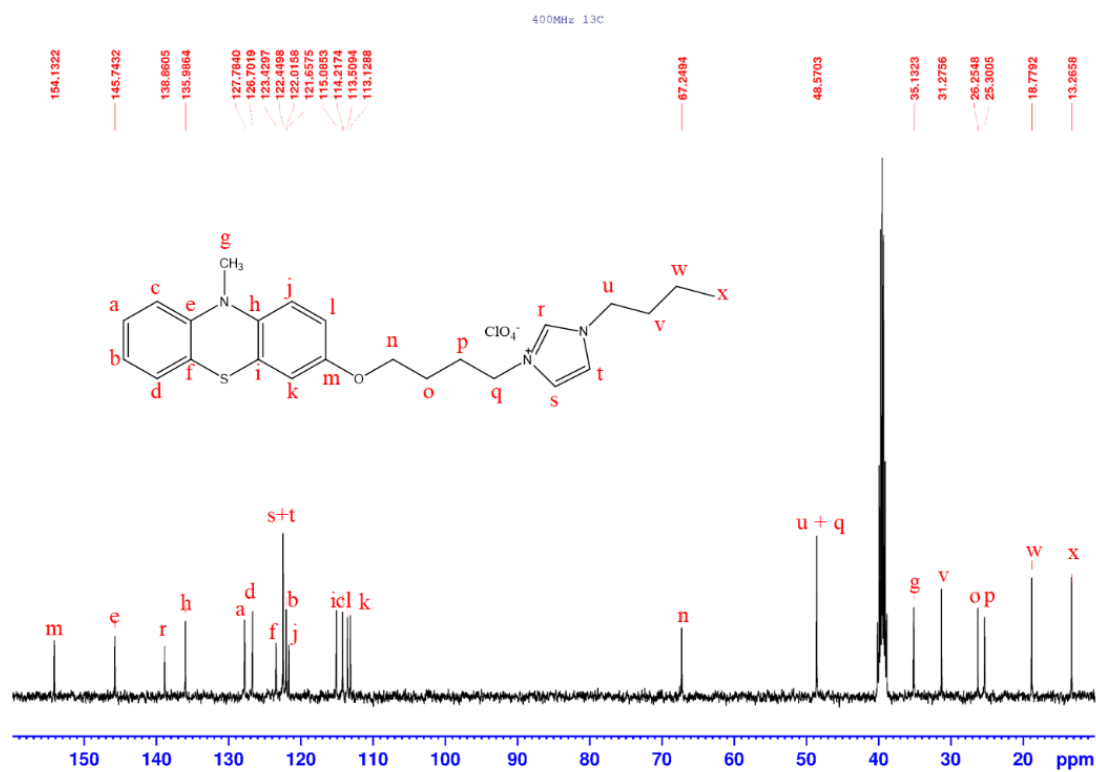
Fig. 4-11 ^{13}C NMR spectrum of NMP-IL.
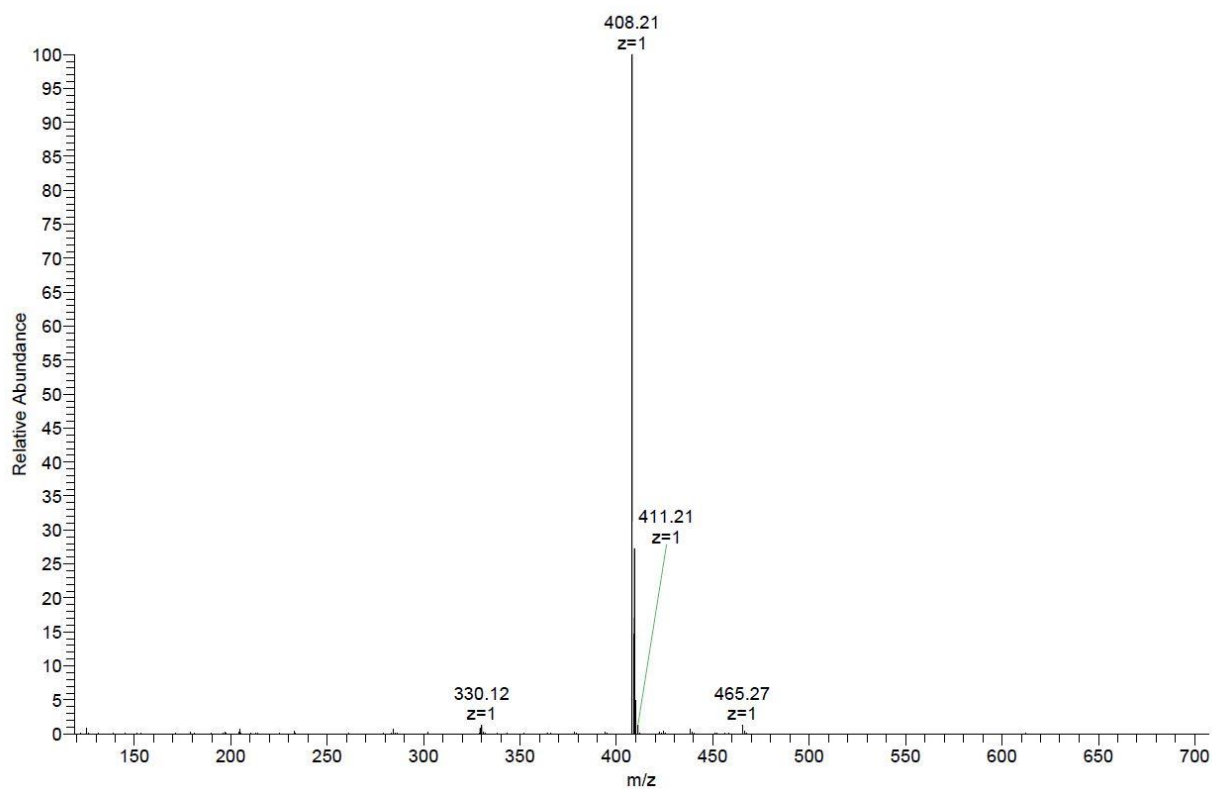
Fig. 4-12 Mass spectra of NMP-IL.

65

4.2.5 Characterization of NMP, NMP-Br and NMP-IL in a three-electrode system

4.2.5.1 CVs of NMP, NMP-Br and NMP-IL

The cyclic voltammogram (CV) used to study the relationship between the redox reaction and applied potential of the NMP, NMP-O-4C and NMP-IL were performed in a three-electrode system. In the solution, 0.03 M NMP, NMP-O-4C and NMP-IL respectively were dissolved in PC also contained 0.1 M TBABF$_4$. The CV was carried out at a scan rate of 100 mV/s, as shown in Fig. 4-13.

Upon the variation of the potential bias, the current density increased or dropped significantly at certain potentials, indicating the occurrence of each redox reaction. The redox reactions of NMP, NMP-O-4C and NMP-IL could be expressed as Eq. (4-1), Eq. (4-2) and Eq. (4-3), respectively.

$$NMP \leftrightarrow NMP^{+\bullet} + e^- \qquad (4\text{-}1)$$

(colorless)　　　(red)

$$NMP\text{-}Br \leftrightarrow NMP\text{-}Br^{+\bullet} + e^- \qquad (4\text{-}2)$$

(colorless)　　　(purple)

$$NMP\text{-}IL \leftrightarrow NMP\text{-}IL^{+\bullet} + e^- \qquad (4\text{-}3)$$

(colorless)　　　(purple)

At the time when the potential bias was larger than the peak potential at 0.563, the NMP-IL would be reduced to NMP-IL$^{+\bullet}$, electrodeposited on the ITO substrate, and it leads a color variation from colorless to purple. The oxidation, reduction and formal potential of NMP, NMP-Br and NMP-IL are collected in Table 4-1. Compared the others, NMP-IL shows the smaller current density. This phenomenon could be observed at the TEMPO-based ionic liquid.
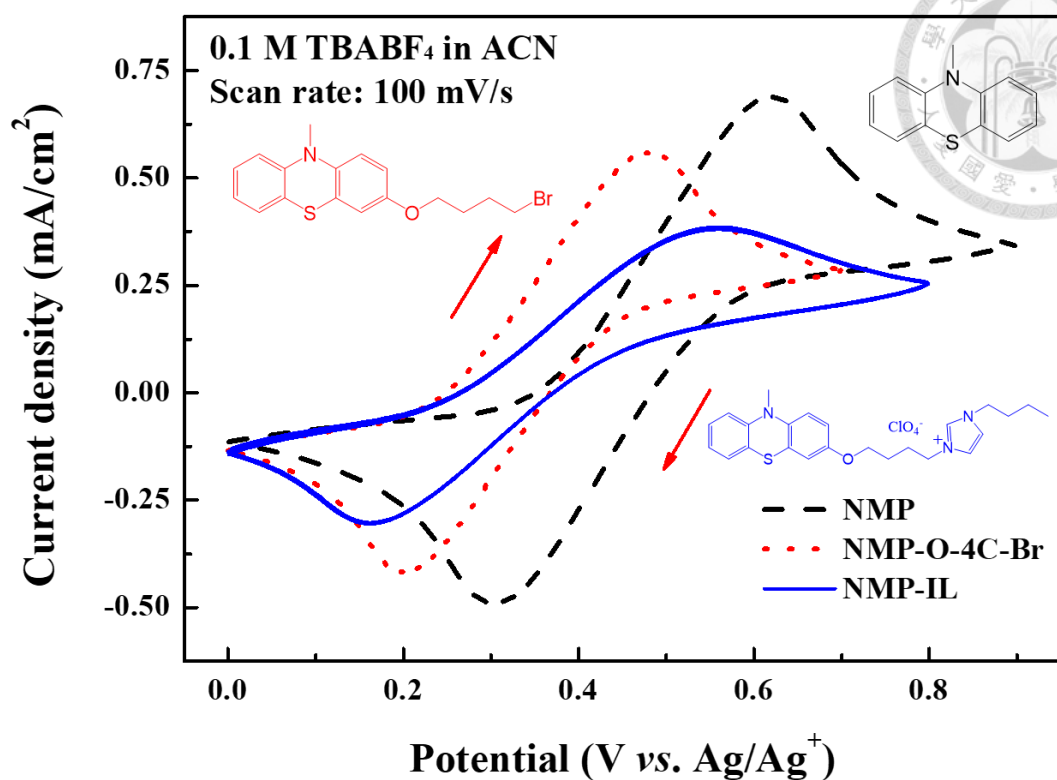
Fig. 4-13 CV of 0.03 M NMP, NMP-Br and NMP-IL in ACN at a scan rate of 100 mV/s in a three electrode system.

Table 4-1 Redox potential of 0.03 M NMP, NMP-Br and NMP-IL in ACN (*vs.* Ag/Ag$^+$).

Redox couples	E	$E_{p,c}$ (V)	ΔE (V)	$E^{0'}$(V)
NMP	0.62	0.302	0.318	0.461
NMP-Br	0.483	0.201	0.282	0.342
NMP-IL	0.563	0.162	0.401	0.363

4.2.5.2 UV-Vis absorbance spectra of NMP, NMP-O-C, NMP-Br and NMP-IL

On the other hand, UV-Vis absorbance spectra of 0.03 M NMP, NMP-O-C, NMP- Br and NMP-IL in ACN contained 0.1 M $TBABF_4$ with maximum absorbance are shown in Fig. 4-14. Based on the results of CV, it indicates the different potential window of NMP, NMP-Br and NMP-IL; therefore, when the potential bias reached 0.9, 0.7 and 0.8 V, the maximum absorbance of NMP, NMP-Br and NMP-IL could be observed. For NMP, it demonstrates high optical change at 520 nm. However, the NMP-Br and NMP-IL both exhibit the main absorbance change at around 575 nm. Compared this result, 3-methoxy-10-methyl-phenothiazine (NMP-O-C) that was synthesized to confirm the effect of carbon chain for NMP and the structure of NMP-O-C is shown in Fig. 4-15. It is found that absorbance peaks of NMP-O-C, NMP-Br and NMP-IL are the same at around 575 nm. A possible explanation for this result that cause a shift of absorbance is the molecular structure change from open ion-radical to hindered ion-radical [127], attributed to the graft of substituents on the NMP.

Based on the results of CV and absorbance spectra, the basic electrochromism of NMP-IL was investigated. It was known that it still demonstrated a large optical contrast and reversible redox reaction upon grafted on ionic liquid.
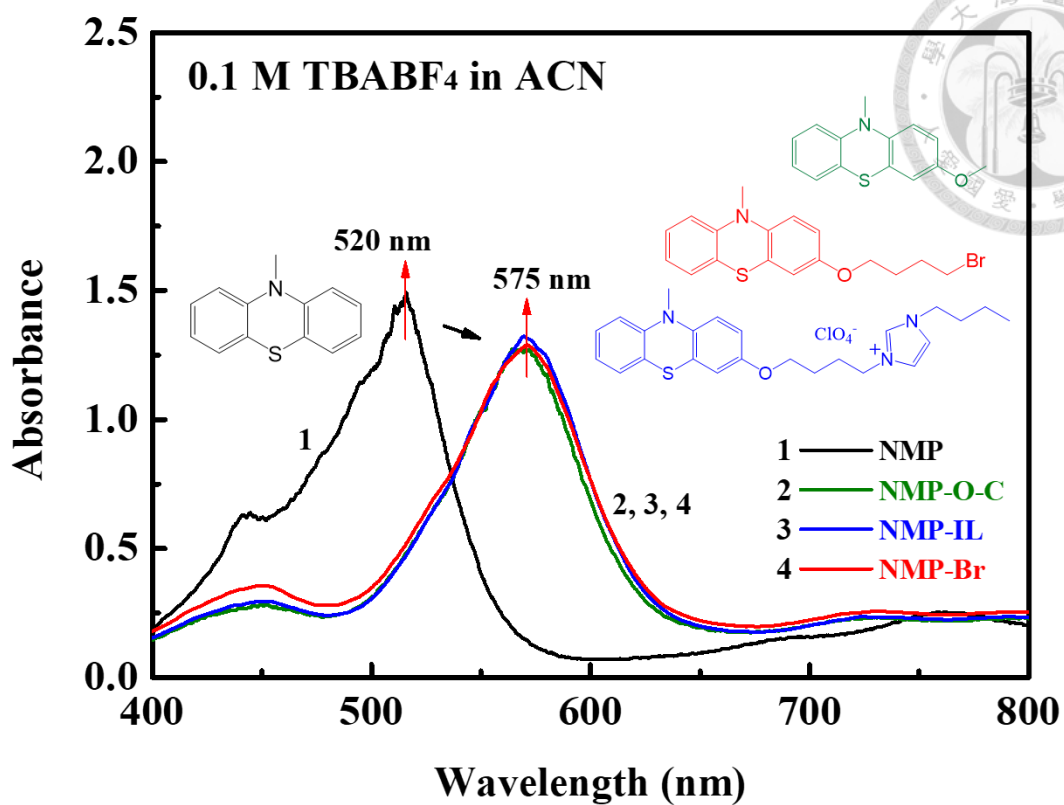
Fig. 4-14 UV-Vis absorbance spectra of 0.03 M NMP, NMP-O-C, NMP-Br and NMP-IL with maximum absorbance in ACN.
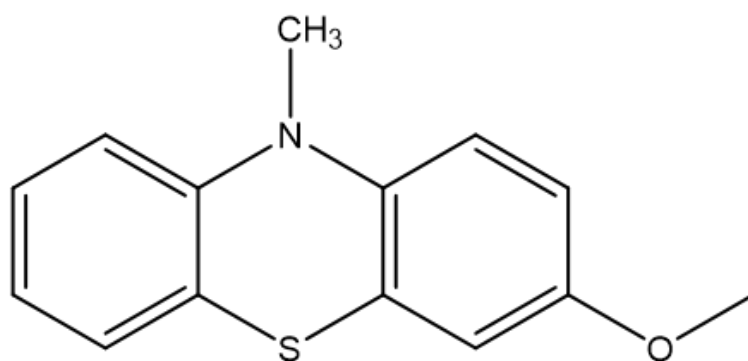
Fig. 4-15 The structure of 3-methoxy-10-methyl-phenothiazine (NMP-O-C).

4.2.6 Characterization of NMP-IL/PV ECD

4.2.6.1 CV of NMP-IL/PV ECD

Fig. 4-16 shows the cyclic voltammogram (CV) of the proposed NMP-IL/PV ECD, performed in a two electrode system. One set of well-defined and reversible redox peaks can be observed for the NMP-IL/PV ECD, with an anodic peak at 1.08 V and a cathodic peak at 0.70 V. The redox peak is attributed to the simultaneous redox reactions of NMP-IL and PV. Redox reactions of NMP-IL and PV can be presented by Eqs. (4-4) and (4-5). Combining these two reactions, the overall reaction of ECD is shown in Eqs. (4-6).

$$NMP\text{-}IL \quad \leftrightarrow \quad NMP\text{-}IL^{+\bullet} \quad + \quad e^- \qquad\qquad (4\text{-}4)$$

$$\text{(colorless)} \qquad\qquad \text{(purple)}$$

$$PV^{2+} \quad + \quad e^- \quad \leftrightarrow \quad PV^{+\bullet} \qquad\qquad (4\text{-}5)$$

$$\text{(colorless)} \qquad\qquad \text{(green)}$$

$$NMP\text{-}IL + PV^{2+} \quad \leftrightarrow \quad NMP\text{-}IL^{+\bullet} + PV^{+\bullet} \qquad\qquad (4\text{-}6)$$
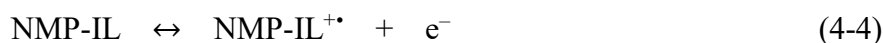
$$\text{(colorless)} \qquad\qquad \text{(dark green)}$$

In Fig. 4-16, the nonzero current density could be observed when the potential is at 1.4 V, implying the recombination reaction of NMP-IL$^{+\bullet}$ and PV$^{+\bullet}$ occurs. In general, the onset potential (E_{onset}) is defined as the potential at which the current density reached 10% of the peak current density. After the applied potential bias reached the E_{onset}, which is 0.71 V for the NMP-IL/PV ECD, NMP-IL is oxidized to NMP-IL$^{+\bullet}$ and PV^{2+} is reduced to PV$^{+\bullet}$ onto the working electrode and the counter electrode, respectively, at the same time. Thereafter, a part of NMP-IL$^{+\bullet}$ and PV$^{+\bullet}$ would diffuse and migrate from the surface of ITO electrode back to the bulk electrolyte, and then NMP-IL$^{+\bullet}$ and PV$^{+\bullet}$ do the redox reaction, forming the NMP-IL and PV, spontaneously. It is defined as recombination reaction and nonzero current density could be explained at the potential bias of 1.4 V.

NMP-IL/PV ECD
Electrolyte: 0.1 M TBABF$_4$ in PC
Scan rate: 100 mV/s
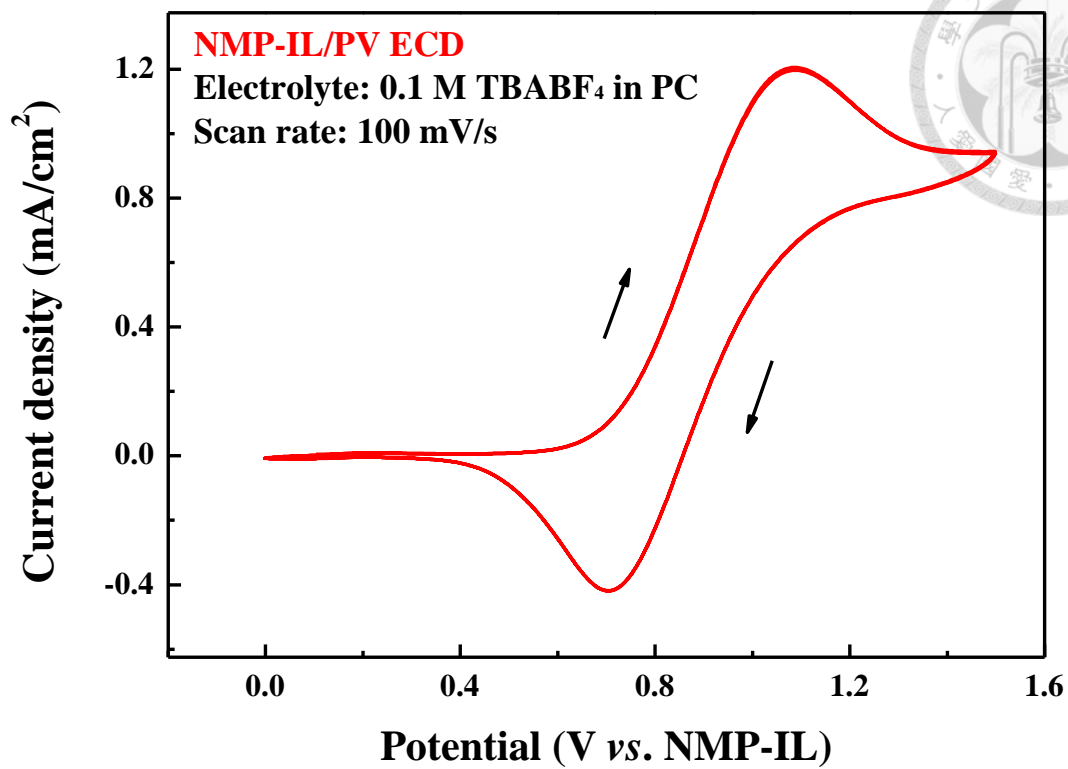
Fig. 4-16 CV of NMP-IL/PV ECD with 0.1 M TBABF$_4$ in PC at a scan rate of 100 mV/s.

4.2.6.2 UV-Vis absorbance spectra of NMP-IL/PV ECD

In order to investigate the electrochromic properties of the ECD, UV-visible (UV-vis) spectra of the NMP-IL/PV ECD was measured under various applied voltages between 0 and 1.3 V, shown in Fig. 4-17. At 0 V, also open-circuit voltage (OCV), the ECD shows absorbance in the full visible region. When the applied voltages bias over 0.6 V, three obvious peaks at 430, 575 and 710 nm could be observed. The increments at 430 and 710 nm are mainly attributed to the PV. Another absorbance variation arises around 575 nm is resulted from both the coloring attribution of NMP-IL and PV.
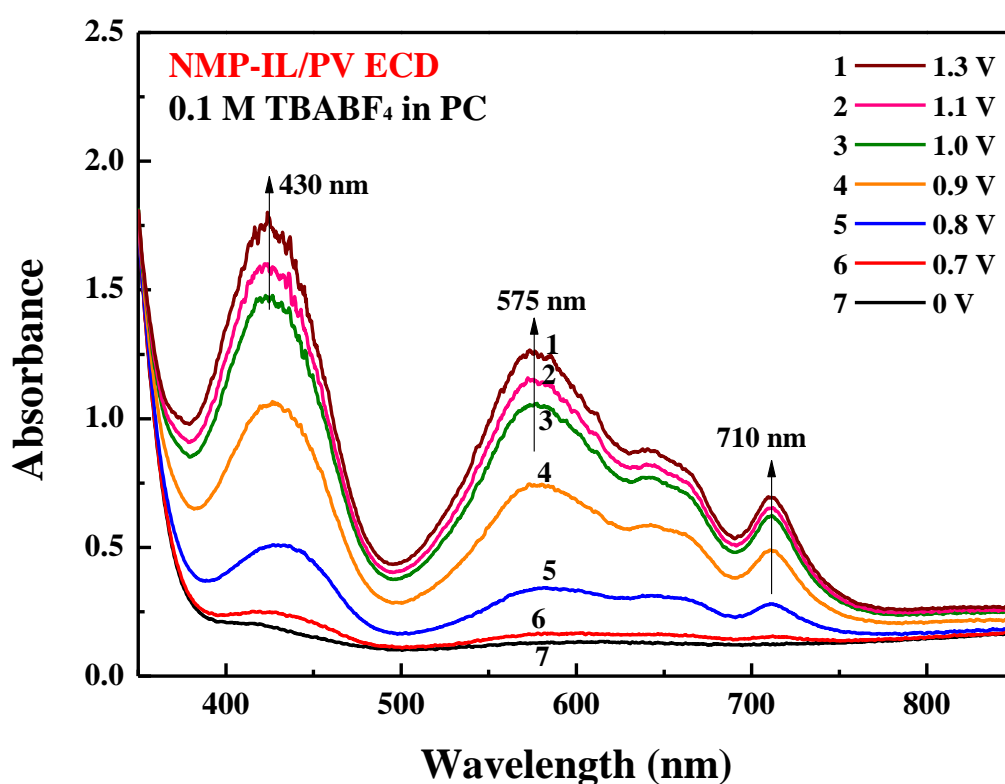
Fig. 4-17 UV-Vis absorbance spectra of NMP-IL/PV ECD at various potential biases from 0 to 1.3 V.

4.2.6.3 Dynamic transmittance responses at 430, 575 and 710 nm for NMP-IL/PV ECD

Since NMP-IL/PV ECD shows the mainly absorbance change at 430, 575 and 710 nm, the transmittance change of the ECD at these specific wavelengths during voltage switching were studied. Fig. 4-18 shows the dynamic transmittance responses for NMP-IL/PV ECD with 10 s interval time. Besides, switching between 0 and 1.3 V, the proposed ECD demonstrated largest transmittance

change that could be obtained. Therefore, we choose 0 and 1.3 V as V_b and V_c, respectively. The data of the t_b, t_c and ΔT of the proposed ECD are collected in Table 4-2.

As presented in Fig. 4-18 and Table 4-2, NMP-IL/PV ECD at each wavelengths exhibit both coloring times and bleaching times shorter than 4 s. Moreover, the transmittance change of 63.7% and 54.5% at 430 and 710 nm can be observed respectively, attributed to the PV. The color-reinforcing effect is achieved at 575 nm, which has the highest ΔT value of 69.2% attributed to the NMP-IL and PV.
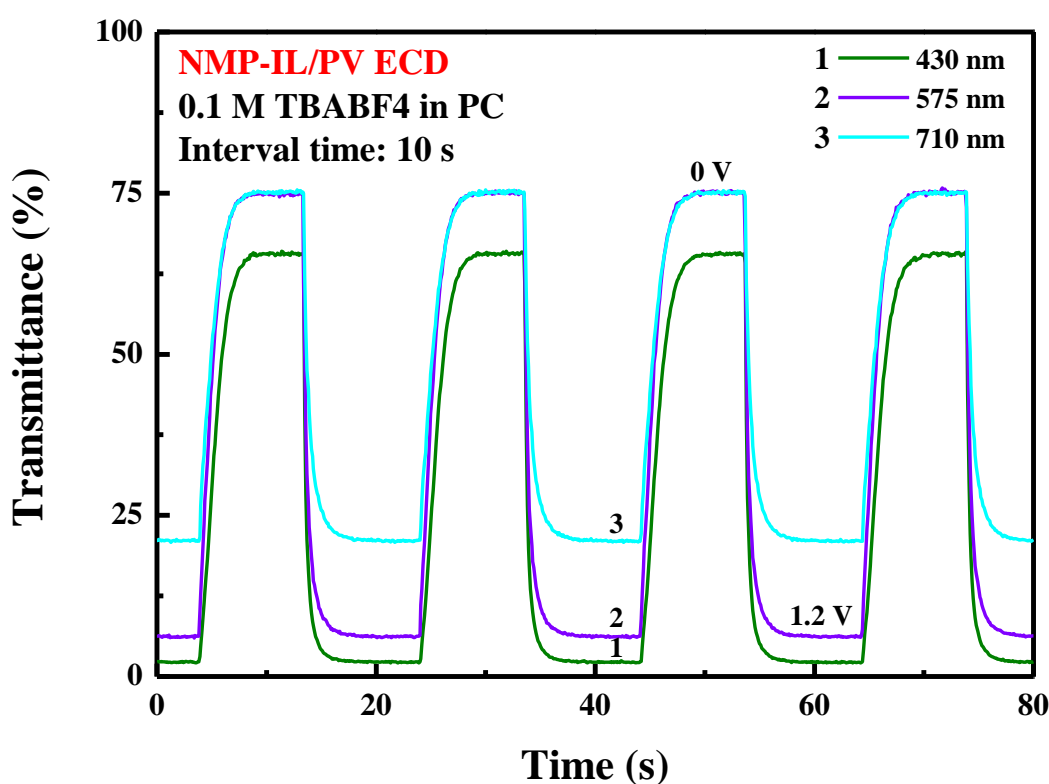
Fig. 4-18 Dynamic transmittance responses at 430, 575 and 710 nm for NMP-IL/PV ECD performed with a potential step between 0 and 1.2 V.

Table 4-2 Dynamic transmittance response of the NMP-IL/PV ECD.

λ (nm)	t	t	T_b (%)[b]	T_c (%)[b]	ΔT (%)
430	3.7	1.3	65.9	2.2	63.7
575	3.1	1.8	75.3	6.1	69.2
710	3.5	2.2	75.4	20.9	54.5

[a] bleaching time (t_b) and coloring time (t_c) are defined as the time required to reach 95% ΔT ;

[b] Transmmitance at bleaching state (T_b) and transmmitance at colored state (T_c)

4.2.6.4 Coloration efficiency of NMP-IL/PV ECD

The relationship between the optical density change (ΔOD) at the 575 nm, which shows color-reinforcing effect, and the injected charge density (Q_d) of the NMP-IL, PV and NMP-IL/PV ECD is presented in Fig. 4-19. The calculated charge densities were based on the integration of the measured current densities against the time (up to a fixed interval time of 10 s). The coloration efficiency (η) was calculated from the slope of the curve from 0.6 to 1.1 V.

The coloration efficiency was calculated to be 171 and 296 cm^2/C of NMP-IL and PV at 575 nm, repsectively. The coloration efficiency of the solution-typed EC materials can be calculated according to the previous literature. Namely, we set O_d as the difference of the measured current density (j_{mea}) and the recombination current density (j_{rec}), resulting the coloring current density (j_{col}) which is closer to the intrinsic charge required to darken solution-typed EC materials. Consequently, the coloration efficiency was calculated to be 531 cm^2/C of NMP-IL/PV ECD at 575 nm. This value is much larger than the normal value of viologen-based ECD incorporating with ferrocene as redox couple. The advantage of complementary ECD is revealed upon the addition of coloration efficiency from individual coloring EC material, NMP-IL and PV. In addition, the dramatic coloration efficiency of NMP-IL/PV ECD shows the thorough reaction between NMP-IL and PV. It suggests that NMP-IL is an attractive candidate for electrochromic redox couple.
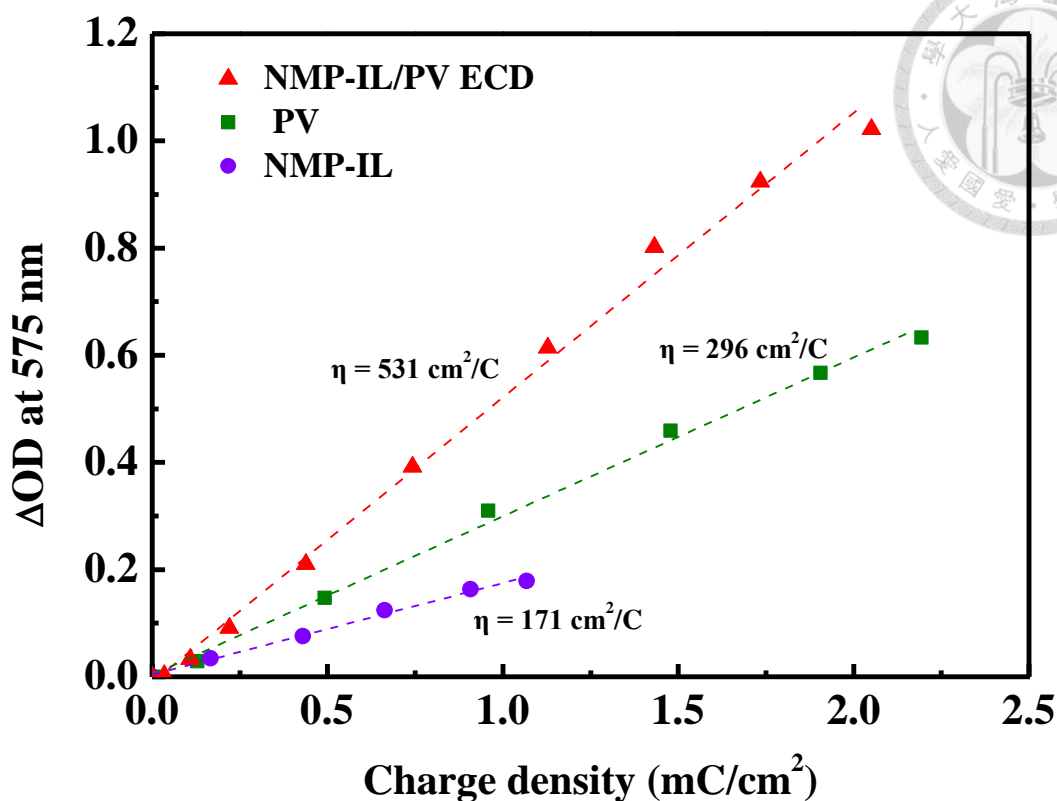
Fig. 4-19 The relationship between the optical changes and the coloring charge density for 10 s of NMP-IL, PV and the NMP-IL/PV ECD at different potential biases.

4.2.6.5 Long-term stability of NMP-IL/PV ECD

The long-term stability of the proposed ECD based on their write-erase ability were tested by stepping the ECD between 0 V (bleached state) and 1.2 V (colored state) with an interval time of 10 s for both coloring and bleaching processes. Dynamic transmittance response cycled for 10000 cycles between coloring and bleaching state at 430, 575 and 710 nm are shown in Fig. 4-20. To qualify the long-term stability, the remained $\Delta T\%$ after n cycles (ΔT_n) of the proposed ECD are collected in Table 4-3.

As shown, exceptional stability that remained around 95% after 4000 cycles can be observed for proposed ECD at 575 nm. Whereas for the ECD at 430 and 710 nm, an obvious decay after 4000 cycles. It has been reported that when $PV^{+\bullet}$ generated upon reduction on the ITO electrode tends to aggregate. The agglomerate inhibits the recombination, which is the most important process during

the bleaching state. Beyond expectations, the aggregation of $PV^{+\bullet}$ seen to be improved after 4000 cycles. The retentions of the NMP-IL/PV ECD are 92.0, 96.2 and 97.8 at 430, 575 and 710 nm respectively after 10,000 cycles. It indicates the NMP-IL is highly stable new electrochromic material and suitable for viologen systems owing to good reversibility as redox couple.
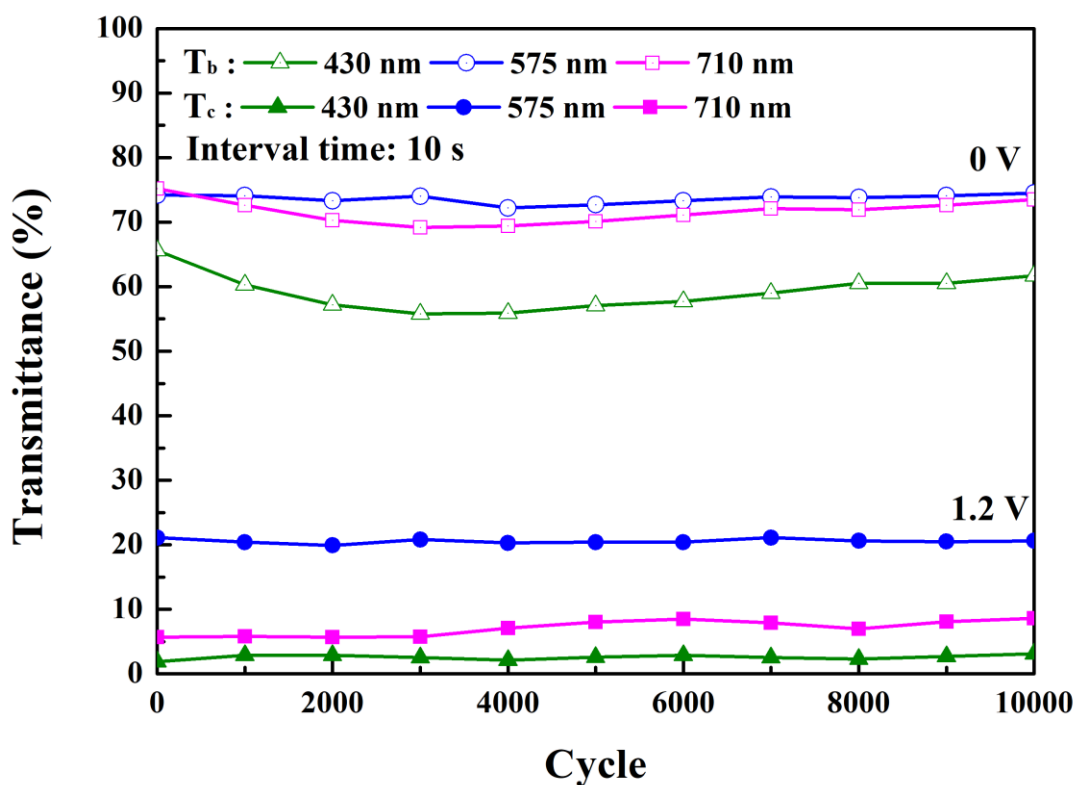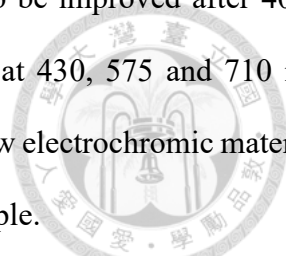
Fig. 4-20 Long-term stability of the NMP-IL/PV ECD.

Table 4-3 Long-term stability of the NMP-IL/PV ECD.

λ (nm)	ΔT	ΔT_{1000} (%)	ΔT_{2000} (%)	ΔT_{4000} (%)	ΔT_{10000} (%)
430	63.7	90.1	85.2	84.5	92.0
575	68.5	99.7	98.7	94.9	96.2
710	54.1	96.1	93.2	90.8	97.8

4.2.6.6 Images of NMP-IL/PV ECD

The images of NMP-IL/PV ECD at both coloring and bleaching states are presented in Fig. 4-21. As mentioned previously, the color of ECD tends to dark green.

Fig. 4-21 Images of NMP-IL/PV ECD at coloring state (1.2 V) and bleaching state (0V).

As a conclusion, there are few literatures collected in Table 3-7 that proposed the ECDs containing redox couple-based ILs, including TEMPO and Fc. However, barely optical change could be found of these redox couple during redox reaction. As presented, the proposed NMP-IL/PV ECD exhibited higher optical contrast (69.2 %) and well long-term stability (> 10,000 cycles) at 575 nm compared to others. The operating potential bias (1.2 V) and switching time (3 s) are also desirable.

Table 4-4 A partial list of literatures on the EC performance of ECDs containing redox couple-based ILs.

ECD	V_b/V_c (V)	t_b/t_c (s)	ΔT (%)	R (%) (n^{th} cycle)	Ref.
PProDOT-Et$_2$/TILBF$_4$[a]	1.0/-1.0	4.0/3.6	62.2	98 (1000)	[128]
[FcC$_{11}$VC$_1$][b][TFSI]$_2$	0/1.0	-	21	-	[129]
[FcNTf][c]/[EV]/IL	0/2.0	5.5/9.5	38.8	94.8 (1000)	[119]
NMP-IL/PV	0/1.2	3.1/1.8	69.2	96.2 (10000)	Chapter 4

[a] 1-butyl-3-{2-oxo-2-[(2,2,6,6-tetramethylpiperidin-1-oxyl-4-yl)amino]ethyl}-1H-imidazol-3-ium tetrafluoroborate.

^b 1-(11-Ferrocenylundecyl)-1'-methyl-4,4'-bipyridinium

^c ferrocenylsulfonyl(trifluoromethylsulfonyl)imide.

4.3 Conclusions

This is the first study for synthesizing the NMP-based IL. Furthermore, the immediate products and final product, NMP-IL, are all confirmed by ^{1}H and ^{13}C NMR and the electrochromic properties are investigated carefully. The strong optical contrast of NMP can be observed at 520 nm. When the functional groups graft on the benzene, the obvious absorbance change to 575 nm is found. It is explained that molecular structures changes from open ion-radical to hindered ion-radical. Namely, the planar structure of NMP convert into NMP-IL which belongs to hindered system. To further realize electrochromism and stability of NMP-IL, the NMP-IL/PV ECD is fabricated. The NMP-IL/PV ECD exhibits largest transmittance change of 69.2% and desirable coloration efficiency of 531 cm^2/C at 575 nm, which is contributed to the overlap of both coloring material. Moreover, the short switching times of less 4s and good long-term stability (remained 92%, 96.2% and 97.8% of its original ΔT after 10,000 cycles at 430, 575 and 710 nm respectively) is obtained. For all the merits mentioned above, the NMP-IL possess potential to be applied in the wide potential window systems.

Chapter 5

Conclusions and Suggestions

5.1 General conclusions

In this thesis, we demonstrated two totally different ECDs, one is thin-film typed ECD based on MEPE and PB, another is solution-typed ECD composed of NMP-IL and PV. Our studies feature in two different aspects, fabricating a panchromatic ECD composed of PolyRuFe, and synthesizing the new class of anodically coloring material, NMP-IL.

In chapter 3, a complementary PolyRuFe/PB ECD was fabricated. The idea of using PolyRuFe and PB is because these two EC materials can provide different wavelength of absorbance change, namely, the panchromatic characteristic can be observed to the PolyRuFe/PB ECD. Furthermore, we investigated the relationship between long-term stability of PolyRuFe/PB ECD and memory effect of PolyRuFe thin film. To increase memory time of PolyRuFe, the MWCNTs were incorporated with PolyRuFe. This strategy is utilizing the adsorption of ClO_4^- by acid treated MWCNTs, remaining the longer memory time of PolyRuFe at the bleaching state.

In chapter 4, we first synthesized the NMP-based ionic liquid. It is found that the absorbance change at 520 nm of NMP shift to 575 nm after grafting the carbon chain onto benzene, forming NMP-IL. It is explained that molecular structure of NMP changes from open ion-radical to hindered ion-radical. Moreover, we fabricated the NMP-IL/PV ECD to investigate the electrochromic performance of NMP-IL in the ECD. The NMP-IL/PV ECD exhibits large transmittance change, the short switching time and desirable coloration efficiency, which is contributed by both coloring EC materials. Good long-term stability is also observed, indicating NMP-IL is a potentially coloring EC material.

5.2 Suggestions

5.2.1 Suggestions for Chapter 3

In chapter 3, we discussed the relationship between long-term stability of PolyRuFe/PB ECD and memory effect of PolyRuFe thin film. It is observed that PolyRuFe-MWCNT thin film shows the longer memory time owing to the adsorption of ClO_4^- by acid treated MWCNTs. According to literature, the double-walled CNTs exhibit the better ability of ClO_4^- adsorption than MWCNTs due to the introduction of more oxygen-containing functional groups, which served as additional adsorption sites. It's expected to introduce the DWCNTs in MEPE system for improving the long-term stability via enhancing the memory effect.

As mentioned before, the oxidative pretreatment is the most crucial step while fabricating the MEPE-based ECD. However, there is rare redox couple can oxidize PolyFe(II) or PolyRu(II) due to their high redox potential. Recently, we found that 1, 4-dimethoxybenzene exhibits the higher redox potential than common redox couples utilizing in electorchromic field, including TEMPO, ferrocene, TMPD and NMP. Thus, 1, 4-dimethoxybenzene is considered to be a potential redox couple for pretreating the PolyRuFe.

5.2.1 Suggestions for Chapter 4
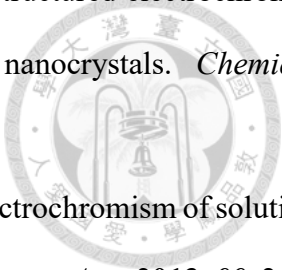
In chapter 4, NMP-IL shows the various advantages of electrochromism, including high optical change, fast response time and good stability. As a new anodically coloring material, it is suitable to fabricate the ECD composed other cathodically EC materials. In order to test the EC stability of NMP-IL in the severe condition, it is suggested to incorporate with EC materials having wide potential window, like PolyCo.

Further, we found that the redox peak of NMP changes to lower potential when the functional groups grafting on its benzene, including NMP-OH, NMP-Br and NMP-IL. Their redox potential is similar to NiHCF, which is the well-known ion storage layer. It is considered to fabricate the low-driving voltage ECD (less than 0.4 V) composed NiHCF and NMP-based redox couple.

References
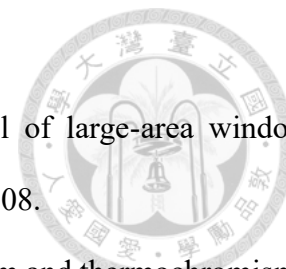
1. Granqvist, C. G., Chromogenic materials for transmittance control of large-area windows. *Critical Reviews in Solid State and Materials Sciences* **1990,** *16* (5), 291-308.

2. Hadjoudis, E.; Vittorakis, M.; Moustakali-Mavridis, I., Photochromism and thermochromism of schiff bases in the solid state and in rigid glasses. *Tetrahedron* **1987,** *43* (7), 1345-1360.

3. Araujo, R. J., Photochromism in glasses containing silver halides. *Contemporary Physics* **1980,** *21* (1), 77-84.

4. Araujo, R. J., Opthalmic glass particularly photochromic glass. *Journal of Non-Crystalline Solids* **1982,** *47* (1), 69-86.

5. Babulanam, S. M.; Eriksson, T. S.; Niklasson, G. A.; Granqvist, C. G., Thermochromic VO2 films for energy-efficient windows. *Solar Energy Materials* **1987,** *16* (5), 347-363.

6. Lampert, C. M., Electrochromic materials and devices for energy efficient windows. *Solar Energy Materials* **1984,** *11* (1-2), 1-27.

7. Svensson, J. S. E. M.; Granqvist, C. G., Electrochromic coatings for "smart windows". *Solar Energy Materials* **1985,** *12* (6), 391-402.

8. Araki, S.; Nakamura, K.; Kobayashi, K.; Tsuboi, A.; Kobayashi, N., Electrochemical optical-modulation device with reversible transformation between transparent, mirror, and black. *Advanced Materials* **2012,** *24* (23), OP122-OP126.

9. Tsuboi, A.; Nakamura, K.; Kobayashi, N., A localized surface plasmon resonance-based multicolor electrochromic device with electrochemically size-controlled silver nanoparticles. *Advanced Materials* **2013,** *25* (23), 3197-3201.

10. Thakur, V. K.; Ding, G.; Ma, J.; Lee, P. S.; Lu, X., Hybrid materials and polymer electrolytes for electrochromic device applications. *Advanced Materials* **2012,** *24* (30), 4071-4096.

11. Yen, H. J.; Lin, K. Y.; Liou, G. S., Transmissive to black electrochromic aramids with high near-infrared and multicolor electrochromism based on electroactive tetraphenylbenzidine units. *Journal of Materials Chemistry* **2011,** *21* (17), 6230-6237.

12. Runnerstrom, E. L.; Llordés, A.; Lounis, S. D.; Milliron, D. J., Nanostructured electrochromic smart windows: Traditional materials and NIR-selective plasmonic nanocrystals. *Chemical Communications* **2014,** *50* (73), 10555-10572.

13. Chen, F.; Fu, X.; Zhang, J.; Wan, X., Near-infrared and multicolored electrochromism of solution processable triphenylamine-anthraquinone imide hybrid systems. *Electrochimica Acta* **2013,** *99*, 211-218.

14. Llordés, A.; Garcia, G.; Gazquez, J.; Milliron, D. J., Tunable near-infrared and visible-light transmittance in nanocrystal-in-glass composites. *Nature* **2013,** *500* (7462), 323-326.

15. Deb, S. K., A Novel Electrophotographic System. *Appl. Opt.* **1969,** *8* (S1), 192-195.

16. Mortimer, R. J.; Rosseinsky, D. R.; Monk, P. M. S., Electrochromic Materials and Devices. *Angew. Chem. Int. Edit.* **2015**, 1-638.

17. Beaujuge, P. M.; Ellinger, S.; Reynolds, J. R., The donor–acceptor approach allows a black-to-transmissive switching polymeric electrochrome. *Nature Materials* **2008,** *7*, 795.

18. Lampert, C. M., Large-area smart glass and integrated photovoltaics. *Solar Energy Materials and Solar Cells* **2003,** *76* (4), 489-499.

19. Argun, A. A.; Aubert, P.-H.; Thompson, B. C.; Schwendeman, I.; Gaupp, C. L.; Hwang, J.; Pinto, N. J.; Tanner, D. B.; MacDiarmid, A. G.; Reynolds, J. R., Multicolored Electrochromism in Polymers: Structures and Devices. *Chemistry of Materials* **2004,** *16* (23), 4401-4412.

20. Mortimer, R. J.; Dyer, A. L.; Reynolds, J. R., Electrochromic organic and polymeric materials for display applications. *Displays* **2006,** *27* (1), 2-18.

21. Kurth, D. G.; Pitarch Lopez, J.; Dong, W.-F., A new Co(ii)-metalloviologen-based electrochromic material integrated in thin multilayer films. *Chemical Communications* **2005,** (16), 2119-2121.

22. Higuchi, M., Stimuli-responsive metallo-supramolecular polymer films: Design, synthesis and device fabrication. *Journal of Materials Chemistry C* **2014,** *2* (44), 9331-9341.

23. Kurth, D. G.; Higuchi, M., Transition metal ions: Weak links for strong polymers. *Soft Matter* **2006,** *2* (11), 915-927.

24.   Han, F. S.; Higuchi, M.; Kurth, D. G., Metallo-supramolecular polymers based on functionalized bis-terpyridines as novel electrochromic materials. *Advanced Materials* **2007,** *19* (22), 3928-3931.

25.   Fu, S. H.; Higuchi, M.; Kurth, D. G., Metallosupramolecular polyelectrolytes self-assembled from various pyridine ring-substituted bisterpyridines and metal ions: Photophysical, electrochemical, and electrochromic properties. *Journal of the American Chemical Society* **2008,** *130* (6), 2073-2081.

26.   Trefonas Iii, P.; West, R., ORGANOSILANE HIGH POLYMERS: OXIDATION OF POLYCYCLOHEXYLMETHYLSILYLENE. *Journal of polymer science. Polymer letters edition* **1985,** *23* (9), 469-473.

27.   Zhang, J.; Hsu, C.-Y.; Higuchi, M., Anion Effects to Electrochromic Properties of Ru-based Metallo-supramolecular Polymers. *Journal of Photopolymer Science and Technology* **2014,** *27* (3), 297-300.

28.   Jelle, B. P.; Hagen, G., Transmission Spectra of an Electrochromic Window Based on Polyaniline, Prussian Blue and Tungsten Oxide. *Journal of the Electrochemical Society* **1993,** *140* (12), 3560-3564.

29.   DeLongchamp, D.; Hammond, P. T., Layer-by-layer assembly of PEDOT/polyaniline electrochromic devices. *Advanced Materials* **2001,** *13* (19), 1455-1459.

30.   Lin, C. F.; Hsu, C. Y.; Lo, H. C.; Lin, C. L.; Chen, L. C.; Ho, K. C., A complementary electrochromic system based on a Prussian blue thin film and a heptyl viologen solution. *Solar Energy Materials and Solar Cells* **2011,** *95* (11), 3074-3080.

31.   Kuo, T.-H.; Hsu, C.-Y.; Lee, K.-M.; Ho, K.-C., All-solid-state electrochromic device based on poly(butyl viologen), Prussian blue, and succinonitrile. *Solar Energy Materials and Solar Cells* **2009,** *93* (10), 1755-1760.

32.   DeLongchamp, D. M.; Hammond, P. T., High-contrast electrochromism and controllable dissolution of assembled prussian blue/polymer nanocomposites. *Advanced Functional Materials* **2004,** *14* (3), 224-232.

33.   Mortimer, R. J.; Rosseinsky, D. R., Electrochemical polychromicity in iron hexacyanoferrate films, and a new film form of ferric ferricyanide. *Journal of Electroanalytical Chemistry* **1983,** *151*

(1-2), 133-147.

34. Gotoh, A.; Uchida, H.; Ishizaki, M.; Satoh, T.; Kaga, S.; Okamoto, S.; Ohta, M.; Sakamoto, M.; Kawamoto, T.; Tanaka, H.; Tokumoto, M.; Hara, S.; Shiozaki, H.; Yamada, M.; Miyake, M.; Kurihara, M., Simple synthesis of three primary colour nanoparticle inks of Prussian blue and its analogues. *Nanotechnology* **2007,** *18* (34).

35. Hara, S.; Shiozaki, H.; Omura, A.; Tanaka, H.; Kawamoto, T.; Tokumoto, M.; Yamada, M.; Gotoh, A.; Kurihara, M.; Sakamoto, M., Color-switchable glass and display devices fabricated by liquid processes with electrochromic nanoparticle "ink". *Applied Physics Express* **2008,** *1* (10), 1040021-1040023.

36. Lee, K. M.; Tanaka, H.; Takahashi, A.; Kim, K. H.; Kawamura, M.; Abe, Y.; Kawamoto, T., Accelerated coloration of electrochromic device with the counter electrode of nanoparticulate Prussian blue-type complexes. *Electrochimica Acta* **2015,** *163*, 288-295.

37. Liao, T. C.; Chen, W. H.; Liao, H. Y.; Chen, L. C., Multicolor electrochromic thin films and devices based on the Prussian blue family nanoparticles. *Solar Energy Materials and Solar Cells* **2016,** *145*, 26-34.

38. Gruver, G. A.; Kuwana, T., Spectroelectrochemical studies of E.E. and E.E.C. mechanisms. *Journal of Electroanalytical Chemistry* **1972,** *36* (1), 85-99.

39. Nelson, R. F.; W. Leedy, D.; T. Seo, E.; N. Adams, R., Anodic oxidation of 5,10-dihydro-5,10-dimethylphenazine. *Anal. Bioanal. Chem.* **1966,** *224*, 184-196.

40. Korth, C.; May, B. C. H.; Cohen, F. E.; Prusiner, S. B., Acridine and phenothiazine derivatives as pharmacotherapeutics for prion disease. *Proceedings of the National Academy of Sciences* **2001,** *98* (17), 9836.

41. Kubota, K.; Kurebayashi, H.; Miyachi, H.; Tobe, M.; Onishi, M.; Isobe, Y., Synthesis and structure–activity relationships of phenothiazine carboxylic acids having pyrimidine-dione as novel histamine H1 antagonists. *Bioorganic & Medicinal Chemistry Letters* **2009,** *19* (10), 2766-2771.

42. Dixit, Y.; Dixit, R.; Gautam, N.; Gautam, D. C., Synthesis and Antimicrobial Activities of Novel Biologically Active Heterocycles: 10H-Phenothiazines, Their Ribofuranosides, and Sulfone

Derivatives. *Nucleosides, Nucleotides and Nucleic Acids* **2009,** *28* (11-12), 998-1006.

43. Singh, G.; Kumar, N.; Yadav Ashok, K.; Mishra, A. K., Potential antimicrobial agents: Trifluoromethyl-10H-phenothiazines and ribofuranosides. *Heteroatom Chemistry* **2003,** *14* (6), 481-486.

44. Gautam, V.; Sharma, M.; Samarth, R. M.; Gautam, N.; Kumar, A.; Sharma, I. K.; Gautam, D. C., Synthesis of Some Substituted 10H-Phenothiazines, Ribofuranosides, and their Antioxidant Activity. *Phosphorus, Sulfur, and Silicon and the Related Elements* **2007,** *182* (6), 1381-1392.

45. Kumar, M.; Rathore, R. K.; Gupta, V.; Gupta, R. R., Studies on diamagnetic susceptibility of biologically active heterocycles: Diamagnetic susceptibility of 1,4-benzothiazines. *Chemical Physics Letters* **1990,** *170* (1), 121-124.

46. Kong, X.; Kulkarni, A. P.; Jenekhe, S. A., Phenothiazine-Based Conjugated Polymers: Synthesis, Electrochemistry, and Light-Emitting Properties. *Macromolecules* **2003,** *36* (24), 8992-8999.

47. Hwang, D.-H.; Kim, S.-K.; Park, M.-J.; Lee, J.-H.; Koo, B.-W.; Kang, I.-N.; Kim, S.-H.; Zyung, T., Conjugated Polymers Based on Phenothiazine and Fluorene in Light-Emitting Diodes and Field Effect Transistors. *Chemistry of Materials* **2004,** *16* (7), 1298-1303.

48. Lai, R. Y.; Kong, X.; Jenekhe, S. A.; Bard, A. J., Synthesis, Cyclic Voltammetric Studies, and Electrogenerated Chemiluminescence of a New Phenylquinoline-Biphenothiazine Donor−Acceptor Molecule. *Journal of the American Chemical Society* **2003,** *125* (41), 12631-12639.

49. Tu, X.; Fu, X.; Jiang, Q., The synthesis and electrochemical properties of anodic electrochromic materials phenothiazine derivatives and their electrochromic devices. *Displays* **2010,** *31* (3), 150-154.

50. Weng, D.; Li, M.; Zheng, J.; Xu, C., High-performance complementary electrochromic device based on surface-confined tungsten oxide and solution-phase N-methyl-phenothiazine with full spectrum absorption. *Journal of Materials Science* **2017,** *52* (1), 86-95.

51. Monk, P. M. S., The effect of ferrocyanide on the performance of heptyl viologen-based electrochromic display devices. *Journal of Electroanalytical Chemistry* **1997,** *432* (1-2), 175-179.

52. Yasuda, A.; Mori, H.; Takehana, Y.; Ohkoshi, A.; Kamiya, N., Electrochromic properties of the n-heptyl viologen-ferrocyanide system. *Journal of Applied Electrochemistry* **1984,** *14* (3), 323-327.

53. Levey, G.; Ebbesen, T. W., Methyl viologen radical reactions with several oxidizing agents. *Journal of Physical Chemistry* **1983,** *87* (5), 829-832.

54. Belinko, K., Electrochemical studies of the viologen system for display applications. *Applied Physics Letters* **1976,** *29* (6), 363-365.

55. Kao, S. Y.; Lu, H. C.; Kung, C. W.; Chen, H. W.; Chang, T. H.; Ho, K. C., Thermally Cured Dual Functional Viologen-Based All-in-One Electrochromic Devices with Panchromatic Modulation. *ACS Applied Materials and Interfaces* **2016,** *8* (6), 4175-4184.

56. Michaelis, L.; Hill, E. S., The viologen indicators. *Journal of General Physiology* **1933,** *16* (6), 859-873.

57. Bird, C. L.; Kuhn, A. T., Electrochemistry of the viologens. *Chemical Society Reviews* **1981,** *10* (1), 49-82.

58. Śliwa, W.; Bachowska, B.; Zelichowicz, N., Chemistry of viologens. *Heterocycles* **1991,** *32* (11), 2241-2273.

59. Ho, K. C.; Greenberg, C. B., Tungsten Oxide-Prussian Blue Electrochromic System Based on a Proton-Conducting Polymer Electrolyte. *Journal of the Electrochemical Society* **1994,** *141* (8), 2061-2067.

60. Cai, G.; Darmawan, P.; Cui, M.; Wang, J.; Chen, J.; Magdassi, S.; Lee, P. S., Highly Stable Transparent Conductive Silver Grid/PEDOT:PSS Electrodes for Integrated Bifunctional Flexible Electrochromic Supercapacitors. *Advanced Energy Materials* **2016,** *6* (4).

61. Layani, M.; Kamyshny, A.; Magdassi, S., Transparent conductors composed of nanomaterials. *Nanoscale* **2014,** *6* (11), 5581-5591.

62. Kobayashi, N.; Hirohashi, R.; Ohno, H.; Tsuchida, E., Electrochromic characteristics for all solid state ECD composed of polymer electrolytes. *Solid State Ionics* **1990,** *40-41*, 491-494.

63. Fletcher, S.; Duff, L.; Barradas, R. G., Nucleation and charge-transfer kinetics at the viologen/SnO2 interface in electrochromic device applications. *Journal of Electroanalytical Chemistry and Interfacial Electrochemistry* **1979,** *100* (1), 759-770.

64. Lin, C.-F.; Hsu, C.-Y.; Lo, H.-C.; Lin, C.-L.; Chen, L.-C.; Ho, K.-C., A complementary

electrochromic system based on a Prussian blue thin film and a heptyl viologen solution. *Solar Energy Materials and Solar Cells* **2011,** *95* (11), 3074-3080.

65.　Green, S.; Backholm, J.; Georén, P.; Granqvist, C. G.; Niklasson, G. A., Electrochromism in nickel oxide and tungsten oxide thin films: Ion intercalation from different electrolytes. *Solar Energy Materials and Solar Cells* **2009,** *93* (12), 2050-2055.

66.　Baba, A.; Tian, S.; Stefani, F.; Xia, C.; Wang, Z.; Advincula, R. C.; Johannsmann, D.; Knoll, W., Electropolymerization and doping/dedoping properties of polyaniline thin films as studied by electrochemical-surface plasmon spectroscopy and by the quartz crystal microbalance. *Journal of Electroanalytical Chemistry* **2004,** *562* (1), 95-103.

67.　Hu, C. W.; Lee, K. M.; Huang, J. H.; Hsu, C. Y.; Kuo, T. H.; Yang, D. J.; Ho, K. C., Incorporation of a stable radical 2,2,6,6-tetramethyl-1-piperidinyloxy (TEMPO) in an electrochromic device. *Solar Energy Materials and Solar Cells* **2009,** *93* (12), 2102-2107.

68.　Zhang, J.; Tu, J. P.; Xia, X. H.; Qiao, Y.; Lu, Y., An all-solid-state electrochromic device based on NiO/WO3 complementary structure and solid hybrid polyelectrolyte. *Solar Energy Materials and Solar Cells* **2009,** *93* (10), 1840-1845.

69.　Lin, T. H.; Ho, K. C., A complementary electrochromic device based on polyaniline and poly(3,4-ethylenedioxythiophene). *Solar Energy Materials and Solar Cells* **2006,** *90* (4), 506-520.

70.　Wang, J. Y.; Yu, C. M.; Hwang, S. C.; Ho, K. C.; Chen, L. C., Influence of coloring voltage on the optical performance and cycling stability of a polyaniline-indium hexacyanoferrate electrochromic system. *Solar Energy Materials and Solar Cells* **2008,** *92* (2), 112-119.

71.　Ho, K. C.; Fang, Y. W.; Hsu, Y. C.; Chen, L. C., The influences of operating voltage and cell gap on the performance of a solution-phase electrochromic device containing HV and TMPD. *Solid State Ionics* **2003,** *165* (1-4), 279-287.

72.　Ho, K.-C.; Fang, Y.-W.; Hsu, Y.-C.; Chen, L.-C., The influences of operating voltage and cell gap on the performance of a solution-phase electrochromic device containing HV and TMPD. *Solid State Ionics* **2003,** *165* (1), 279-287.

73.　Moon, H. C.; Lodge, T. P.; Frisbie, C. D., Solution Processable, Electrochromic Ion Gels for

Sub-1 V, Flexible Displays on Plastic. *Chemistry of Materials* **2015,** *27* (4), 1420-1425.

74. Chidichimo, G.; Imbardelli, D.; De Simone, B. C.; Barone, P.; Barberio, M.; Bonanno, A.; Camarca, M.; Oliva, A., Spectroscopic and Kinetic Investigation of Ethyl Viologen Reduction in Novel Electrochromic Plastic Films. *The Journal of Physical Chemistry C* **2010,** *114* (39), 16700-16705.

75. Gruver, G. A.; Kuwana, T., Spectroelectrochemical studies of E.E. and E.E.C. mechanisms. *Journal of Electroanalytical Chemistry and Interfacial Electrochemistry* **1972,** *36* (1), 85-99.

76. Watanabe, Y.; Imaizumi, K.; Nakamura, K.; Kobayashi, N., Effect of counter electrode reaction on coloration properties of phthalate-based electrochromic cell. *Solar Energy Materials and Solar Cells* **2012,** *99*, 88-94.

77. Hu, C. W.; Sato, T.; Zhang, J.; Moriyama, S.; Higuchi, M., Multi-colour electrochromic properties of Fe/Ru-based bimetallo- supramolecular polymers. *Journal of Materials Chemistry C* **2013,** *1* (21), 3408-3413.

78. Roig, A.; Navarro, J.; Garcia, J. J.; Vicente, F., Voltammetric study of the stability of deposited Prussian blue films against succesive potential cycling. *Electrochimica Acta* **1994,** *39* (3), 437-442.

79. Silva, G. A.; Costa, L. M. M.; Brito, F. C. F.; Miranda, A. L. P.; Barreiro, E. J.; Fraga, C. A. M., New class of potent antinociceptive and antiplatelet 10H-phenothiazine-1-acylhydrazone derivatives. *Bioorganic & Medicinal Chemistry* **2004,** *12* (12), 3149-3158.

80. Chandra, D.; Sharma, V. N.; Mital, R. L., Studies on some new phenothiazines. *Canadian Journal of Chemistry* **1967,** 45, 761-767.

81. Zhang, W. W.; Yu, Y. G.; Lu, Z. D.; Mao, W. L.; Li, Y. Z.; Meng, Q. J., Ferrocene - Phenothiazine conjugated molecules: Synthesis, structural characterization, electronic properties, and DFT-TDDFT computational study. *Organometallics* **2007**, 26, 865-873.

82. Kim, S.-K.; Lee, J.-H.; Hwang, D.-H., EL properties of an alternating copolymer composed of phenothiazine and thiophene heterocycles. *Synthetic Metals* **2005,** *152* (1), 201-204.

83. Wang, W.; Sheng, C.; Che, X.; Ji, H.; Miao, Z.; Yao, J.; Zhang, W., Design, Synthesis, and Antifungal Activity of Novel Conformationally Restricted Triazole Derivatives. *Archiv der*

Pharmazie **2009,** *342* (12), 732-739.

84. Messali, M.; Aouad, R. M.; El-Sayed, S. W.; Al-Sheikh Ali, A.; Ben Hadda, T.; Hammouti, B., New Eco-Friendly 1-Alkyl-3-(4-phenoxybutyl) Imidazolium-Based Ionic Liquids Derivatives: A Green Ultrasound-Assisted Synthesis, Characterization, Antibacterial Activity and POM Analyses. *Molecules* **2014,** *19* (8), 11741-11759.

85. Beniwal, V.; Kumar, A., Thermodynamic and molecular origin of interfacial rate enhancements and endo-selectivities of a Diels-Alder reaction. *Physical Chemistry Chemical Physics* **2017,** *19* (6), 4297-4306.

86. Yao, C.-J.; Zhong, Y.-W.; Yao, J., Five-Stage Near-Infrared Electrochromism in Electropolymerized Films Composed of Alternating Cyclometalated Bisruthenium and Bis-triarylamine Segments. *Inorganic Chemistry* **2013,** *52* (17), 10000-10008.

87. Andres, P. R.; Schubert, U. S., New Functional Polymers and Materials Based on 2,2′:6′,2″-Terpyridine Metal Complexes. *Advanced Materials* **2004,** *16* (13), 1043-1068.

88. Dong, Y.-B.; Wang, P.; Huang, R.-Q.; Smith, M. D., Syntheses and Structures of Ag(I)-Containing Coordination Polymers and Co(II)-Containing Supramolecular Complex Based on Novel Fulvene Ligands. *Inorganic Chemistry* **2004,** *43* (15), 4727-4739.

89. Hu, C.-W.; Sato, T.; Zhang, J.; Moriyama, S.; Higuchi, M., Multi-colour electrochromic properties of Fe/Ru-based bimetallo-supramolecular polymers. *Journal of Materials Chemistry C* **2013,** *1* (21), 3408-3413.

90. Han, F. S.; Higuchi, M.; Ikeda, T.; Negishi, Y.; Tsukuda, T.; Kurth, D. G., Luminescence properties of metallo-supramolecular coordination polymers assembled from pyridine ring functionalized ditopic bis-terpyridines and Ru(ii) ion. *Journal of Materials Chemistry* **2008,** *18* (38), 4555-4560.

91. Kanao, M.; Higuchi, M., Synthesis of Metallo-Supramolecular Polymers with Bis-NNN-Tridentate Ligand for Electrochromic Devices. *Journal of Photopolymer Science and Technology* **2015,** *28* (3), 363-368.

92. Han, F. S.; Higuchi, M.; Kurth, D. G., Diverse Synthesis of Novel Bisterpyridines via Suzuki-

Type Cross-Coupling. *Organic Letters* **2007,** *9* (4), 559-562.

93.   Ide, T.; Takeuchi, D.; Osakada, K.; Sato, T.; Higuchi, M., Aromatic Macrocycle Containing Amine and Imine Groups: Intramolecular Charge-Transfer and Multiple Redox Behavior. *The Journal of Organic Chemistry* **2011,** *76* (22), 9504-9506.

94.   Hsu, C.-Y.; Zhang, J.; Sato, T.; Moriyama, S.; Higuchi, M., Black-to-Transmissive Electrochromism with Visible-to-Near-Infrared Switching of a Co(II)-Based Metallo-Supramolecular Polymer for Smart Window and Digital Signage Applications. *ACS Applied Materials & Interfaces* **2015,** *7* (33), 18266-18272.

95.   Wu, J.-T.; Liou, G.-S., A novel panchromatic shutter based on an ambipolar electrochromic system without supporting electrolyte. *Chemical Communications* **2018,** *54* (21), 2619-2622.

96.   Kao, S.-Y.; Lu, H.-C.; Kung, C.-W.; Chen, H.-W.; Chang, T.-H.; Ho, K.-C., Thermally Cured Dual Functional Viologen-Based All-in-One Electrochromic Devices with Panchromatic Modulation. *ACS Applied Materials & Interfaces* **2016,** *8* (6), 4175-4184.

97.   Shin, H.; Kim, Y.; Bhuvana, T.; Lee, J.; Yang, X.; Park, C.; Kim, E., Color Combination of Conductive Polymers for Black Electrochromism. *ACS Applied Materials & Interfaces* **2012,** *4* (1), 185-191.

98.   Weng, D.; Shi, Y.; Zheng, J.; Xu, C., High performance black-to-transmissive electrochromic device with panchromatic absorption based on TiO2-supported viologen and triphenylamine derivatives. *Organic Electronics* **2016,** *34*, 139-145.

99.   McCargar, J. W.; Neff, V. D., Thermodynamics of mixed-valence intercalation reactions: The electrochemical reduction of Prussian blue. *Journal of Physical Chemistry* **1988,** *92* (12), 3598-3604.

100. Mortimer, R. J.; Reynolds, J. R., In situ colorimetric and composite coloration efficiency measurements for electrochromic Prussian blue. *Journal of Materials Chemistry* **2005,** *15* (22), 2226-2233.

101. Maestri, M.; Armaroli, N.; Balzani, V.; Constable, E. C.; Thompson, A. M. W. C., Complexes of the Ruthenium(II)-2,2′:6′,2″ -Terpyridine Family. Effect of Electron-Accepting and -Donating Substituents on the Photophysical and Electrochemical Properties. *Inorganic Chemistry* **1995,** *34* (10),

2759-2767.

102. Schott, M.; Szczerba, W.; Posset, U.; Šurca Vuk, A.; Beck, M.; Riesemeier, H.; Thünemann, A. F.; Kurth, D. G., In operando XAFS experiments on flexible electrochromic devices based on Fe(II)-metallo-supramolecular polyelectrolytes and vanadium oxide. *Solar Energy Materials and Solar Cells* **2016,** *147*, 61-67.

103. Chen, W.-H.; Chang, T.-H.; Hu, C.-W.; Ting, K.-M.; Liao, Y.-C.; Ho, K.-C., An electrochromic device composed of metallo-supramolecular polyelectrolyte containing Cu(I) and polyaniline-carbon nanotube. *Solar Energy Materials and Solar Cells* **2014,** *126*, 219-226.

104. Ho, T. D.; Zhang, C.; Hantao, L. W.; Anderson, J. L., Ionic Liquids in Analytical Chemistry: Fundamentals, Advances, and Perspectives. *Analytical Chemistry* **2014,** *86* (1), 262-285.

105. Scrosati, B.; Hassoun, J.; Sun, Y.-K., Lithium-ion batteries. A look into the future. *Energy & Environmental Science* **2011,** *4* (9), 3287-3295.

106. Park, M.; Zhang, X.; Chung, M.; Less, G. B.; Sastry, A. M., A review of conduction phenomena in Li-ion batteries. *Journal of Power Sources* **2010,** *195* (24), 7904-7929.

107. Lewandowski, A.; Świderska-Mocek, A., Ionic liquids as electrolytes for Li-ion batteries—An overview of electrochemical studies. *Journal of Power Sources* **2009,** *194* (2), 601-609.

108. de Souza, R. F.; Padilha, J. C.; Gonçalves, R. S.; Dupont, J., Room temperature dialkylimidazolium ionic liquid-based fuel cells. *Electrochemistry Communications* **2003,** *5* (8), 728-731.

109. Gírio, F. M.; Fonseca, C.; Carvalheiro, F.; Duarte, L. C.; Marques, S.; Bogel-Łukasik, R., Hemicelluloses for fuel ethanol: A review. *Bioresource Technology* **2010,** *101* (13), 4775-4800.

110. Wang, P.; Zakeeruddin, S. M.; Moser, J.-E.; Grätzel, M., A New Ionic Liquid Electrolyte Enhances the Conversion Efficiency of Dye-Sensitized Solar Cells. *The Journal of Physical Chemistry B* **2003,** *107* (48), 13280-13285.

111. Wang, P.; Zakeeruddin, S. M.; Moser, J. E.; Nazeeruddin, M. K.; Sekiguchi, T.; GrÄTzel, M., A stable quasi-solid-state dye-sensitized solar cell with an amphiphilic ruthenium sensitizer and polymer gel electrolyte. In *Materials for Sustainable Energy*, Co-Published with Macmillan

Publishers Ltd, UK: 2010; pp 88-93.

112. Ito, S.; Zakeeruddin, S. M.; Humphry-Baker, R.; Liska, P.; Charvet, R.; Comte, P.; Nazeeruddin, M. K.; Péchy, P.; Takata, M.; Miura, H.; Uchida, S.; Grätzel, M., High-efficiency organic-dye-sensitized solar cells controlled by nanocrystalline-TiO2 electrode thickness. *Advanced Materials* **2006,** *18* (9), 1202-1205.

113. Ye, Y.-S.; Rick, J.; Hwang, B.-J., Ionic liquid polymer electrolytes. *Journal of Materials Chemistry A* **2013,** *1* (8), 2719-2743.

114. Qian, W.; Jin, E.; Bao, W.; Zhang, Y., Clean and selective oxidation of alcohols catalyzed by ion-supported TEMPO in water. *Tetrahedron* **2006,** *62* (4), 556-562.

115. Chu, T.-C.; Lin Ryan, Y.-Y.; Lee, C.-P.; Hsu, C.-Y.; Shih, P.-C.; Lin, R.; Li, S.-R.; Sun, S.-S.; Lin Jiann, T.; Vittal, R.; Ho, K.-C., Ionic Liquid with a Dual-Redox Couple for Efficient Dye-Sensitized Solar Cells. *ChemSusChem* **2013,** *7* (1), 146-153.

116. Bui-Thi-Tuyet, V.; Trippé-Allard, G.; Ghilane, J.; Randriamahazaka, H., Surface and Electrochemical Properties of Polymer Brush-Based Redox Poly(Ionic Liquid). *ACS Applied Materials & Interfaces* **2016,** *8* (42), 28316-28324.

117. Forgie, J. C.; El Khakani, S.; MacNeil, D. D.; Rochefort, D., Electrochemical characterisation of a lithium-ion battery electrolyte based on mixtures of carbonates with a ferrocene-functionalised imidazolium electroactive ionic liquid. *Physical Chemistry Chemical Physics* **2013,** *15* (20), 7713-7721.

118. Zhang, W.; Qiu, L.; Chen, X.; Yan, F., Imidazolium Functionalized Bis-2,2,6,6-Tetramethyl-piperidine-1-oxyl (TEMPO) Bi-redox Couples for Highly Efficient Dye-Sensitized Solar Cells. *Electrochimica Acta* **2014,** *117*, 48-54.

119. Gélinas, B.; Das, D.; Rochefort, D., Air-Stable, Self-Bleaching Electrochromic Device Based on Viologen- and Ferrocene-Containing Triflimide Redox Ionic Liquids. *ACS Applied Materials & Interfaces* **2017,** *9* (34), 28726-28736.

120. Liao, Y.; Jiang, P.; Chen, S.; Xiao, F.; Deng, G.-J., Synthesis of phenothiazines from cyclohexanones and 2-aminobenzenethiols under transition-metal-free conditions. *RSC Advances*

2013, *3* (40), 18605-18608.

121. Kao, S.-Y.; Kawahara, Y.; Nakatsuji, S. i.; Ho, K.-C., Achieving a large contrast, low driving voltage, and high stability electrochromic device with a viologen chromophore. *Journal of Materials Chemistry C* **2015,** *3* (14), 3266-3272.

122. Lu, H.-C.; Kao, S.-Y.; Chang, T.-H.; Kung, C.-W.; Ho, K.-C., An electrochromic device based on Prussian blue, self-immobilized vinyl benzyl viologen, and ferrocene. *Solar Energy Materials and Solar Cells* **2016,** *147*, 75-84.

123. Chang, T.-H.; Lu, H.-C.; Lee, M.-H.; Kao, S.-Y.; Ho, K.-C., Multi-color electrochromic devices based on phenyl and heptyl viologens immobilized with UV-cured polymer electrolyte. *Solar Energy Materials and Solar Cells* **2018,** *177*, 75-81.

124. Monk, P. M. S.; Fairweather, R. D.; Ingram, M. D.; Duffy, J. A., Evidence for the product of the viologen comproportionation reaction being a spin-paired radical cation dimer. *Journal of the Chemical Society, Perkin Transactions 2* **1992,** 2(11), 2039-2041.

125. Goddard, N. J.; Jackson, A. C.; Thomas, M. G., Spectrelectrochemical studies of some viologens used in electrochromic display applications. *Journal of Electroanalytical Chemistry and Interfacial Electrochemistry* **1983,** *159* (2), 325-335.

126. van Dam, H. T.; Ponjeé, J. J., Electrochemically Generated Colored Films of Insoluble Viologen Radical Compounds. *Journal of the Electrochemical Society* **1974,** *121* (12), 1555-1558.

127. Rosokha, S. V.; Kochi, J. K., Continuum of Outer- and Inner-Sphere Mechanisms for Organic Electron Transfer. Steric Modulation of the Precursor Complex in Paramagnetic (Ion-Radical) Self-Exchanges. *Journal of the American Chemical Society* **2007,** *129* (12), 3683-3697.

128. Fan, M.-S.; Lee, C.-P.; Vittal, R.; Ho, K.-C., A novel ionic liquid with stable radical as the electrolyte for hybrid type electrochromic devices. *Solar Energy Materials and Solar Cells* **2017,** *166*, 61-68.

129. Tahara, H.; Baba, R.; Iwanaga, K.; Sagara, T.; Murakami, H., Electrochromism of a bipolar reversible redox-active ferrocene–viologen linked ionic liquid. *Chemical Communications* **2017,** *53* (16), 2455-2458.
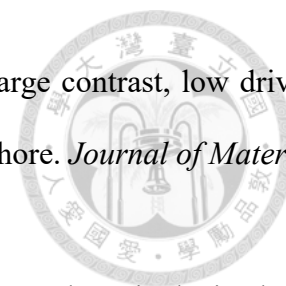
Date of Birth: Nov. 10th, 1993

Place of Birth: Kaohsiung, Taiwan

Sexual/Marital Status: Male/Single

Email Address: alan8020001@gmail.com;

r05524050@ntu.edu.tw

Education

    M. S. study, Chemical Engineering   September 2016 – July 2018

    National Taiwan University, Taiwan

    B. S. study, Chemical Engineering   September 2012 – June 2016

    National Chung Cheng University, Taiwan

Research Experience

1. Electrochemistry: Fundamental analysis using voltammetry, amperometry, rotating disk electrode

2. Material synthesis

    (a) Synthesis of electrochromic materials: Metallo-supramolecular polymers (MEPEs), Prussian blue analogues, phenothiazine-based groups, conducting polymers, viologens.

    (b) Synthesis of gel-state electrolytes

    (c) Synthesis of metal layered double hydroxides, metal oxide, metal nitride

3. Synthesis of metal-organic frameworks (MOFs):

    Porphyrin-based MOF (MOF-525) nanocrystal

4. Electrocatalysis:

    Electrocatalysis for oxygen evolution reaction (OER) and oxygen reduction reaction (ORR)

5. Familiar with electrochemical work stations (Autolab, CHI), scanning electron microscopy (SEM), Nuclear Magnetic Resonance (NMR), Mass spectrometer (MS), UV-Vis spectrophotometer, Fourier transform infrared spectroscopy (FTIR)

Publications

1. **<u>Li-Yin Hsiao</u>**, Ting-Hsiang Chang, Hsin-Che Lu, Yen-Chun Wang, Kuo-Chuan Ho* and Masayoshi Higuchi*, A panchromatic electrochromic device composed of Ru(II)/Fe(II)-based heterometallo-supramolecular polymer and Prussian blue. (Under preparation)

2. **<u>Li-Yin Hsiao</u>**, Chien-Hsin Wu, Ying-Chi Huang, Yoshikazu Ninomiya, Min-Hsin Yeh, Yen-Chun Wang, Masayoshi Higuchi*, Ru-Jong Jeng*, Kuo-Chuan Ho*, N-Methylphenothiazine Derived Ionic Liquid as a Redox Couple with Phenyl Viologen for Electrochromic Device. (Under preparation)

3. Yen-Chun Wang, Hsin-Che Lu, **<u>Li-Yin Hsiao</u>**, Kuo-Chuan Ho*, A Complementary Electrochromic Device Composed of Nanoparticulated Ruthenium Purple and Fe(II)-based Metallo-supramolecular Polymers. (Under preparation)

Conference Presentations

1. **<u>Li-Yin Hsiao</u>**, Hsin-Che Lu, Sheng-Yuan Kao, Ting-Hsiang Chang, Yen-Chun Wang, Kuo-Chuan Ho, "A Complementary Electrochromic Device Composed of Co(II)-Based Metallo-Supramolecular Polymer, Prussian Blue and Ferrocene," The 2017 MRS Fall Meeting & Exhibit, Boston, U.S.A., November 26- December 1 (2017). (*Oral presentation*)

2. Yen-Chun Wang, Hsin-Che Lu, **<u>Li-Yin Hsiao</u>**, Kuo-Chuan Ho, "A Complementary Electrochromic Device Composed of Nanoparticulated Ruthenium Purple and Fe(II)-based Metallo-supramolecular Polymers," The 2017 MRS Fall Meeting & Exhibit, Boston, U.S.A., November 26- December 1 (2017). (*Oral presentation*)

3. **<u>Li-Yin Hsiao</u>**, Chien-Hsin Wu, Ying-Chi Huang, Yoshikazu Ninomiya, Min-Hsin Yeh, Yen-Chun Wang, Masayoshi Higuchi, Ru-Jong Jeng, Kuo-Chuan Ho, "N-Methylphenothiazine Derived Ionic Liquid as a Redox Couple with Phenyl Viologen for Electrochromic Device," IME-13, Chiba, Japan, August 27-31 (2018). *(Poster).*

4. Yen-An Lu, Bo-Xun Wang, **<u>Li-Yin Hsiao</u>**, Yen-Chun Wang, Ting-Hsiang Chang, Kuo-Chuan Ho, "Highly Stable Black-to-Transmissive Electrochromic Devices Composed of Phenolacetyl Viologen and 5,10-Dihydro-5,10-dimethylphenazine," IME-13, Chiba, Japan, August 27-31 (2018). *(Poster).*

5. Yen-Chun Wang, Hsin-Che Lu, **<u>Li-Yin Hsiao</u>**, Kuo-Chuan Ho, "A Complementary Electrochromic Device Composed of Nanoparticulated Ruthenium Purple and Fe(II)-based Metallo-supramolecular Polymers," IME-13, Chiba, Japan, August 27-31 (2018). *(Poster)*